CR-102747

SOME ASPECTS OF VISCOUS CHEMICALLY REACTING MODERATE ALTITUDE ROCKET EXHAUST PLUMES

R. B. Edelman, M. J. Abbett, G. Weilerstein,

O. Fortune, & J. Genovese

FINAL REPORT

March 1970

Prepared Under Contract NAS8-21264

Prepared for

George C. Marshall Space Flight Center
Marshall Space Flight Center, Alabama 35812

GENERAL APPLIED SCIENCE Labs.,Inc.
MERRICK AND STEWART AVENUES, WESTBURY, L I, NEW YORK 11590 • 516-333-6960
A SUBSIDIARY OF THE MARQUARDT CO

SOME ASPECTS OF VISCOUS CHEMICALLY REACTING MODERATE ALTITUDE ROCKET EXHAUST PLUMES

R. B. Edelman, M. J. Abbett, G. Weilerstein,

O. Fortune, & J. Genovese

General Applied Science Laboratories, Inc.
Merrick and Stewart Avenues
Westbury, L.I., New York

FINAL REPORT

March 1970

Prepared Under Contract NAS8-21264

Prepared for

George C. Marshall Space Flight Center
Marshall Space Flight Center, Alabama 35812

ABSTRACT

This report represents an analytical study of several processes relevant to the structure of moderate altitude rocket exhaust plumes. The work covers an analytical framework for a viscous and chemically reacting plume; the Mach disc, the mixed flow problem, and condensation effects.

The contractors report number is GASL TR 737.

TABLE OF CONTENTS

		Page
	Abstract	ii
	Nomenclature	ix
I	Introduction	1
	A. Status of Previous Plume Flow Programs	2
	B. Specific Objectives of This Effort	3
II	Discussion of the Problem	4
	A. Required Modifications of Existing Program	4
	B. The Triple Point-Mach Disc	4
	C. The Transonic-Flow	5
III	Analysis	7
IV	Details of the Modifications of the MOCV Program	10
	A. The Expansion at the Nozzle Exit Lip-Starting Line	10
	B. Detection of the Intercepting(Barrel) Shock	11
	C. Intercepting Shock Computations	12
	D. Triple Point Location and Solution	14
	E. Reflected Shock Computation	14
	F. The Subsonic Region	15
	G. The Sonic Point on the Axis	16
V	Sample Computation	17
VI	The Mach Disc	18
	A. The Problem	19
	B. Outline of the Theory	21
	C. Verification of the Theory and Comparions With Other Theories	25
	D. Discussion of Other Theories	29
	E. Concluding Remarks	32
VII	Evaluation of Methods to Compute the Transonic Inviscid Flow in an Underexpanded Plume	33
	A. Considerations	33
	B. Discussion of the Qualities of the Three Approaches with Respect to the Four Criteria and the Evaluation	35

TABLE OF CONTENTS (contd)

		Page
VIII	Solution of the Steady Flow in a Two-Dimensional deLaval Nozzle as the Asymptotic Limit of an Unsteady Flow	43
	A. Introduction	43
	B. Formulation of the Initial Value Boundary Value Problem	44
	C. The Nature of the Entrance Plane Discontinuity	47
	D. Solution of the Problem	48
	E. Conclusion	60
IX	Chemical Kinetics in Plume Flows	61
X	Phase Transition	66
	A. Analysis	66
	B. The Condensation Process	72
	C. Chemistry Model	83
XI	Summary	85
	Appendix A	86
	References	88
	Table I	93
	Table II	94

LIST OF FIGURES

		Page
1	Schematic of Flow Field-Supersonic Missile With Underexpanded Exhaust	95
2	Triple Point Configuration	96
3	Schematic of Flow Downstream of Mach Disc	97
4	Schematic of MOCV Computational Procedure	98
5	Sketch- Starting Mesh of Edelman & Weilerstein	98
6	Sketch of Starting Mesh for Current Effort	99
7	Sketch of Regular Characteristic Mesh Superimposed on Computational Mesh	100
8a	Sketch Illustrating Computational Procedure	101
8b	Sketch of Computation at Intercepting Shock	101
9	Sketch of Triple Point Computation	102
10	Sketch of Subsonic Core Streamtube	103
11	Sample Calculation	104
12	Inviscid Plume of an Underexpanded Nozzle	105
13	Core Streamtube Mach Number vs Axial Distance for Various Assumed Triple Point Locations	106
14	Slip Line Slope vs Core Mach Number for Various Assumed Values of Triple Point Locations	107
15	Various Computed Pressure Distributions	108
16	Angle Between Mach Disc and Incident Flow vs Axial Position of Assumed Triple Point	109
17	Parameters Pinpointing the Solution	110
18	Comparison of Theoretical and Experimental Point Locations	111
19	Computed Flow Field for $x_{T.P.}/r_j = 4.79$	112
20	Schematic of Underexpanded Sonic Nozzle in a Quiescent Environment	113
21	Schematic of Underexpanded Sonic Nozzle in the Absence of Internal Shocks	113

LIST OF FIGURES (contd)

		Page
22	Schematic of Internal Shock Structure in the Vicinity of the Triple Point	114
23 24	Normalized Mass Flow vs Axial Distance	115
25	Flow Near and Downstream of the Triple Point Mach Disc	116
26	Computational Region for Transonic Flow	116
27a	Region to be Computed as Steady Supersonic Flow	117
27b	Region to be Computed with Unsteady Procedure	117
28	Two-Dimensional deLaval Nozzle	118
29	Schematic of the Unsteady Initial Value Boundary Value Problem	118
30	Quasi-One-Dimensional deLaval Nozzle Unsteady Flow	119
31	Schematic of the Entrance Plane "Black Box"	119
32	Quasi-One-Dimensional deLaval Nozzle Computational Grid	119
33	Computational Scheme at Entrance Discontinuity	120
34	Quasi-One-Dimensional deLaval Nozzle	121
35	Quasi-One-Dimensinnal deLaval Nozzle - Pressure Distribution at Several Times	122
36	Pressure vs Time on Downstream Side of the Discontinuity-Quasi-One-Dimensional deLaval Nozzle	123
37	History of Work Performed at the Entrance Plane-Quasi-One-Dimensional deLaval Nozzle	124
38	Entropy Jump at Entrance Plane Discontinuity-Quasi-One-Dimensional deLaval Nozzle	125
39	Discontinuity Work and Entropy Jump Histories for "Overchoked" and "Underchoked" Quasi-One-Dimensional Nozzles	126

LIST OF FIGURES (contd)

		Page
40	Mach Number Behind the Discontinuity for "Overchoked" and "Underchoked" in Quasi-One-Dimensional Nozzles	127
41	Pressure Behind the Discontinuity in "Overchoked" and "Underchoked" Quasi-One-Dimensional Nozzles	128
42	Computational Grid in Physical Space Time=Constant	129
43	Schematic of Mapping of Physical Space Auto Computation Space - Fixed Time	130
44	Schematic of Computational Procedure at a Wall Mesh Point (Upper Wall Shown)	131
45	Schematic of Computational Procedure on Downstream Side of Discontinuity	132
46	Two-Dimensional deLaval Nozzle - Specified Geometry	133
47	Pressures and Velocities Downstream of Discontinuity-Two-Dimensional	134
48	Entropy Jump at Discontinuity Surface - Two-Dimensional Nozzle	135
49	Computed Steady Centerline and Wall Pressure Distribution Two-Dimensional Nozzle	136
50	Computed Steady State Centerline and Wall Mach Number Distribution - Two-Dimensional Nozzle	137
51	Early Quasi-Complete Combustion of Hydrocarbon-Air Chemistry Model	138
52	Final Quasi-Complete Combustion Hydrocarbon-Air Chemistry Model	139
53	Comparison of Quasi-Complete Combustion Models Equilibrium Chemistry for a Propane-Air System	140
54	Comparison of Quasi-Complete Combustion Models With Equilibrium Chemistry for a Propane-Air System	141
55	Velocity and Temperature Profiles at Station $A/A_{jet} = 22$	142

LIST OF FIGURES (contd)

		Page
56	Gaseous Specie Mass Fraction Distribution at $A/A_{jet} = 22$	143
57	Condensed Water Profiles at Several Downstream Stations	144
58	Condensate Size Distribution in the First Category at $A/A_{jet} = 22$	145
59	The Characteristic Mesh	146
60	Schematic of Triple Point Configuration	147

NOMENCLATURE

A	area
a	speed of sound
b	defined by Eq. (12)
D_i	defined by Eq. (14)
F	defined by Eq. (16)
g	defined by Eq. (13)
H	total enthalpy
h	static enthalpy (sensible + chemical) of i^{th} specie
j	0 for 2-dimensional flow 1 for axisymmetric flow
Le	Lewis Number
ℓ	length along characteristic
M	Mach number
Pr	Prandtl number
p	pressure
q	velocity modulus
r	y ordinate
S	entropy
T	static temperature
t	time
u	viscosity or streamline velocity component
v	lateral velocity component
$\dot{w}_i$	chemical production term for i^{th} specie
x	streamwise coordinate
y	lateral coordinate

Greek

α_i	mass fraction of i^{th} specie
γ	specific heat ratio
ϵ	characteristic direction
θ	flow deflection angle
ρ	density
σ	surface tension
τ	tan θ
Ψ	stream function

Superscript

*	sonic condition or critical droplet state

Subscript

$\mathcal{C}_L$	centerline
e	supersonic external flow
i	subsonic internal flow or initial state
j	jet or nozzle state
L	condensate
N.S.	normal shock

s	shock
T.P.	triple point
t,0	stagnation state
v	vapor
v_{∞}	saturation state
∞	undisturbed environmental state

Additional symbols defined locally within the text.

I. INTRODUCTION

The description of rocket engine exhaust plumes has long been of interest because of a variety of important problems associated with the plume flow field structure. These problems involve a number of mechanisms which in the most general case, are coupled together within a framework of chemical and fluid dynamical processes. Radiation and convective heating of the vehicle and surrounding structure, communication and detection, impingement and contamination constitute the bulk of these problems[1,2,3].

The main characteristics of an axisymmetric moderate altitude rocket exhaust flow field are shown in Figure 1. The vehicle velocity is supersonic and the exhaust is underexpanded at the exit plane, leading to a "lip" shock which starts at the trailing edge of the nozzle. Often there are one or more nozzle shocks (not shown) which are caused by compression from the nozzle walls. The expansion waves at the trailing edge reflect as compression waves of the opposite family, often coalescing to form the intercepting (barrel) shock. The strength of the intercepting shock increases downstream due to further reflected waves which may be further enhanced due to the axisymmetric focusing effect. Downstream, the triple point-Mach disc configuration will introduce an imbedded region of subsonic flow. At the triple point a slip line contact discontinuity is formed and the intercepting shock is reflected as a shock of the opposite family.

Depending on flight and nozzle exit conditions, mixing between the ambient and exhaust gases can significantly affect the gross as well as the local properties of the flow. If the fuel has not been completely burned by the time it reaches the exit plane, it will then form a potentially combustible mixture as it mixes with the high speed air.

Thus, the plume problem involves a complex coupling of inviscid and viscous phenomena which in general includes the effects of combustion kinetics.

The purpose of this report is to describe some analysis and computational capability required for the prediction of such moderate altitude plume flow fields.

A. Status of Previous Plume Flow Programs

1. Inviscid Flow Field - The supersonic inviscid plume flow field for perfect, frozen, or equilibrium gas mixtures can be accurately and economically computed using the method of characteristics, and there are many such computer programs in existence, though few have the intercepting shock structure. The inclusion of finite rate chemistry in the usual fashion introduces economic limitations because the integration of the species production terms along streamlines by standard techniques such as Runge-Kutta lead to exceedingly long computing times.[4] In 1965 a major advance on the problem was made by G. Moretti[4]. Subsequent modifications and improvements[5,6] in Moretti's solution technique have extended even further the ability to solve complex chemical kinetics problems accurately while maintaining feasible running times.

The problem of the interaction between the subsonic-supersonic regions downstream of the Mach disc is itself complex but in certain cases can be treated by invoking a quasi-one-dimensional streamtube approximation for the subsonic flow, once the triple point location has been determined. These problems are discussed in later sections of this report.

2. Viscous Effects - The simplest and most common means of including viscous effects is to first determine the inviscid flow field and then to solve for a shear layer along the streamline which separates (in the inviscid solution) the exhaust gases from the external stream. This presupposes, of course, that the mixing layer remains relatively thin and that mixing effects do not significantly alter the inviscid field. However, when the mixing layer spreads significantly, it is not reasonable to lay a mixing analysis over an inviscidly computed flow field. However, the work in References 7, 8 and 9 have presented the basis for the treatment of such flows having simultaneously, (i) appreciable lateral pressure gradients, (ii) viscous effects over appreciable lateral dimension, and (iii) non-equilibrium chemistry.

3. The Viscid-Inviscid Analysis - The above analysis has been under development for a number of years and detailed in Reference 9. Basically, the idea is to consider those flows in which both inertia and viscous forces affect the pressure field while transport effects are of the boundary layer type ; thus, an initial value formulation is appropriate. The Navier Stokes equations are approximated in a manner such that the complete Euler terms are retained, while the viscous and heat

conduction terms are approximated in the same way as is usually done in classical boundary layer analyses. The method of characteristics is used to obtain a pressure-streamline deflection relation which includes the transport and species production terms in the inhomogeneous part of the compatibility relations along characteristics. The energy, streamwise momentum, and species production equations are integrated along streamlines after the pressure gradient has been determined from the characteristic computation.

At GASL, Edelman and Weilerstein[9] applied this technique to the solution of the supersonic plume of an underexpanded exhaust nozzle, among other configurations. That computer program, which included finite rate chemical effects did not have the capability of computing the internal shock structure and was limited to the hydrogen-air system.

B. Specific Objectives of This Effort

The following sections describe the modifications and extensions of the above computer program to include the internal shock structure. Detailed treatments of the Mach disc and transonic flow problems are also presented.

II. DISCUSSION OF THE PROBLEM

A. Required Modifications of Existing Program

This section will describe the important aspects of the general problem and how these relate to the work performed on this effort. This involves the inclusion of the intercepting shock, triple point-Mach disc, reflected shock, and transonic flow region solutions in the GASL MOCV computer program*.

Because the MOCV program developed by Edelman and Weilerstein contained no internal shock structure it was necessary to consider the following elements: (1) initial detection of the intercepting shock; (2) inclusion of the intercepting shock computation in the basic computer program; (3) determination of the triple point location; (4) solution of the triple point-Mach disc configuration; (5) inclusion of the reflected shock computation; (6) solution of the transonic flow downstream of the Mach disc. There are no fundamental difficulties associated with 1, 2 or 5 and they will receive no further attention in this section. 3, 4 and 6 all have associated with them fundamental problems which need additional discussion.

B. The Triple Point-Mach Disc

At the inception of this work, no one had, as yet, developed a completely satisfactory criterion for locating the triple point, and our initial intention was to make the computer program as flexible as possible by including as options each of the three most well known theories [10,11,12]. However, during the course of this work, a self-contained theory was developed which is firmly grounded on the basic interaction which determines the triple point location. As this theory was being developed, the usefulness of including the other three theories as program options diminished, and currently the triple point location is a datum.

Once the triple point has been located, it is necessary to obtain its configuration and that of the Mach disc. For the flows

---

* Reference will be made to the method of solution as the Method of Characteristics with Viscosity (MOCV) and to the associated computer code as the MOCV computer program.

we are considering, the triple point solution seems always to correspond to that shown in Figure 2, at least so long as no one does not consider scales on the order of the shock thickness or less.

C. The Transonic-Flow

The transonic flow downstream of the Mach disc also needs to be given special attention. For small to moderate-sized plumes, the core region is grossly one-dimensional [10] (see Section VI) and a quasi-one-dimensional streamtube approximation is remarkably accuracte over a wide range of nozzle exhaust conditions for supersonic plumes in a static ambient. The effect of the supersonic flight velocity is to shrink the lateral dimension of the plume, making the one-dimensional approximation for the core region even better. Also, viscous effects are neglected in the subsonic region and along the slip line where pressure/streamline-deflection effects predominate (the velocity difference across the slip line will ordinarily be quite small). So, in this effort, the transonic region is treated quasi-one-dimensionally, inviscidly, with an inviscid matching along the slip line.

The quasi-one-dimensional flow has associated with it, a pressure-area relationship while the supersonic outer flow is characterized by a pressure-streamline deflection law. In order to match along the slip line we must tie these two relations together, to match them. This is done by relating the slip line ordinate with its slope as sketched in Figure 3.

Consider everything known at some station x_o. Then to march ahead, we have, along the slip line,

$p = p_e(\theta)$ from the supersonic side (1a)

$p = p_i(y)$ from the subsonic side (1b)

$y = y(\theta)$ from analytic geometry and differential calculus (1c)

Putting (1c) in (1a) gives

$p = p_e(y)$ from the supersonic side (1a')

The matching involves, at a specified x, finding y(x) such that

$$p_e(y(x)) = p_i(y(x)).$$

So long as we are not near the place where the interior flow becomes sonic, we can expect to be able to march ahead, determining the slip line shape and axial pressure distribution from the indicated matching. Near the sonic point we can expect numerical difficulties because of the change in sign of the derivative of the area relation for the inside. This difficulty is best illustrated by differentiating (1a) and (1b) to get, along the slip line,

$$\frac{dp_e}{dx} = \frac{dp}{d\theta}\,\frac{d\theta}{dy}\,\frac{dy}{dx} \qquad \text{from the outer flow} \qquad (2a)$$

$$\frac{dp_i}{dx} = \frac{dp_i}{dy}\,\frac{dy}{dx} \qquad \text{from the inner flow} \qquad (2b)$$

Now as we proceed through the sonic point of the inner flow, dp_i/dy changes sign. If we had been able to solve the flow upstream of this point exactly (including the triple point - Mach disc solution), we would find that dp_e/dy changes sign (actually $d\theta/dy$) at the same abscissa as does dp_i/dy. But we cannot hope for such accuracy, and we must expect in the numerical solution, the changes in sign of dp_e/dy and dp_i/dy to occur at different abscissae, say x^*_e and x^*_i, the difference depending on the accuracy of the solution. The result will be, of course, difficulty in converging in the interaction for the matching along the slip line.

III. ANALYSIS

In this section we will first write the equations which comprise the MOCV analysis. Details can be found in the report by Edelman and Weilerstein[9]. Then, we will explain the splitting of the equations into "hyperbolic" and "parabolic" groupings indicating how each group is solved.

The Equations - We are considering axisymmetric flows and denote the axial and radial coordinate directions by (x,y) respectively. After non-dimensionalizing and dropping higher order transport terms, in intrinsic coordinates the describing equations are:

Global Continuity

$$(\rho q)_s + \frac{j\rho q}{r} \sin\theta + \rho q \theta_n = 0 \tag{3}$$

S-momentum

$$\rho q\, q_s + p_s = \frac{1}{r^j}\left[r^j \mu \frac{\partial q}{\partial n}\right]_n \tag{4}$$

n-momentum

$$\rho q^2 \theta_s + P_n = 0 \tag{5}$$

Species Continuity

$$\rho q (\alpha_i)_s = \dot{\rho w}_i + \frac{1}{r^j}\left[r^j \mu \frac{Le}{Pr} (\alpha_i)_n\right]_n \tag{6}$$

Energy

$$\rho q H = \frac{1}{r^j}\left[r^j \frac{\mu}{Pr} H_n\right]_n + \frac{1}{r^j}\left[\left(1-\frac{1}{pr}\right)\mu (q^2/2)_n\right]_n + \frac{1}{r^j}\sum_i \left[(Le-1) r^j \frac{\mu}{Pr} h_i (\alpha_i)_n\right]_n \tag{7}$$

where

$$H = \sum_i \alpha_i h_i(T) + q^2/2 \tag{8}$$

$$\rho = \frac{P}{RT \sum_i \frac{\alpha_i}{W_i}} \tag{9}$$

$$h_i = h_i(\alpha_i, T) \tag{10}$$

These equations are combined to yield two compatibility equations, relating changes in p and θ,

$$\frac{d\tau}{d\ell} \pm b \frac{dp}{d\ell} = \pm g \tag{11}$$

$$b = \frac{1 + \tau^2}{\rho q^2 \operatorname{Tan} \epsilon} \qquad \tau = \operatorname{Tan} \theta \tag{12}$$

$$q = \frac{(1+\tau^2)\sin \epsilon}{F} \left[\frac{\mu}{\rho q} \left(H_{nn} + \frac{\cos \theta}{y} H_n\right) - \frac{\mu}{\rho} \left(1 + \frac{F}{q^2}\right)\left\{q_{nn} + \right.\right. \tag{13}$$

$$\left.\left. + \frac{q_n \cos \theta}{y} \right\} - \sum_i h_i D_i + \frac{\rho RTF}{p} \sum_i \frac{D_i}{W_i} - \frac{F \sin \theta}{y} \right]$$

$$D_i = \frac{u}{\rho q} \alpha_{inn} + \frac{\mu}{\rho q} \frac{\cos \theta}{y} \alpha_{in} + \frac{\dot{w}_i}{q} \tag{14}$$

one along each of the two characteristics respectively inclined at the angles $\pm \epsilon_k$ to the streamline direction. The ϵ_k are given by

$$\operatorname{Tan} \epsilon_{1,2} = \pm \sqrt{\frac{F}{\rho q^2 \left(\frac{F}{p} - \frac{1}{\rho} - \frac{F}{\rho q^2}\right)}} \tag{15}$$

where

$$F = T \sum_i \alpha_i \frac{dh_i(T)}{dT} \tag{16}$$

$\dot{w}_i$ represents the rate of production of the i^{th} specie as a result of chemical reactions and is a known function of species concentrations, temperature, and density.

Equations (3) - (10) comprise eight equations* for the eight dependent variables, p, ρ, T, H, h, Q, θ, α_i. Of the five partial differential equations, Equations (3) - (7), the two compatibility equations (Equation(11)), are used in place of the global continuity and the normal momentum equations, and comprise the "hyperbolic" part of the system. Then the streamwise momentum, energy, and species continuity equations, (Eqs. (4), (6), (7)) integrated along streamlines, comprise the "parabolic" part of the system. They are solved by an explicit finite difference procedure, as are the characteristic compatibility equations.

Consider the solution to be known at some axial station x, as sketched in Figure 4. Then a characteristic mesh can be drawn, as indicated. Associated with this mesh is a minimum domain , Δx, of influence.

First the compatibility equations are solved on the characteristic mesh (with uneven axial spacing). Then, by interpolations on p and θ, the ordinate, inclination, and pressure at $x + \Delta x$ of the streamlines originating at mesh points at x are determined. With the now known pressure gradient the parabolic part of the system is solved in order: streamwise momentum, energy, species continuity.

---

* For convenience we will refer to all the species continuity equations as one equation.

IV. DETAILS OF THE MODIFICATIONS OF THE MOCV PROGRAM

In this section we will present the details of the analysis as well as of the required changes to the MOCV computer program. As mentioned before, the computer program used by Edelman and Weilerstein[9], was a basic program which established firmly the computational feasibility and usefulness of the basic MOCV concept outlined in the introduction. Some of the changes necessary to bring the MOCV computer program beyond this state are included in the following discussion.

A. The Expansion at the Nozzle Exit Lip - Starting Line

When the underexpanded exhaust gases reach the nozzle exit lip, they expand due to the lower external pressure (Figure 1). Locally, this expansion, which is inviscidly dominated, is a Prandtl-Meyer expansion. The exhaust gas streamlines turn into the external air stream, which is directed in the axial direction just upstream of the lip. An oblique shock is required to turn the external stream, since it cannot continue on its way due to the interaction with the exhaust gases. At the lip, the shock and expansion strengths must match so that the pressure and flow direction of the external and exhaust streams are compatible. In a purely inviscid flow, a slip line (contact discontinuity) would separate the two flows downstream of the lip. In our case, where we are including mixing of the two streams, we will refer to the streamline corresponding to the inviscid slip line as the separating streamline (SSL).

Edelman and Weilerstein[9], accounted for this expansion-shock structure, and the pertinent equations are presented in their report. However, in continuing downstream of the exit plane, they did not include the local details of the Prandtl-Meyer expansion in that computation. Consider the following schematization in Figure 5, of their finite difference grid at the exit plane and the immediately subsequent axial station. Point K at the initial station n = 1, has the pressure and flow direction determined by matching the shock and expansion strength (see above) and has the state associated with the chemical properties of the ambient gas.

The next lower mesh point k = K-1 is a regular exhaust nozzle point. Although locally not very detailed this finite difference is adequate for flow field computations not involving the detection of an intercepting shock. However, to compute an intercepting shock caused by the reflection, of the expansion waves off, essentially, the separating streamline, requires a

considerably more detailed treatment in the local near region. Such a procedure is illustrated in Figure 6. The expansion fan is divided into a number of intervals in the usual fashion for characteristic computations. In making the first axial step, the points K-I through K-1 are treated as a simple wave with frozen chemistry. All the other points are computed in the usual manner. The initial step is kept small enough so that, for the purpose of these computations, the simple wave approximation is adequate.

B. Detection of the Intercepting (Barrel) Shock

The intercepting shock is formed by the coalescence of compression waves resulting, basically, from the reflection of the lip expansion waves from the dividing streamline*. In a standard method of characteristics computation, it is easy to detect an envelope shock by the crossing of characteristics of the same family, in this case the right running (upper half plane) or first family characteristics. However, our characteristic mesh is redefined at each axial station, and a number of interpolations on the local characteristic grid are performed during the normal course of the computation. By the very nature of the computational procedure, it is impossible to detect the shock by the crossing of two first family characteristics originating from regular mesh points at a given axial station.

Since this situation results from the fact that the computational grid is established according to streamlines rather than characteristics, one solution is to superimpose a regular characteristic grid on the basic computational mesh, Figure 7. The characteristic mesh is composed of all the first family characteristics originating at either initial mesh points at the exhaust plane or regular mesh points on the lip shock. Thus, we can identify and follow downstream a number of distinct first family characteristics. When two of these characteristics cross we will have detected the "beginning" of the intercepting shock.

* The shock can be formed by other means, also, as by non-uniformities in nozzle exhaust properties, even when the exhaust pressure is balanced with the external pressure.

An alternative technique is to scan across the flow field to determine the maximum positive lateral pressure gradient. The intercepting shock is initiated at the point of maximum lateral pressure gradient when it exceeds a specified value. Although the details for both techniques have been worked out it is the latter that has been implemented in the MOCV program. In particular, the pressure profile is scanned and if the pressure shows a rise such that $\Delta p / p_{min} \geq .1$ between two grid points, a shock is initiated there.

C. Intercepting Shock Computations

Once we have detected the existence of the intercepting shock, it is necessary to include this shock in all subsequent computations downstream of its inception. Basically, this leads to a fairly standard method of characteristics treatment of a supersonic flow field with an embedded shock, except that we are working with a modified characteristic mesh and are including certain viscous and heat conduction effects. Now, the modified characteristic mesh actually simplifies the computational procedure considerably in the presence of imbedded shocks. Viscous and heat conduction effects are a complication since the integration of the "parabolic" equations along streamlines requires a knowledge of certain derivatives normal to the streamlines (e.g., g_n, g_{nn}, H_{nn}, α_{in}). Near the imbedded shock it becomes difficult to evaluate these terms since most of them are not continuous at the shock. In such cases, when we must evaluate these terms for a streamline whose mesh point is just adjacent to the shock, we use their values at the next adjacent mesh point on the same side of the shock. This approximation seems justified because, in the neighborhood of the shock, the changes due to the shock should dominate those due to viscous and heat conduction effects (excluding those within the shock), so any loss in accuracy from these extrapolations should have "higher order" effects.

The calculation procedure is as follows, (refer to Figures 8a and 8b):

Consider the flow, including the shock angle, to be completely specified at some station x_n. There are two mesh points (k_s,n) and (k_s+1,n) located on the shock; one on the upstream side, the other on the downstream side. The unknowns are the ordinates y_{n+1} of the shock, the shock slope, and the conditions on its upstream and downstream sides. To obtain this information, first the ordinate of the shock point $(k_{s\,n+1})$ at x_{n+1} is determined by using the shock slope at x_n and the already determined step size

$\Delta x = x_{n+1} - x_n$. The conditions in front of the shock $(k_s, n+1)$ are obtained by a regular characteristic streamline computation, interpolating on the data at $x = x_n$ to get the required data at points A, B, and C, Figure 8b.

Then the Rankine-Hugoniot jump conditions are simultaneously solved with the compatibility equation along the first family characteristic, $\overline{DF}$, yielding the shock angle and the conditions behind the shock at point $(k_s+1, n+1)$.

Letting subscripts 1 and 2 denote conditions on the upstream and downstream sides of the shock respectively, q denote the modulus of the velocity vector, θ_s the angle the shock makes with the incident x (upstream) flow, and τ the streamline slope, the jump equations are (for species frozen across the shock):

$$v_{t_1} = q_1 \cos \theta_s \qquad (17)$$

$$v_{m_1} = q_1 \sin \theta_s \qquad (18)$$

(17) and (18): velocity components normal and parallel to the shock

$$v_{t_2} = v_{t_1} \qquad (19)$$

$$(\alpha_i)_2 = (\alpha_i)_1 \qquad (20)$$

$$p_2 = p_1 + \rho_1 v_{n_1}^2 (1-\rho_1/\rho_2) \qquad (21)$$

$$h_2 = h_1 + \frac{1}{2} v_{n_1}^2 [1-(\rho_1/\rho_2)^2] \qquad (22)$$

$$T_2 = T_2(h_2, (\alpha_i)_2) \qquad (23)$$

$$v_{n_2} = \sqrt{2(h_1-h_2)+v_{n_1}^2} \qquad (24)$$

$$\delta = \theta_s - \tan^{-1}(v_{n_2}/v_{n_1}), \text{ the turning angle} \qquad (25)$$

$$\tau_2 = \tan(\tan^{-1}\tau_1 - \delta) \qquad (26)$$

The unknowns are : p_2, ρ_2, T_2, h_2, v_{n_2}, $(\alpha_i)_2$, τ_2, δ, θ_s, v_{t_2}.

Equations (19)-(25) are eight equations for ten unknowns. The other two equations are the equation of state

$$\frac{\rho_1}{\rho_2} = \frac{p_1}{p_2}\,\frac{T_2}{T_1} \quad \text{since } (\alpha_i)_2 = (\alpha_i)_1 \tag{27}$$

and the compatibility equation along the first family characteristic (Ref. 9 Eq. (38), with the minus sign)

$$\frac{d\tau}{d\ell} - \frac{1+\tau^2}{\rho q^2 \tan\theta}\,\frac{dp}{d\ell} = -g. \tag{28}$$

Because of the non-linearity of these equations, they are solved by iterating on the shock angle θ_s and, within that iteration, on the density ratio ρ_1/ρ_2.

D. Triple Point Location and Solution

Currently, the location of the triple point is a datum to be supplied by the program user. Once the computation has reached the triple point, the local triple point solution is determined. The intercepting shock angle and the flow conditions at (1) and (2) Figure 9, will have already been obtained from the regular flow field - intercepting shock computation using information only from upstream of the triple point. Then the solution at (3) and (4), including the reflected and Mach disc shock orientations, are obtained iteratively. A guess is made of the Mach disc angle, and the solution at (4), including p_4^o and θ_4^o is determined. Since $p_4=p_3$, the reflected shock is oriented by requiring $p_3^o = p_4^o$. There will then result a θ_3^o corresponding to p_3^o. In general, we cannot expect to have $\theta_3^o = \theta_4^o$, which it must since (3) and (4) are separated by a contact discontinuity. Hence, the shock angles are iterated on until $\theta_4^i = \theta_3^i$ and $p_4^i = p_3^i$ simultaneously.

E. Reflected Shock Computation

The computation of the reflected shock is identical to that outlined in IV-C for the intercepting shock except that the shock is of the other family.

F. The Subsonic Region

The subsonic region downstream of the Mach disc is treated quasi-one-dimensionally. This solution is coupled internally to the MOCV computation so that the entire solution is automatically generated.

Consider the quasi-one-dimensional flow to be completely known at some station x_n, and denote the values at this station by a subscript 1, Figure 10. It is desired to compute the flow at the next station, $x = x_n + \Delta x$, designated by a subscript 2. Letting A_1 and A_2 indicate the cross sectional area at each station, $\dot{m} = \rho_1 q_1 \quad A_1 = \rho_2 q_2 A_2$ be the total mass flow, H_o the stagnation enthalpy (no heat or momentum transport across the slip stream), then the equations for p_2, A_2, ρ_2, q_2, h_2, T_2, $(\alpha_i)_2$, are

Continuity

$$\frac{d\rho}{\rho} + \frac{dq}{q} + \frac{dA}{A} = 0 \tag{29}$$

Momentum

$$\rho q dq + dp = 0 \tag{30}$$

Energy

$$q dq + dh = dH = 0 \tag{31}$$

Caloric State

$$h_2 = h_2(p_2, \rho_2, \alpha_{i2}) \tag{32}$$

Rate

$$q \frac{d\alpha_i}{dx} = f(p, \rho, \alpha_i) \quad i = 1,2,3,\ldots n. \tag{33}$$

Thermal State

$$p_2 = R\left(\sum \frac{\alpha_i}{W_i} \right) \rho_2 T_2 \tag{34}$$

There are six equations for seven unknowns. Usually one specifies, for a streamtube, the pressure or area as a function of x, thus completing the system of equations. In our problem, the matching along the slip line between the inner and outer regions provides the "missing equation."

Equations (30) and (31) can be put in finite difference form and Equation (29) in integrated form:

$$\rho_1 q_1 A_1 = \rho_2 q_2 A_2 = \dot{m} \tag{29a}$$

$$\frac{1}{2}\rho dq^2 + dp = 0 \tag{30'}$$

$$\frac{\rho_1 + \rho_2}{4}(q_2^2 - q_1^2) + (p_2 - p_1) = 0 \tag{30a}$$

$$\frac{1}{2} dq^2 + dh = 0 \tag{31'}$$

$$\frac{1}{2}(q_2^2 - q_1^2) + (h_2 - h_1) = 0 \tag{31a}$$

G. The Sonic Point on the Axis

Downstream of the Mach disc, there will be a region where the quasi-one-dimensional core flow will accelerate to supersonic velocities. As previously mentioned, one can not expect to be able to smoothly continue the solution through this region without special treatment. However, the restart capability of the computer program enables the user to circumvent this problem by intelligent extrapolation through the sonic region. This is preferred over an automatic extrapolation within the program, for it enables the user to maintain maximum control where the computation becomes singular. Some approaches on the detailed treatment of related transonic flows are discussed later in this report, Sections VII and VIII.

V. SAMPLE COMPUTATION

A sample computation to check the program logic has been made with the intercepting shock-triple point-reflected shock structure. This case is for a highly underexpanded (pressure ratio of 50.1: 1) Mach 3.18 H_2O jet in a uniform Mach 3.25 air stream. In this first computation, viscosity was taken to be zero and the species were frozen. The computed flow is shown in Figure 11.

To perform this sample computation took about 30 minutes on the IBM 360-65-7094 emulator. The basic program logic and coding has been completed, but there remains the task of putting the computer program on a large enough computer so that the finite rate option can be run while including the intercepting shock-triple point structure.

The computed flow field is shown in Figure 11. It would be of interest to compare this result with a real gas inviscid characteristics calculation.

VI. THE MACH DISC

In the previous discussion the Mach disc was treated rather globally in the sense that its location and geometry is determined semiempirically. This section attempts to place the Mach disc problem on a more rational basis.

In the past decade, at least two hypotheses and two theories have been proposed to locate the triple point-Mach disc, none of which is entirely satisfactory from the standpoint of being completely nonempirical or of yielding consistently good results. Here, a self-contained theory is proposed and developed which accounts for the basic fluid mechanical interaction that determines when and where a Mach disc forms in an underexpanded exhaust plume. Quantitative results are presented to illustrate the interaction and to verify the theory.

The flow field is first qualitatively divided into two subregions; 1) a quasi-one-dimensional streamtube consisting of the flow near the centerline, and 2) the rest of the flow. A discussion of how the interaction between these two parts of the flow field determines when and where the Mach disc forms follows.

The expansion waves from the exhaust plane reflect as compression waves which coalesce to form the intercepting shock. The shock, immersed in the expansion, gathers strength from additional compression waves and, if the flow is axisymmetric, from the focusing effect. Downstream, where the expansion loses strength, the integrated effect of the compression waves can result in the need for a very strong adverse axial pressure gradient. The supersonic core flow, which is supercritical, is unable to generate the required adverse axial pressure gradient by interacting with the supersonic outer flow. Instead, the supercritical streamtube reacts to the required downstream pressure increase by jumping to a subcritical (subsonic) state via a strong shock, the Mach disc.

Downstream of the Mach disc, the subsonic core flow acts as the physical agent whereby information of the interaction between the inner and outer flows is transmitted upstream to the Mach disc and fixes its location. In the theory, the Mach disc location is quantitatively determined by the requirement

that the subsonic core flow must pass smoothly through a throat-like region, thereby becoming supersonic. Thus, the entire plume flow field solution depends on one parameter, the triple-point location, which is determined by this throat-like condition.

This theory is compared with experiment and with other theories for a Mach 1.5 exhaust plume in a static ambient ($p_{exhaust}/p = 4$). The eigenvalue character of the solution (the triple point location being considered the eigenvalue) is strikingly demonstrated by the numerical results when various solutions, each for a specified triple point location, are compared.

A brief discussion of the relationship between this and other theories concludes the discussion. In particular, it is noted when the basic interaction mechanism is implicitly (if partially) reflected in other theories.

A. The Problem

The basic features of the inviscid plume flow field of an underexpanded nozzle are shown in Figures 12a and 12b for static and supersonic ambient respectively. The expansion waves from the nozzle lip reflect from the dividing constant pressure (or separating) streamline as compression waves, subsequently coalescing to form the intercepting (barrel) shock. Depending on the flow conditions, the intercepting shock may reflect regularly at the centerline or it may terminate in a triple point-Mach disc configuration, illustrated in Figure 12. Behind the Mach disc is a region of subsonic flow bounded above by a slip stream emanating from the triple point.

A complete theory which can predict the existence or non-existence of the Mach disc has not been available, nor has there existed a satisfactory theory for determining the triple point location when the Mach disc is present, though four theories (most are empirical correlations) have been proposed to this end.

Adamson and Nicholls[10] (A&N), by correlations, hypothesized that on the axis the static pressure behind the Mach disc equals the ambient static pressure. In one sense,

this can be thought of as an asymptotic theory since $p_{\mathcal{C}_L} \to p_\infty$ as $x_{\mathcal{C}_L} \to \infty$. However, it seems to be quite good a theory for predicting, in many instances, the first of a sequence of Mach discs. Eastman and Radtke [11] (E&R) proposed a completely empirical method for locating the triple point. They observed that when they plotted the axial pressure distribution behind the intercepting shock, the point where the pressure has a minimum correlates fairly well, in many cases, with the triple point abscissa. Although their study was for a static ambient they expected it to also apply to cases having uniform supersonic free stream. Bowyer, D'Attore and Yoshihara [12] (BDY) hypothesized that the Mach disc was locally normal to the incident flow at the triple point. They then located the triple point by looking for a point on the intercepting shock where the flow is consistent with this assumption. In a recent paper, Abdelhamid and Dosanj [13] (A&D) present a theory based on the global conservation considerations for sections perpendicular to the jet centerline. The first three are all criteria for locating the Mach disc; they are not theories for determining when, as well as where the Mach disc forms. By implication, one would think that the non-existence of a point at which any of these criteria is satisfied could be interpreted as meaning that the Mach disc does not exist in that case. However, this view does carry some problems, the most important being that in axisymmetric flow one never gets regular reflection at the centerline.

Of these theories, that of Adamson and Nicholls has the most surface appeal because it has a direct connection between the triple point-Mach disc and the downstream flow. We certainly expect an interaction between the triple point solution and the subsonic flow downstream of the Mach disc, and, in fact, the solution of our problem should basically reflect on a large rather than local scale, the dynamic equilibrium of the flow in this region. However, the condition that immediately behind the Mach disc the pressure should equal the ambient is an asymptotic type of condition (in spite of the fact that it is not proposed or used asymptotically) and does not a priori seem to be characteristic of the more "regional" sort of balance which one would have in a consistent theory.

This is a report of a theory which explains in detail how and when a Mach disc is formed from the plume intercepting shock and when the intercepting shock will reflect obliquely from the centerline. A theory and procedure for determining the location of the triple point when the Mach disc is present is developed. Then, quantitative results obtained lend support to the theory. In the final section, a few comments on the four aforementioned theories add perspective to the problem.

B. Outline of the Theory

1. Why Does the Mach Disc Form - Probably the biggest stumbling block in find the criterion for locating the triple point has been the lack of understanding of why the triple point Mach disc configuration forms. The answer does not appear to be particularly complicated. In fact, the empirical correlation of Eastman and Radtke reflects very strongly the physical mechanism involved. In what follows we will be considering two-dimensional symmetric or three-dimensional axisymmetric flows.

Let us direct our attention to the fluid in the exit plane of an underexpanded exhaust nozzle immersed in a static ambient (Figure 12a). The first thing felt by the exhaust gas is the expansion emanating from the nozzle lip. These expansion waves accelerate the fluid and turn it away from the centerline. At any axial station, near the axis, the amount of turning increases in the direction normal to the axis. The expansion waves reflect off the constant pressure streamline as compression waves which are propagated along right running characteristics. The compression waves often are strong enough to coalesce, forming the intercepting (barrel) shock. Because of the strong favorable pressure gradient in front of the shock, the pressure behind the shock decreases axially, even though the strength of the shock is probably increasing. The favorable axial pressure gradient, resulting from the expansion at the nozzle lip, gradually diminishes in strength downstream. The strength of the barrel shock, in turn, increases axially due to additional compression waves from the constant pressure surface and, when the flow is axisymmetric, to the focusing effect. These two effects can cause the axial pressure gradient behind the shock to change from favorable to adverse. When the compression waves are strong enough (moderate to large underexpansion ratios) the strong adverse pressure gradient can become concentrated over very short distances. For low to moderate underexpansion, the flow is grossly one-dimensional. One can even think of it as being, near the centerline, grossly constant area flow. A grossly inviscid, supersonic, constant area flow will realize such a strong positive pressure change by means of a strong shock,[14] the Mach disc. That is, the Mach disc forms when the essentially quasi-

one-dimensional flow near the axis of the plume must realize a strong adverse pressure increase over a very short distance.

To put it another way, split the flow into two parts, a quasi-one-dimensional streamtube along the centerline and the rest of the flow. In the favorable axial pressure gradient the cross-sectional area of the centerline streamtube will increase, the amount of increase being determined by the interaction of the streamtube with the outer flow. Since it is supersonic, the streamtube is supercritical, and $d\delta/dp < 0$, where δ corresponds to the width (radius) of the streamtube; and there is no problem associated with the interaction so long as $dp/dx < 0$. However, as Crocco [15] points out, the supercritical centerline flow, interacting with the supersonic outerflow is not able to generate an adverse axial pressure gradient. Instead, the supercritical streamtube will react to the required downstream pressure increase by jumping to a subcritical (subsonic) state. This is accomplished, in our problem, by means of a strong shock, the Mach disc.

2. When Does the Mach Disc Form - Now it is clear why we sometimes do not get a Mach disc structure. If (in two-dimensional flow) the intercepting shock is formed by a relatively concentrated compression so that it approaches the centerline while still in the strong part of the expansion, there may be no change in the sign of dp/dx behind the shock and no need for the centerline flow to change from supercritical to subcritical, hence, no Mach disc. In particular, the predominance of Mach disc structures (on a significant scale) in axisymmetric flow is due to the axisymmetric focusing effect which tends to increase the compression so much that, even though the shock may be in a strong part of the expansion fan, the compression locally dominates and leads to a change in the sign of the pressure gradient.

Thus, quantitatively, the "when" is put by the theory as follows. If the flow without the Mach disc requires a very large adverse axial pressure gradient, then the Mach disc will form. How can one determine what "large" means here? If a solution is possible without a Mach disc, it will not form. That is, if regular reflection with completely supersonic flow is possible at the point where the intercepting shock intersects the axis, there will be no Mach disc. If regular reflection is not possible, we understand that such a large pressure increase is required that it must be achieved with a stronger (than weak-oblique) shock, the Mach disc. In axisymmetric flow, focusing has the effect of concentrating the compressions so that a very

large adverse pressure gradient is always induced prior to the point where the intercepting shock intersects the axis*.

3. Where Does the Mach Disc Form - The last part of the theory is an explanation of the mechanism by which the triple point-Mach disc location is set. This condition reflects quantitatively the interaction between the subsonic core and supersonic outer flow downstream of the Mach disc. The condition is that the triple point location is determined by the requirement that the centerline flow, which is subsonic just downstream "throat-like" region where the flow becomes supersonic. That is, singularities are not accepted in this region. In the quasi-one-dimensional approximation, which is the only case considered here, the streamtube cross-sectional area will have a minimum there.

In order to clearly see this interaction and how it determines the triple point location, it is helpful to strip the flow to its very barest skeleton. The heart of the resulting model, as of the actual phenomenon, is the quasi-one-dimensionality of the flow near the axis. This means that, even though the flow just behind the Mach disc is subsonic, the steady problem is still properly formulated as an initial value problem**with the triple point location as a parameter. So, starting at the exhaust plane if the triple point were given, the entire flow field can be determined, at least conceptually. The solution procedure can be outlined by referring to Figure 12. The entire flow up to the triple point is obviously determined once the exhaust and ambient conditions have been specified. With the triple point location specified, the solution of the shock configuration there can be determined by a straight forward computation. The initial slope of the contact discontinuity would be one result of the triple point computation. The flow downstream of the triple point can then be determined by

1) computing the supersonic region (by the method of characteristics, say);

2) computing the subsonic flow using a steady quasi-one-dimensional model;

3) matching 1) and 2) along the contact discontinuity, thus locally determining the axial pressure gradient.

---

*However, this phenomenon may be localized enough so that on a micro scale regular reflection is (apparently) acceptable.

**This is not to say that there are not regions of severe numerical difficulties of boundary value type, as we shall see.

As one proceeds downstream with this calculation, the core flow streamtube will tend to become subsonic.*

By assuming a triple point location, the triple point-Mach disc solution can be obtained and used as initial conditions for a solution of the interaction problem downstream. In general, the resulting initial value problem will not possess a consistent smooth solution. The pressure gradient generated will tend to either $\pm \infty$, with $M_{\mathcal{L}} \rightarrow \begin{matrix} 0 \\ 1 \end{matrix}$, simultaneously with $(dy/dx)_{edge} \rightarrow \pm \infty$**. Only for one value of the triple point location will $(dp/dx)_{\mathcal{L}}$ remain finite while $M_{\mathcal{L}} \rightarrow 1$ as $dy/dx \rightarrow 0$ in a throat-like region. That is, the throat-like region is a saddle point type singularity depending on the triple point location as a parameter.

Now suppose that the location of the triple point is not specified and one wants to determine it. How can we settle on the correct solution?

---

* If $M_{\mathcal{L}}$ remains subsonic as $x \rightarrow \infty$, we must conclude that a completely inviscid theory is inadequate. In addition, there is no doubt that when the centerline streamtube flow goes sonic at some station, x_s, it will be numerically difficult, if not impossible, to match along the slip line in the immediate vicinity of x_s. But this is a numerical problem and does not mean that the model (i.e., quasi-one-dimensional core streamtube, inviscid flow) is inadequate. For instance, a similar problem arises when one attempts to determine the streamtube pressure distribution by integrating the quasi-one-dimensional equation through a sonic throat with the area specified.

** Actually, one will probably not see in a numerical solution of the first case, $dp/dx \rightarrow \infty$ since the admissable solutions have a very small increase in pressure (streamtube is subsonic). However, the behavior of $(dy/dx)_{slip\ line}$ confirms the tendency for dp/dx to become unbounded.

The triple point location can be considered to be a parameter of the inviscid solution for the plume flow field. The value of the parameter is then determined by the requirement that the subsonic centerline flow downstream of the Mach disc pass smoothly through the throat-like region.

4. Synopsis of the Theory - At this point a synopsis of the theory is helpful to identify the essential ingredients and clarify their respective roles.

Why Does the Mach Disc Form?

1) Expansion of the central region of the exhaust plume.

2) Compression waves form intercepting shock.

3) Splitting of plume into core and outer regions.

4) Compression overcomes expansion leading to large adverse pressure gradient which causes supersonic core to go subcritical via Mach disc.

When Does the Mach Disc Form?

5) When solution with regular reflection does not exist; that is, when the compression is strong enough to create very large adverse axial pressure gradient.

Where Does the Mach Disc Form?

6) Triple point location determined by requirement that the flow is the subsonic core just downstream of Mach disc pass smoothly through a singular throat-like region, thereby becoming supersonic.

C. Verification of the Theory and Comparison With Other Theories

In this section the third part of the theory (how the triple point is located when there is a Mach disc) is verified by a computational example which illustrates quite well the singular behavior of the solution in the throat region and the eigenvalue character of the theory. A series of computations have been made, each having a different value for $x_{T.P.}$ the triple point abscissa. An analysis of the behavior of the streamtube

solution downstream of $x_{T.P.}$ as a function of $x_{T.P.}$ comprises the quantitative support of the theory. The example chosen has been determined primarily by the requirements of available computer programs and the desire to compare with experiment. The conditions for this example are:

- perfect gas, inviscid, constant specific heat ratio, $\gamma = 1.4$;
- static ambient;
- parallel flow at jet exhaust plane, Mach = 1.5;
- underexpansion ratio $p_j/p_\infty = 4.0$;
- axisymmetric.

This case, one of those reported by Love, et al.,[16] has a Mach disc diameter comparable to the nozzle exit diameter, so the interaction should be strong enough and on a large enough scale so that we can feel confident that numerics will not cloud the issue, though they can moderately effect the quantitative results. In the following computation, it appears that numerics has affected the results quantitatively to no more than a few percent and qualitatively not at all.

One note of caution is in order here. The quantitative results of these computations depend on things like mesh size, interpolation schemes, computer program organization, etc. For orientation purposes only, the computational procedure is outlined here. Additional details are given in Appendix A. A given computation requires the specification of

- initial data (i.e., conditions at exhaust plane: pressure, flow direction, etc.),
- γ_j, the exhaust specific heat ratio,
- p_∞, the ambient pressure,
- $x_{T.P.}/r_j$, the triple point abscissa dividend by the exhaust radius,
- computer program controls (e.g., mesh size).

The supersonic portions of the flow field are computed by the method of characteristics. The intercepting shock is detected when two right running characteristics coalesce, the determination of its shape and strength being subsequently part of the flow field computation. When the abscissa of the intercepting shock reaches the value specified for the triple point, a triple point solution is generated. Then the computation continues, including the solution of the subsonic quasi-one-dimensional flow downstream of the Mach disc. The centerline pressure gradient and the shape of the slip line downstream of the triple point are determined by the interaction between the subsonic inner flow and the supersonic outer flow (see Appendix A).

If the specified triple point abscissa is appreciably less than the solution, the pressure behind the Mach disc there will be too high and the contact discontinuity will make too great an angle with the axis to be consistent with the downstream throat condition. With a relatively large $(\theta)_{S.S.}$ we will have (for a smooth solution) the area of the streamtube increasing appreciably. The result is that the downstream pressure will increase, tending to stagnate the flow in the streamtube, in this case an unacceptable solution. Similarly, the pressure will be too low and $\theta_{S.S.}$ too small (algebraically) if the specified triple point abscissae is too large. Then, with $\theta_{S.S.}$ significantly negative, a strong favorable downstream pressure gradient will be generated, accelerating the streamtube to sonic velocities as $\theta_{S.S.} \rightarrow -\infty$. Actually, the situation is not so simple since near the correct triple point abscissae neither case will quickly prevail, and the "branch" we are on will not become evident until the pressure gradient actually begins to increase or decrease catastrophically (in the first case this is evident by the catastrophic increase in $\theta_{S.S.}$). Consider the results.

The axial variation in core streamtube Mach number (Figure 13) clearly shows the two branches depending on whether the assumed value for $x_{T.P.}$ is greater than or less than the solution. In particular, notice the "peaking" of the stagnation branch as the parameter $x_{T.P.}$ approaches the solution.

One of the most revealing figures is a plot of $(dy/dx)_{S.S.}$ vs M_{ℓ} (Figure 14). The saddle point behavior is quite evident, particularly in the tendency of $d\theta(M)/dM$ to become discontinuous at $\theta=0$ as $M=1$ is approached on the stagnating branch. Notice the convergent-divergent character of that branch when the figure is rotated 90° clockwise. It is clear from these two figures that, within the accuracy of these computations, this theory

brackets $x_{T.P.}/r_j$ between 4.79788 and 4.8*. This is good agreement with the experimental result of Love, et al which placed the Mach disc on the axis of $x/r_j = 4.9$.

A wealth of information is contained in Figure 15, which conveys the important pressure histories, namely

a) the ambient pressure,

b) the centerline pressure in the absence of a Mach disc,

c) the pressure immediately behind a normal shock on the axis (important in the theory of Adamson and Nicholls),

d) the pressure behind the intercepting shock in the absence of a triple point Mach disc (important in the theory of Eastman and Radtke),

e) the pressure immediately behind the downstream of the triple point for each of the values of $x_{T.P.}/r_j$ actually computed,

f) the predictions of A & N, E & R, BDY and the present theory.

Again, the two branches can be seen, though less clearly since the behavior of p(x) on the "stagnating branch" is not at all spectacular, as in the "accelerating branch".

One of the most striking observations to be made is the fact that the pressure immediately behind the strong shock at the triple point is, within quite a good tolerance, equal to the pressure behind the normal shock on the axis. This correspondence is even closer, in this case, if one considers the Mach disc to be slightly curved toward the exhaust plane as one proceeds away from the axis. This points to the possibility that the pressure behind the Mach disc is essentially constant, and this matter should be investigated further (see also Ref. 12).

The predictions of the theories of Adamson and Nicholls and of Eastman and Radtke can be easily extracted from Figure 15. A plot of the angle between the incident flow and the strong shock branch of the triple point solution vs. the assumed value of $x_{T.P.}/r_j$ (Figure 16) yields the predictions for $x_{T.P.}/r_j$

* One could, of course, continue indefinitely to narrow down this range, being only limited by storage and accuracy of the computer, financial resources, and patience.

according to Bowyer, D'Attorre and Yoshihara. Note the appearance of the curve in Figure 16, the well defined slope of (θ Mach disc-θ flow) vs $x_{T.P.}/r_j$.

In this theory, the solution can be pinpointed by considering how close we came to passing through the "throat" for each assumed value of the triple point location. On the stagnating branch, the quantity $(1-(M_{\text{℄}})_{max}$ measures closeness well, while on the accelerating branch, the value of the slip-stream slope, $(dy/dx)_{S.S.}$ where M = 1, is appropriate. These two curves strikingly point to the value of $x_{T.P.}$ (Figure 17).

The predictions of four of the theories are compared with each other and with experiment in Figure 18. Because of uncertainties in reading data and estimated inaccuracies in the computations, a band is included on each side of the predicted values in order to try and compensate for quantitative uncertainties which the theories should not be required to suffer. Neglecting possible inaccuracies in the computation, the maximum difference between two theories is about 20%, which is not so terrible considering that three of the theories are essentially semiempirical. The theory for $x_{T.P.}$ of this report agrees, in this case, to within almost 1% of the experimental value of $(x_{\text{Mach disc}})_{\text{℄}}$.

Finally, the computed flow field structure for $x_{T.P.}/r_j$ 4.79788 and 4.7 again show the two branches of the eigenvalue problem (Figure 19) with $x_{T.P.}/r_j$ = 4.79788 being almost right on the solution.

D. Discussion of Other Theories

Since this is the fifth in a series of theories* for solving the triple point-Mach disc problem, a discussion and comparison between some of these theories is certainly in order.

The rule of Eastman and Radtke ties in the triple point location with what would be the adverse downstream axial pressure gradient if there were no triple point. In this respect it reflects the physical interaction actually occurring and which is qualitatively and quantitatively included in the present theory.

*Though I consider the theories of Eastman and Radtke and of Bowyer, D'Attoree, and Yoshihara to be empirical "rules of thumb" (or hypotheses) (which could be elevated to the theory status) since they were proposed without reasons or explanations of why they work or why they should be expected to work.

Eastman and Radtke do not have the possibility of saying when the triple point does or does not exist, except that one must assume that the absence of a pressure minimum prior to the intersection of the intercepting shock with the centerline would imply regular reflection there. However, one must expect to encounter the situation in which the centerline flow and intercepting shock do not then admit to regular reflection, in which case the rule of E & R would fail completely. A & D state that in two dimensional flow E & R will always fail because there is no pressure minimum. This statement seems to depend on the exhaust flow being uniform and parallel, and it appears that it is not generally true. For example, non-uniform exhaust flow could easily lead to an adverse axial pressure gradient downstream.

With the help of Figure 15 we can understand why the apparently asymptotic conditions ($p_{\mathcal{C}} \to p_\infty$ as $x_{\mathcal{C}} \to \infty$) of A & N works on a non-asymptotic interaction. Note that, for the case computed, the curve showing the pressure behind a normal shock on the centerline has a significant negative slope and that, near the triple point-Mach disc abscissa, the pressures behind the normal shock are near $p_{\mathcal{C}} \to p_\infty$. In Figure 19, note that for $x_{T.P.}/r_j = 4.8$ the leading right characteristic from the expansion where the reflected shock intersects the constant pressure boundary intersects the slip stream (from the triple point) at about $x/r_j = 7.2$. Since the flow is subsonic behind the Mach disc ($M \sim 0.35$), there is no possibility of having a significant increase in p without having reversed flow there (we rule this out from experimental results). So, with the large negative gradient of $(p_{\mathcal{C}})_{N.S.}$*, it is easy to get a downstream limit of $x_{T.P.}$, since we expect to have $p_{\mathcal{C}} \to p_\infty$ within reasonably short distances. In the same way, for $x_{T.P.}$ too short, $(p_{\mathcal{C}})_{N.S.}$ is appreciably higher than p_∞, in a region where there is a continual feeding of compression waves from the reflected expansion waves. This would result in centerline pressures appreciably greater than p_∞, something which is unreasonable in the current configuration since the compressions result from reflected expansions from a boundary with $p = p_\infty$. Thus, A & N's semi-empirical theory gives relatively good results because, locally, behind the Mach disc the pressure cannot differ by large amounts with its asymptotic value and the large negative slope of $(p_{\mathcal{C}})_{N.S.}$ delimits a small interval within which the Mach disc must be found.

The motivation for A & D's theory seems to be the maximum mass-flow-rate criterion of quasi-one-dimensional stream-tube theory, that for a fixed stagnation condition there is a minimum

---

* N.S. means normal shock

cross-sectional area where the mass flow rate is a maximum and the velocity is sonic. This fact seems to have been carried over to the plume problem. In order to fit it into the present discussion, it is necessary to outline the theory.

Consider a uniform underexpanded sonic jet exhausting into a quiescent environment. Since the flow is sonic and uniform there, the exhaust mass-flow rate is the maximum allowable for the implied stagnation conditions. The free boundary streamline has a barrel shape, Figure 20, which, if there were no shocks, one might at first sight extend as in Figure 21. Treating the flow as quasi-one-dimensional, the minimum allowable area with supersonic flow could occur at x_1, where $A_1=A_{EP}=A^*$, since the flow is sonic at the exhaust plane. They then theorized that an intercepting-shock-Mach disc was necessary earlier than x_1 in order to allow the reflected shock to strikethe free boundary, turning it away from its disastrous journey toward the centerline.

The Mach disc location is then supposedly determined from global conservation considerations. One assumes an abscissa for the Mach disc and computes the flow upstream of the Mach disc-reflected shock (area to the left of ABC, Figure 22). At this point there is a merging of theory and computational procedure. Apparently, the axial mass flow component across BC is assigned to the cross-sectional area CD and the axial component across AB to the area DE; then the sum of the two is the mass flow across CE. A sequence of such computations is made for different Mach disc locations, and not surprisingly, different sums are obtained for the mass-flow across the various sections. Call these sums W_i, where i corresponds to the i^{th} assumed value, x_i, of the Mach disc abscissa. Finally, a point of $W(x_i)/W^*$ is made, where W^* is the mass-flow for the sonic exhaust, which appears as in Figure 23, and the Mach disc location corresponds to $W(x_i)/W^* = 1.0$.

The important point here is that there is a mixing of theory and computational procedure to arrive at the condition in Figure 23. Actually, if the above approximations were not made in obtaining the mass-flow across CE, (i.e., if the solution procedure had no approximations), a different curve for $W(x_i)/W^*$ would have been obtained, and it would have looked like Figure 24. In fact, such a curve could easily be constructed from the present results. In this figure, there would be a maximum $x_i = x_{i_{max}}$. such that for $x_i > x_{i_{max}}$ the "accelerating branch" will lead to sonic core flow (without the throat condition being satisfied) prior to reaching the abscissa where the reflected

shock intersects the free boundary. This will correspond to a Mach disc location considerably downstream of the actual solution. It should be emphasized that in the present computations, for $x_{T.P.}$ as large as 6.4, there were no problems associated with the free boundary coming too close to the axis.

So, why does the theory of A & D work? It is evidently attributable to the fact that; 1) approximations are made in estimating the mass-flow across the area CE, and, 2) the manner in which these approximations are made can be correlated with the Mach disc location.

Of the other four theories, only that of E & R reflects directly, though crudely, the physical interaction which actually determines the triple point configuration. However, this statement must be slightly qualified with the note that although the BDY seems to work reasonably well, it embodies more empiricism and minimum of mechanism.

E. Concluding Remarks

The triple point location is determined by an upstream-downstream interaction, transmitted through the subsonic core downstream of the Mach disc. The present theory incorporates this interaction with an approximation which leads to an eigenvalue problem ($x_{T.P.}$ is the eigenvalue).

VII. EVALUATION OF METHODS TO COMPUTE THE TRANSONIC INVISCID FLOW IN AN UNDEREXPANDED PLUME

The analytical and numerical solution of steady, inviscid, mixed (i.e., subsonic-transonic-supersonic) flows has been one of the most difficult problem areas in theoretical fluid mechanics. The Euler equations for steady flow change from elliptic to hyperbolic when the Mach number increases from less than to greater than the sonic velocity. Thus, the subsonic region is characterized by boundary-value problem formulations (cf. Laplace's equation) while initial-value problem formulations (cf. wave equation) typify supersonic flows. The type of data to be specified for a well set problem differs in the two cases (cf. Dirichlet or Newmann conditions for Laplace's equation, Cauchy conditions for the wave equation). Prior to obtaining the solution to mixed flow problems, the boundary separating the boundary-value and initial-value regions is not known so that there is a fundamental problem, which has not yet been solved, in setting up the proper initial value-boundary value formulation to solve a well set mixed flow problem.

Fortunately, these difficulties have not deterred scientists and engineers from gathering their courage and plunging into this theoretical (and experimental) morass. Basic studies of approximate mathematical models of the complete equations have increased our understanding while sometimes providing analytical tools for the solution of model problems. Numerical techniques for solving the complete equations have been developed, though they usually are characterized by significant analytical and/or numerical difficulties.

The purpose of this study is to select a numerical method for the solution of the two-dimensional mixed flow downstream of the Mach disc in an underexpanded exhaust plume. Three approaches will be considered: integral relations,[17,18,19,20] relaxation [17,20], and time dependent[17,23]. The selection will be made on the basis of a weighted qualitative evaluation of the relative merits of each approach with respect to certain important critiera.

A. Considerations

The considerations on which the selection is to be made fall into four groupings: convenience, accuracy, analytical and numerical difficulties, and adaptability to the basic problem,

the solution of the mixed flow downstream of the Mach disc in an underexpanded plume. In this section, the meaning and importance of this grouping and the basis for the evaluation are given.

1. Convenience – A numerical technique is convenient if: (1) the analysis is not too complex, (2) it is easily translated into a computer program, when necessary, and (3) the computer program: a) is reliable and easy to use, b) does not require unacceptable computing times, and c) does not have unacceptably large high speed access storage requirements.

A few remarks about each of these points are in order. Items 1) and 2) are important because, though the resulting computer program may be acceptable with respect to item 3), too complex an analysis of excessive difficulty translating it into a computer code may mean that the initial analysis and computer code development cost is too great to justify their pursuit. One part of this consideration is well known to anyone familiar with computer programs; the errorless translation of complex analysis into a computer program can require considerable effort and expense.

A computer code is easy to use if a user (other than the developer) can use it to obtain information he thinks it should supply without becoming frustrated before receiving the answers. Of course, a good user's manual, consistent input, etc., all contribute to this quality, but these aspects are not part of our considerations. Rather, sometimes analyses lead to computer codes which are basically difficult to use. For instance, if the numerical solution is sensitive to small changes or inconsistencies in the input data, the tool can soon become a source of frustration rather than answers. Another item in this vein is that the computer code must be reliable.

The acceptability of computational times is difficult to concretize, for it depends on the problem, the computer, and the user. But, for our purposes it is easy to establish one measure of acceptability, because our problem is part of a larger one. Therefore, any solution is certainly acceptable if its computing time requirements are about the same as, or less than those of the solution for the rest of the plume. That is not to say, of course, that it cannot be more, for sometimes it is acceptable to have the solution of one part

of a problem contributing substantially more than its "fair share" to computing costs.

Finally, the computer code must not require unacceptably large high speed access storage program. This requirement is rapidly diminishing in importance as larger, faster computers are being introduced.

2. Accuracy - Each of the approaches is potentially exact in the sense that sufficient monetary and computer resources will permit one to obtain a solution within any given tolerance. But our machines and, pocket books are limited, and the important question here is, "can I get the required accuracy within current computer capabilities and, if so, at what expense?".

3. Analytical and Numerical Difficulties - As pointed out in the first section, there are fundamental formulation and solution problems associated with transonic flows. The question is, how do they affect and how are they reflected in the three approaches? For example, numerical and analytical problems along a singular line are characteristic of the solution of transonic flows by the method of integral relations. Their effect, if any, on computer code development, accuracy, reliability, flexibility, etc., is an important factor in this evaluation.

4. Adaptability to the Problem is the most important consideration. We are looking for an accurate numerical solution of the transonic region in an underexpanded plume, and this solution must fit in as a part, a sub-program, of a solution for the entire plume flow field. Considerations which may restrict or prevent an approach from taking its position as one part of the whole are of highest importance. Flexibility is also very important; if one approach is considerably more flexible in this respect, it must be considered to have a distinct advantage over the others.

These, then, are the most important considerations in this evaluation. They are not of equal weight, but complete failure with respect to any of them would eliminate a contending approach from the competition.

B. Discussion of the Qualities of the Three Approaches with Respect to the Four Criteria and the Evaluation

Rather than order this discussion with respect to the four criteria, it is preferable to discuss, in turn, the important merits and demerits of each approach. While making

somewhat more difficult the comparison with respect to any one of the criteria, this will provide a much better overall view of the fitness of each of the approaches. Also, it permits the elimination somewhat quickly of those considerations which are not as important as others.

For instance, computing time is not a particularly important item in the comparison because, grossly, each of the approaches results in typical computing times on the order of a few minutes or less on an IBM 360/75 or a UNIVAC 1108 computer (inviscid, perfect gas). These times are not as short as one could like, but they also are not unacceptably long, particularly when we consider increased speed of computers like the CDC-6600 and machines we may expect in the next few years. These times can vary appreciably depending on the accuracy desired. The important point is that none of the approaches appears to have a significant advantage in computing speed.

As far as storage requirements, the method of integral relations should have a distinct advantage, for one usually can retain good accuracy with very few strips (at least when the flow is in chemical equilibrium, this is not true for the non-equilibrium case, and there the method of integral relations has a distinct shortcoming). However, as previously mentioned, this is not one of the more important considerations since we seem to have reached the point where several machines (systems, if you prefer) having almost unlimited (for practical purposes) storage are now or soon will be available.

Accuracy is also not a consideration which can quickly eliminate any of the three approaches, for they all can provide sufficiently accurate results. However, two important considerations do arise here. It seems that it is a fairly complicated process (algebraically) to set up a relaxation scheme which is second order accurate in the mesh size, so that relaxation procedures will probably usually involve first order schemes. This is not true for unsteady methods, which can be thought of as relaxation procedures, where a number of relatively simple second order accurate differencing schemes are available. Experience has shown that usually the increased number of operations per step in a second order scheme is more than offset by the greater accuracy, so that for a given required accuracy the second order scheme is more economical than a first order scheme with a finer mesh (requires less computing time and computer storage). Thus, we can expect

a second order accurate unsteady method to usually be more economical than a first order accurate relaxation scheme. Also, both the relaxation and unsteady methods provide a very convenient mechanism for increasing accuracy, just decrease the mesh size. Though it may be possible to set up a generalized method of integral relations for an arbitrary number of strips, it is probably a fairly complicated process, certainly in comparison with the easy mesh size control for the other two approaches. So we can expect more inconvenience varying accuracy with the method of integral relations.

In order to facilitate the discussion of the rest of the considerations for the three approaches, a slight modeling of the problem is helpful. In Figure 25, the solution up to and including the triple point - Mach disc is assumed known, and the solution of the flow downstream thereof is sought. There must be a matching along the slip stream between the subsonic-transonic inner flow and the supersonic outer flow. In order to discuss the relative merits of the three approaches, first consider the matching to be done sequentially, so that the solution will be obtained by iterating between the inner and outer regions. At any step in the iteration, the boundary, including the slip stream shape, of the transonic region is fixed and known. Then we must solve for the flow in the shaded region of Figure 25.

Referring to Figure 26, initial data along the line AB would be supplied from the solution of the flow upstream of and up to the triple point-Mach disc. Of course, some assumptions about the Mach disc shape would be required (once the triple point location has been specified) in order to obtain the state of the flow on AB. As already noted, the slip stream shape, BC, is specified. As modeled, the solution of the region ABCD is just the same as that for a finite length convergent-divergent axisymmetric deLaval nozzle and experience gained on the nozzle problem can be used in the current evaluation. So, temporarily the discussion is directed toward the solution of the flow in a two-dimensional or axisymmetrical convergent-divergent nozzle. A discussion of the merits and shortcomings of the three approaches with respect to this problem will help to place some later comments in perspective.

Relaxation techniques have been around a long time and used to be one of the most commonly used tools of the analyst needing numerical results for complicated physical problems. Depending

on the relaxation procedure, the analyses and their translation to computer programs usually can be accomplished without insurmountable trouble, but sometimes at the expense of very inefficient relaxation procedures. The basic difficulty is that efficient relaxation procedures require judgement during the relaxation process, and simple algorithms are usually not efficient. For this problem one can expect to be able to make decent computer programs without particularly trying analytical or numerical difficulties. The boundary conditions on the walls and exit plane can, however, be a source of trouble, or at least of inaccuracies, since they basically involve the specification of combinations of derivatives or a derivative and the value of the function, the parts of which must be determined during the course of the computation (the flow need not be irrotational).

The main shortcomings of relaxation techniques are:

- second order accurate relaxation schemes can be quite complicated and impractical on a digital computer,
- first order accurate schemes will probably require quite small mesh sizes leading to long computing times for acceptable accuracy,
- the boundary conditions on the nozzle wall (slip stream) can be a source of numerical trouble and inaccuracies.

In the past fifteen years the Method of Integral relations has been one of the most actively developed techniques for the numerical solution of complicated fluid mechanical problems. It has been established as a very powerful tool in a wide variety of problems (e.g., boundary layer, blunt body, subsonic and transonic nozzle flows, pointed cone at angle of attack, etc.).

Depending on the problem and the accuracy desired, the resulting analysis can be simple or complicated (algebraically, that is). Though it may be possible to construct a general computational algorithm for an arbitrary number of strips it appears that existing analyses and computer programs are invariably restricted to one approximation (i.e., the number of strips is fixed). When such a procedure is followed, one does not have

much flexibility in improving the accuracy if the available computer code is not accurate enough. However, this is not in itself an overpowering shortcoming, for the method of integral relation has been shown to yield quite accurate results with very few strips at least for inviscid chemically inert flows, (Ref. 18).

A more serious shortcoming of the method has to do with the singular behavior of the resulting ordinary differential equations (Ref. 17, 19, 21, 22) in the transonic region. This behavior, which often does not receive the attention it deserves, reflects the fact the method of integral relations essentially replaces an elliptic partial differential equations with a two point boundary value problem for a system of ordinary differential equations, the latter to be solved iteratively as an initial value problem by the "shooting" method. The result is that procedural problems accompanying the solution of mixed flow problems by the Method of Integral Relations are basic to the formulation and, hence, are likely to remain as sources of problems in the development of a computer code.

In addition, looking ahead to the inclusion of finite rate chemical effects, the method of integral relations would require a very large number of strips in order to provide needed accuracy when the mass fraction profiles are non-monotonic.

In the past few years the use of the unsteady time dependent approach, for the solution of steady mixed flow problems has become quite popular. The basic motivation is simple and can be readily schematized:

- the mixed flows considered have large subsonic regions where the steady Euler equations are elliptic,
- elliptic partial differential equations are characteristic of boundary value problems,
- boundary value problems are difficult to solve,
- mixed (elliptic-hyperbolic) problems are even more difficult to solve,
- initial value problems are as a class; easier to solve,
- initial value formulations characterize unsteady flows, whether the flow be subsonic, transonic, or supersonic,

- if we consider the steady flow solution to be the time-asymptotic limit of an unsteady flow, the steady mixed-flow problem can be obtained by solving an initial value problem (and that is comparatively easy),
- the time asymptotic solution is reached relatively quickly in many cases.

There are two particularly appealing aspects of the unsteady approach; 1) it always leads to initial value problems, whether the steady problem is of boundary value or initial value type, and 2) there is a connection between the steady solution sought and an implied transient. Usually, it is possible to identify the transient with an actual physical process, the approach is even more appealing.

The experience with this approach on the blunt body problem has been quite impressive [23,24] and would lead one to believe that it would also be well suited to the nozzle problem. However, it seems that some investigators working on this problem have encountered unexpected and, at first sight anyway, inexplicable numerical difficulties [25,26]. These numerical problems usually appeared in the latter stages of a computation as the solution should have been tending toward a steady state. Apparently the solution usually "blew up" with much the same characteristics associated with numerical instability. This is particularly upsetting because the time dependent approach should be well suited to this problem. In particular, the technique for computing wall points as given by Moretti and Abbett [23] should yield quite accurate solutions at and near the wall (i.e., at the slip stream).

This background discussion on the merits and demerits of the three approaches does not point conclusively to any of them as being markedly superior, at least with respect to the flow in a two-dimensional deLaval nozzle. However, we have not as yet given due attention to the adaptability of the methods to the problem of the flow downstream of the Mach disc when the triple point location has been specified. The solution of this problem will involve an iteration between the inner subsonic-transonic and the outer supersonic flows, and the shape of the slip stream is one of the unknowns. It is easy to see that if the iteration

is performed as a sequence of steady problems, the solution will be a formidable problem indeed. However, the unsteady approach provides a very handy, natural mechanism with which to achieve this solution, namely, iterating in time as illustrated in the following figures and discussion.

First, a solution for the supersonic flow is obtained neglecting the triple point-Mach disc-reflected shock structure (Figure 27a). (The purpose of continuing the solution of the intercepting shock beyond the specified triple point abscissa will be evident momentarily.) Then a triple point solution is generated at the specified $x_{T.P.}$, i.e., the shape of the Mach disc is assumed, the flow immediately behind the Mach disc is obtained, a first guess at the slip stream shape is made, and the corresponding reflected shock is computed (Figure 27b). Also indicated in Figure 27b, is (by cross hatching) the region of overlapping supersonic flow computed by continuing the intercepting shock downstream of $x_{T.P.}$. (In Figure 27b, $\overline{CD}$ is a right running "limiting characteristic" of the subsonic region.) Now, the "iteration" via the unsteady approach can be achieved by computing the entire region $\overline{ABCDEA}$ as a time dependent flow, the solution to the steady problem being obtained when the unsteady flow becomes steady. In the actual solution procedure, the slip stream $\overline{BD}$, would divide the flow into two separate computational regions, $\overline{ABDEA}$ and $\overline{BCDB}$. Both the reflected shock, $\overline{BC}$, and the slip stream, BD, would move during the unsteady phase of the computation; thus the iteration is really replaced by a relaxation in time of the entire region $\overline{ABCDEA}$.

The power of this approach over the others is evident; the time dependency provides a natural mechanism for relaxing to the final, steady solution. Neither of the other two approaches provides such a conceptually convenient means of obtaining the slip stream shape.

The above discussion is based upon a priori knowledge of the triple point location. This could be specified using the empirical criteria discussed in Section VI. However, as described in Section VI, the Mach disc and downstream transonic flow are coupled and a theory was presented which has the potential of eliminating the empiricism. The unsteady, "relaxation" technique discussed above could be employed in this theory.

Thus, the triple point location, $x_{T.P.}$ and the Mach disc shape could be determined simultaneously by allowing the triple point-strong shock also to move during the unsteady process. However, since the added computational effort and problems can be expected to be significant, we will concentrate on the original problem with $x_{T.P.}$ and the Mach disc shape specified and on the model problem, the two-dimensional deLaval nozzle. The theory of Section VI will be reserved for future development steps.

There is an additional numerical problem area which did not become evident until late in this study. The expansion emanating from the intersection of the reflected shock with the constant pressure boundary (point C in Figure 27) "covers" part of the transonic region in at least some cases and probably in all (Section VI), and thus must be included in the computational region no matter which approach is used. This is, of course, only a source of numerical aggravation, but it must be considered no matter how the solution procedure is set up.

Now that the attributes of the three approaches have been discussed, a summing up, an evaluation can be made. In fact, the conclusions is rather obvious. In most areas none of the three approaches has an overpowering advantage, except that the time dependent approach is far ahead as far as flexibility and adaptability to the problem so it appears to be the best choice.

As already mentioned, previous investigators have encountered inexplicable numerical difficulties in attempting to compute the flow in a two-dimensional deLaval nozzle by using the unsteady approach with the Lax-Wendroff differencing procedure. Since both the approach and that differencing procedure have been shown to be admirably applicable to transonic flows, it is unlikely, that these difficulties are insurmountable. Therefore, since this approach appears to be the most promising in the long run, a study of this problem is in order to determine whether or not there are basic, insurmountable problems associated with time dependent solutions of two-dimensional transonic deLaval nozzle flows.

VIII. SOLUTION OF THE STEADY FLOW IN A TWO-DIMENSIONAL DELAVAL NOZZLE AS THE ASYMPTOTIC LIMIT OF AN UNSTEADY FLOW

A. Introduction

The steady subsonic-supersonic inviscid flow in a two-dimensional converging-diverging deLaval nozzle exhibits all the basic idiosyncracies of mixed flows. The subsonic flow, where the Euler equations are elliptic, is correctly set as a boundary value problem, but without the solution one does not know the shape of or boundary conditions on part of the boundary (the sonic line, say). On the other hand, the hyperbolic nature of the Euler equations in the supersonic region leads to initial value formulations downstream of the limiting characteristic line. (The data on any initial line in the supersonic region depends, of course, on the solution of the upstream flow.) The extreme mathematical difficulties connected with such mixed flow problems have hindered their solution, particularly solutions of direct problems when the entrance flow and the nozzle geometry are specified. In this report a numerical procedure for obtaining the solution for the steady flow in a deLaval nozzle as the time limit of an unsteady flow is developed.

The typical steady problem is considered in which the state of the entering flow (0A, Figure 28 and the wall geometry (AB) Figure 28, are prescribed, and the solution is to obtained in the interior (0ABC), Figure 28. At least three reports [25,27,28] have appeared in which this problem has been attacked by time dependent techniques. In each of these cases, the authors appear to have encountered rather severe problems with the finite nozzle. Migdal, Klein, and Moretti [29], side tracked the problems of a subsonic entrance plane boundary condition by considering the problem with an infinite upstream reservoir. The technique developed in this report permits the specification of the steady entering flow boundary conditions at a subsonic boundary during the unsteady process.

The procedure, which is developed in Sections B and C, is slightly unorthodox and includes a discontinuity surface at the nozzle entrance, suggested by G. DaForno at GASL. Since mass crosses the entrance surface and since the flow on either side is subsonic, the discontinuity is not an ordinary one. The analyses

and a discussion of some preliminary results for a quasi-one-dimensional and a two-dimensional nozzle are presented in Section D. In this discussion the gas is considered to be inviscid and thermally and calorically perfect with constant specific heat ratio, γ.

B. Formulation of the Initial Value Boundary Value Problem

Before getting down to the specifics of the problem formulation, some brief comments of a general nature are in order.

The objective of this study is to obtain the solution of a steady inviscid flow as the asymptotic (in time) limit of an unsteady flow. Since the time dependent approach has been shown to be a very powerful method for obtaining numerical solutions to blunt body flows, it is an obvious candidate for the two-dimensional nozzle problem. However, this problem differs from that one in that an upstream boundary is given in the subsonic regime where the entering flow is specified as a boundary condition to the steady problem.*

In developing a procedure to obtain the solution to a steady flow problem as the limit of an unsteady flow, it is important that

1) there is a steady solution to the problem, and

2) the problem formulation includes a vehicle through which the (correct) steady solution can be reached.

This vehicle is usually, if not always, the boundary conditions of the unsteady problem. Very roughly, steady boundary conditions will bring the unsteady flow to a steady state. However, the treatment in the unsteady problem of the "steady" boundary conditions is often not straightforward.

*Contrast this with the blunt body problem where the free stream velocity is supersonic.

The solution sought in this study is the steady flow in a two-dimensional deLaval nozzle (see Figure 28) having subsonic entrance and supersonic exit velocities. The boundary conditions for the steady problem* conditions are:

the nozzle geometry (i.e., $y(x)$ for $\overline{OA}$, $\overline{AB}$ and $\overline{BC}$),

the state of the flow crossing $\overline{OA}$ (say total pressure, total enthalpy, velocity, and flow direction, (p_t, H, q, θ) as functions of y along $\overline{OA}$)

velocity component normal to the wall vanishes at the wall.

Since the flow is assumed supersonic at the exit, $\overline{BC}$, no additional condition can be prescribed there.

In obtaining the steady solution as the time limit of an unsteady one, the following initial value - boundary value problem (Figure 29) is to be solved. At time $t = 0$, initial data is prescribed in the entire section $\overline{OABC}$.

Boundary conditions on the $x = 0$ plane,** the rectangle $\overline{OADE}$ ($\overline{DE} \to \infty$ as $t \to \infty$), will be prescribed as the boundary conditions appropriate along $\overline{OA}$ for the steady problem. This is part of the vehicle insuring that the (correct) steady solution will result from the time dependent computation. On the exit plane $\overline{BCFG}$ the flow is assumed to always be supersonic enough so that disturbances on that plane do not have an appreciable numerical influence on the upstream flow in the nozzle.

The data to be prescribed on the two planes, $t = 0$, $x = 0$, are:

u,v	the two velocity components,
p_t	the total pressure, and
H	the total enthalpy,

* For convenience, only nozzles symmetric about the x axis are sketched and discussed.

** As a matter of convenience only, the entrance surface will often be referred to and considered as a planar surface.

or some other suitable combination of these quantities. Then for a perfect polytropic gas,

$h = h(p,\rho)$ is the static enthalpy,

$H = h + \frac{u^2 + v^2}{2}$ is the total enthalpy

$a^2 = a^2(h)$ is the sound speed,

and

$\frac{p}{p_t} = f(a^2, q^2)$ is the ratio of static to total pressure,

where

$q^2 = u^2 + v^2$ is the square of the velocity modulus.

The initial plane, $t = 0$, is a space-like surface, and we have prescribed the proper information for a well set Cauchy problem with respect to time. On the other hand, the $x = 0$ plane is a time-like surface along which we have prescribed more data than is permitted as boundary data to continue the Cauchy problem with a well set Goursat problem*. This should not be a cause of worry, however, for there is no reason to expect this problem to be well formulated as a Cauchy initial value-boundary value problem. The specification of Goursat data on $x = 0$ would guarantee that the solution is continuous there, at least in the small. In particular, it would guarantee that the characteristic compatibility equations would be satisfied consistent with the prescribed data on the plane $x = 0$. However, it would not permit the imposition of all the boundary conditions of the steady problem there, but they are necessary to insure that the unsteady solution approach the (correct) steady solution. This is accomplished by permitting the unsteady solution to be discontinuous at the entrance surface. This discontinuity is the second part of the vehicle which will guarantee that unsteady flow approaches the steady solution. When there is a continuous steady solution, the strength of the entrancy discontinuity must become vanishingly small as $t \to \infty$ and the steady solution is approached.

* Actually a Cauchy problem followed by a sequence of Goursat problems.

C. The Nature of the Entrance Plane Discontinuity

In the preceding section the need for a discontinuity surface at the entrance plane was indicated by examining the mathematical nature of the initial value-boundary value problem. From physical arguments the essential attributes of this surface can be induced. In order to strip away unnecessary complications, consider a quasi-one-dimensional deLaval nozzle. The pressure, density, and velocity (p, ρ, u) are to be specified, (constant) in time, at the entrance to the nozzle. Since the flow just behind the entrance plane is subsonic, disturbances from downstream are propagated upstream and eventually reach the entrance plane where they will interact with the incoming flow. Because of this effect, some form of work/energy is required to maintain the specified conditions at the entrance plane. Although it is more natural to consider this to be mechanical work, in fact it is perfectly legitimate to conceive of the required energy to be in the form of heat and/or mechanical work.

This report concentrates on the mechanical problem. Some device which is an artifice, must perform work in order to maintain the flow conditions prescribed at the entrance. This device can be thought of as a black box of negligible thickness. Though it evidentally has a definite task, the details of how it accomplishes this task can remain a mystery, though some of those properties it must have in order that it accomplish its task in a satisfactory manner can be deduced.

First, it must maintain a steady mass flow rate. This is necessary to insure that a steady state will be reached. Quantitatively this is $\rho_2 u_2 = \rho_1 u_1$ where subscripts 1 & 2 refer to the flow immediately upstream and downstream of the discontinuity, respectively, Figures 30 and 31. Thus, p_1, ρ_1, u_1, are the specified steady state values . In doing this it will operate in one of two modes, constant pressure or constant velocity, depending on the downstream flow. If at one instant there is a high pressure just downstream of the entrance to the nozzle, the box will have to compress the gas to pressures consistent with the downstream ones.

On the other hand, if there is a low pressure downstream, there would seem to be no problem in maintaining $p_2 = p_1$ at the exit of the box. Second, it must do work on the gas, as required, to maintain the specified mass flow rate against the

resistance of the flow downstream of the entrance plane. Conceptually, energy (in the form of work or heat) could be extracted from the gas. However, this possibility must be ruled out on the ground that it admits unacceptable solutions. In particular, one solution would be to extract all the available energy from the gas, resulting in a steady but unmeaningful solution. The requirement that work must be done on the gas means that the entropy of the gas should always be increased (or, at best, unaffected) by the box.

In the pressure mode, the constant mass flow rate can be achieved by maintaining at the box's exit, the velocity equal to the incoming values. In being forced through at this velocity, the gas will be compressed to static pressures higher than p_1. With $u_2 = u_1$, continuity of mass flow rate gives $\rho_2 = \rho_1$. Then $p_2 > p_1 \rightarrow T_2 > T_1$ and (for a perfect gas, constant specific heat ratio) $s_2 > s_1$, i.e., the specific entropy of the gas is increased, as required.

On the other hand, if the downstream flow offers no resistance, the flow can be forced through at constant pressure. Then, in maintaining $p_2 = p_1$, the box will accelerate the incoming flow to a velocity $u_2 \geq u_1$; hence $\rho_2 \leq \rho_1$, $T_2 \geq T_1$ and $s_2 \geq s_1$, again.

The above arguments purposely do not delve into the actual processes going on within this black box. Rather, the exit conditions are fixed so that they are consistent with the flow immediately downstream and with the principal that work is only done on the gas. As stated, this latter condition results in having $s_2 > s_1$.

D. Solution of the Problem

1. Quasi-One-Dimensional DeLaval Nozzle - In order to verify the feasibility of the basic concept, it is not necessary to obtain the solution to a two-dimensional deLaval nozzle; the quasi-one-dimensional case will suffice.

In what follows, much of the computational technique developed for the solution of the blunt body problem is employed, Ref's 23 & 24. In determining the unsteady solution we will divide the nozzle into three regions: the entrance plane, the interior, and the exit plane (Figure 32). At $x = 0$, the entrance plane, we have the discontinuity surface which represents the now familiar black box. The interior region will be covered by a finite difference grid having equal mesh spacing.

The computational procedure in this interior is very straightforward. Assuming the entire flow to be given at some time t_o, we want to compute the entire flow at $t_1 = t_o + \Delta t$. The interior (in x) points at $t_o + \Delta t$ are obtained by expanding the dependent variables in a 2nd order Taylor series about their respective mesh points, at t_o. This is essentially the Lax-Wendroff [30] scheme in non-conservation form*. In particular,

$$u(x,t_o + \Delta t) = u(x,t_o) + u_t(x,t_o)\Delta t + u_{tt}(x,t_o)\frac{\Delta t^2}{2} \qquad (35)$$

with similar expressions for the other dependent variables. The first derivative terms, like u_t, are obtained directly from the differential equations for unsteady quasi-one-dimensional flow. The second derivative terms are obtained by differentiating the differential equations with respect to time. The resulting mixed derivatives, like u_{xt}, are evaluated by differentiating the original equations with respect to x, the space variable, thus expressing the mixed time-space derivatives in terms of space derivatives only.

The convergence and stability characteristics of the scheme[30] applied to gas dynamic problems are not investigated in this study, for there is quite a large literature on this subject. Suffice it to say that we can be confident that the scheme is convergent and conditionally stable, the maximum stable step size being given by

$$\Delta t \leq \alpha \min \left(\frac{\Delta x}{u+a} \right) \qquad (36)$$

where α is of the order 1 and the minimum is the minimum over all the mesh points at each time step.

To obtain the actual expressions for u_t, u_{tt}, p_t, etc., we have the basic differential equations for quasi-one-dimensional unsteady flow (in standard notation).

---

* Any number of other finite difference schemes (e.g., Lax, Rusanov, etc.) could have been chosen.

$$\rho_t + \rho u_x + u\rho_x + \frac{\rho u}{A}\frac{dA}{dx} = 0$$

$$u_t + uu_x + \frac{p_x}{\rho} = 0 \qquad (37)$$

$$s_t + us_x = 0$$

where ρ is the density, p the pressure, u the velocity, s the entropy, A the cross sectional area (A = A(x) is specified), and the subscripts x and t denote the partial derivative with respect to that independent variable. Writing $R = \ell n\rho/\rho_o$, $P = \ell np/p_o$, with ρ_o and p_o some reference conditions, then $\frac{S-S_o}{C_v} = P-\gamma R$ and the equations become

$$R_t = -\left[uR_x + u_x + \frac{u}{A}\frac{dA}{dx}\right]$$

$$u_t = -\left[uu_x + \frac{p}{\rho}P_x\right] \qquad (38)$$

$$S_t = -uS_x$$

$$P_t = S_t + \gamma R_t$$

Then

$$R_{tt} = -\left[u_t R_x + uR_{xt} + u_{xt} + \frac{u_t}{A}\frac{dA}{dx}\right] \qquad (39)$$

$$R_{xt} = R_{tx} = -\left[u_x R_x + uR_{xx} + u_{xx} + \frac{u_x}{A}\frac{dA}{dx} + \frac{u}{A}\frac{d^2A}{dx^2} - \frac{u}{A^2}\left(\frac{dA}{dx}\right)^2\right]$$

etc.

At the entrance plane we have the discontinuity with

$$\rho_2 u_2 = \rho_1 u_1 \quad \text{(steady mass flow rate)}$$

and either

$$u_2 = u_1 \qquad p_2 = p_1$$

$$\text{or} \tag{40}$$

$$p_2 = p_2(u_2) \qquad u_2 = u_2(p_2)$$

where $p_2(u_2)$ (and $u_2(p_2)$) quantitatively embodies the requirement that the flow on the downstream side of the entrance plane must be consistent with the flow in the rest of the nozzle. The functional form of $p_2(u_2)$ is obtained by writing the characteristic compatability equation (corresponding to Eq. (38))

$$\frac{du}{dt} - \frac{a}{\gamma}\frac{dP}{dt} = -\frac{au}{A}\frac{dA}{dx} \tag{41}$$

along the characteristic direction defined by

$$\frac{dx}{dt} = u-a \tag{42}$$

Here d/dt is the total derivative of the dependent variable and a is the local sound speed, $a = \sqrt{\gamma p/\rho}$. Computationally, Eq. (41) is written in finite difference form between the entrance plane at $t = t_1 = t_o + \Delta t$ and an interior point at $t = t_o$, the location of the interior point being the intersection with the line $t = t_o$ of the characteristic passing through the entrance plane at t_1, and having slope dx/dt = u-a (Figure 33). The difference form of Eq. (41) is

$$u_2-u^* = +\frac{a}{\gamma}(P_2-P^*) - \frac{au}{A}\frac{dA}{dx}\Delta t$$

where the coefficients are averaged along the characteristic.

Once the solution has been determined at the entrance point and at the interior points, at time $t=t_o+\Delta t$, the values at the exit point are obtained by extrapolation from the interior points. Though this is not formally correct, it has been shown to be an acceptable numerical short cut so long as the flow there is supersonic enough so that the upstream feeding is numerically negligible, References 23 and 24.

A good evaluation of the procedure can be obtained by comparing computed results with an exact steady solution (cf., NACA Report 1135[31], 1953). To this end, consider a long quasi-one-dimensional deLaval nozzle. The first test case considered* corresponds to the steady flow of a $\gamma = 1.4$ gas accelerating continuously from Mach 0.5 to Mach 1.8. The specified area variation with the exact steady state values for Mach number and pressure ratio are shown in Figures 34a through 34c. As initial conditions for the unsteady flow we put the steady solution with the exception that at $x/\sqrt{A^*} = 4$ ($A/A^* = 1.88$, corresponding to $M = 0.6$ in the steady solution) we put a pressure equal to twice the steady value. Thus, a compression will propagate upstream and downstream due to this initial pressure jump. When the compression wave traveling upstream strikes the entrance plane it will be reflected. If the entrance were a solid boundary, the compression wave would reflect as a compression. In the present case the entrance plane is somewhere between a solid and free boundary. Because we can expect less energy to be associated with free boundaries, the primary component of the reflected wave will probably be an expansion.

One of the most interesting items to study is the pressure distribution in the nozzle at various times (Figure 35). p_o, ρ_o are the isentropic stagnation pressure and density of the exact steady solution. The path and dispersion of the primary compression wave down the nozzle are easily followed. Less distinct and more dispersed is the primary reflected wave, which is an expansion, though there is really no difficulty in following it. The pressure history on the downstream side of the discontinuity is shown in Figure 36. Note that within steps corresponding to a non-dimensional time of 20, the solution is essentially stablized within less than 0.1% of the steady state value. The history of $W/H_{entrance} = H_2 - H_1/H_1$, the instantaneous work level (Figure 37) exhibits the expected behavior; that is, it is always positive. It is evident that W can be determined, in this case, to an accuracy of not quite 0.1%** The entropy jump history is shown in Figure 38.

---

* A test of the mesh size effect was made in another case, the results being, as expected, that decreasing the number of mesh points decreases the accuracy. For example, decreasing the number of mesh points by a factor of two decreased the accuracy of the computed "steady state" (at the same time) by a factor of three.

** The area is specified to 0.01% and the derivatives of the area are obtained by finite difference.

One of the most interesting features of this procedure is that it admits steady solutions to entrance conditions for which there is no continuous steady solution. The discontinuous behavior at the entrance plane permits this. For instance, if the prescribed entrance Mach number is larger than that consistent with sonic flow at the throat (in continuous steady flow), the black box can reach a steady state in which the gas is continuously being compressed (and decelerated) at the entrance. Similarly, the box can accelerate a "too slow" flow so that the sonic velocity is reached at the throat. We refer to these two cases as "over-choked" and "under-choked" respectively. An example of each of these cases has been computed for the same nozzle area distribution already discussed. The work and entropy jump (Figure 39) histories show the expected rapid initial increase followed by a gradual leveling off to the steady value. As expected, the final steady state has a Mach number behind the discontinuity equal to the value consistent with a steady, choked flow for the specified contraction ratio (Figure 40), but the steady state pressure level differs in each case (Figure 41).

2. Two-Dimensional Nozzle - There are several important differences between the flow in quasi-one-dimensional and two-dimensional deLaval nozzles. Though conceptually basically the same, in detail the entrance plane discontinuity is somewhat more complicated in two dimensions.

A general outline of the computational procedure for obtaining the solution to the two-dimensional unsteady flow is discussed prior to giving the details. Assuming the entire flow to be known on some constant time plane $t = t_o$, we want to be able to step ahead to obtain the solution to another time plane $t_1 = t_o + \Delta t$. In (x,y,t) space the nozzle is covered by a finite difference mesh which, for a constant value of t_1 appears as shown in Figure 42. As in the quasi-one-dimensional case, the solution at interior mesh points at $t_1 = t_o + \Delta t$ can be obtained using a number of explicit or implicit differencing procedures; we will again use the non-conservation form of the Lax-Wendroff method. The upper wall points can be computed by the method of characteristics as developed by Moretti and Abbett[32]. At the entrance surface the

specified local steady mass flow rate is maintained which, when coupled with a characteristic compatibility equation from the interior flow, yields a solution for the flow on the downstream side of the discontinuity. When all these points have been computed at t_1, data for the exit plane points again can be obtained by extrapolation from the interior flow, so long as the flow remains more than slightly supersonic at the exit plane.

For flexibility, it is desirable to develop the computer program which the capability of curved entrance surface; that is, the entrance surfaces could be somewhat curved in x,y space. This, combined with the curvature of the upper wall, leads to problems in constructing in the physical (x,y,t) space, a finite difference grid for the numerical solution of the problem. A well tried remedy is to map the nozzle onto a rectangle so that one can set up a relatively convenient numerical procedure. Then the three-dimensional computational domain is a rectangular parallelepiped upon which it is easy to construct a computational grid. Of course, the equations of motion differ in the transformed space.

Let (x,y,t) denote a cartesian coordinate system in physical space, with velocity components (u,v) and with the x axis positive in the general flow direction (the nozzle need not be symmetric). The wall geometry is denoted by $y = s(x)$ on the upper wall and by $y = b(x)$ on the lower wall. The nozzle entrance and exit surfaces are denoted by $x = f(y)$ and $x = g(y)$ respectively. The computational space is denoted by (X,Y,T), and the transformation is shown in Figure 43. Then the Euler equations become

$$R_T = - \left[BR_Y + ER_X + \frac{v_Y}{\delta} + \frac{D}{\delta_1} v_X + \frac{c}{\delta} u_y + \frac{u_X}{\delta_1}\right.$$

$$u_T = - \left[Bu_Y + Eu_X + \frac{p}{\rho\delta} \left(CP_Y + \frac{\delta}{\delta_1} P_X\right)\right]$$

$$v_T = - \left[Bv_Y + Ev_X + \frac{p}{\rho\delta} \left(P_Y + \frac{\delta}{\delta_1} DP_X\right)\right]$$

$$S_T = - \left[BS_Y + ES_X\right]$$

with

$$C = b_x(Y-1) - YS_x$$

$$D = f_y(X-1) - Xg_y$$

$$B = \frac{(v+cu)}{\delta}$$

$$E = \frac{(u+vD)}{\delta_1}$$

Again, these equations are differentiated with respect to X,Y, and T to get the second time derivatives of R, u, v and S, to be used in Equations like (35).

The wall boundary points are computed by the method given in Moretti and Abbett [32] and outlined here. A local cartesian coordinate system (ξ,η,t) in physical space with velocity components (U,V) is set up normal to the wall at each mesh point (see Figure 44).

In the (η,t) plane the Euler equations are written in a characteristic form relating V and P. The equation is

$$\frac{a}{\gamma}\frac{dP}{dt} - \frac{dV}{dt} = -\left[\frac{a}{\gamma} UP_\xi + aU_\xi - UV_\xi\right]$$

where

$$\frac{d}{dt} = \frac{\partial}{\partial t} + \frac{\partial}{\partial \eta}\frac{d\eta}{dt}$$

along the direction

$$\frac{d\eta}{dt} = V - a.$$

Since $V \equiv 0$ at the wall, this can be written in difference form to give P at $t_1 = t_o + \Delta t$ in terms of the flow at time $t = t_o$. Thus

$$P(t_o+\Delta t) = P^*(t_o) + \left(\frac{\gamma}{a}\right)V^*(t_o) - \overline{\left[UP_\xi + \gamma U_\xi - \frac{\gamma}{a} UV_\xi\right]}\,\Delta t$$

where the asterisk denotes values at time t_o on the characteristic line of slope $d\eta/dt = V - a$ (see Figure 44) and the bar denotes average values along that line. The velocity component and the entropy are determined by first order explicit finite difference equations for the second momentum and the entropy equations. These are, since $V = 0$ on the wall,

$$U_t + UU_\xi = - p_\xi/\rho \rightarrow U(t_o+\Delta t) = U(t_o) - [UU_\xi + p_\xi/\rho]\ \Delta t$$

$$S_t + US_\xi = 0 \rightarrow S(t_o+\Delta t) = S(t_o) + \bar{U}S_\xi\ \Delta t$$

It is true that this difference scheme is unconditionally unstable at interior mesh points, but experience has shown that it is adequate at the boundary points, the stabilization probably being due to a combination of the one-sided finite differences and the use of the characteristic equation for the relation between the pressure and the velocity component normal to the wall.

The entrance surface discontinuity requires specialized treatment, somewhat more elaborate than in the quasi-one-dimensional case. The two operational modes, having jumps respectively in pressure and velocity, still characterize the box, though it may operate in different modes simultaneously at each point of the entrance plane. For example, at a given time there may be a pressure jump near the centerline and a velocity jump near the nozzle wall. Again, this is necessary in order to insure that, locally, work is being done on the gas, resulting in entropy increases as the gas traverses the box. Thus, even if the conditions prescribed on the upstream side are uniform, two-dimensional effects propagating upstream will usually result in lateral pressure gradients at the downstream side of the box. Of course, nonuniform upstream conditions can have the same effect. So, during the unsteady process, the lateral pressure gradients will induce velocity components which are locally normal to the inflow velocity vector. Since either the pressure or normal velocity component are specified at the box's exit (which one being determined by the requirement $\Delta S \geq 0$), it is natural to seek two equations relating the pressure and both velocity components at time $t_o + \Delta t$ to the nozzle flow at time t_o. The characteristic equations along two bi-characteristics provide such a relation.

Consider a cartesian coordinate system (ξ,η,t) (Figure 45) whose origin is at a mesh point on the downstream side of the discontinuity. The ξ axis is oriented locally normal to the discontinuity (Figure 45), and the velocity components in the (ξ, η) directions are (U,V) respectively. The bi-characteristics through (0,0,0) are given parametrically by

$$\frac{d\xi}{dt} = U + a \cos \alpha \quad ; \quad \frac{d\eta}{dt} = V + a \sin \alpha$$

where a is the local sound speed and α is a parameter. For given α, the compatibility equation along the corresponding bi-characteristic is

$$\frac{Dp}{Dt} + \rho a \cos \alpha \frac{DU}{Dt} + \rho a \sin \alpha \frac{DV}{Dt} =$$

$$- \rho a^2 [U_\xi \sin^2 \alpha - (U_\eta + V_\xi) \sin \alpha + \cos \alpha + V_\eta \cos^2 \alpha]$$

where D/Dt means differentiation in the bi-characteristic direction. The bi-characteristic in the plane normal to the discontinuity (on the downstream side) corresponds to $\alpha = \pi$, so the bi-characteristics corresponding to $\alpha = 3\pi/4$ and $5\pi/4$ should provide a good combination of lateral and streamwise momentum transport. This combination was used in the computation discussed below. The remaining equations are the local continuity of mass flow rate across the discontinuity, $\rho_2 U_2 = \rho_1 U_1$, the perfect gas equation of state, and one of the two conditions

$$p_2 = p_1 \qquad \text{or} \qquad U_2 = U_1$$

depending upon which results in $\Delta S \geq 0$.

A side comment on numerics is in order at this point. The use of the characteristic equations requires a number of interpolations on the basic computational mesh. This can be a cause of numerical trouble when adjacent mesh points at the discontinuity are operating in different modes, ($p_2=p_1$, or $U_2=U_1$). Therefore, it is necessary to set up a procedure for switching from one mode to the other between mesh points. One procedure, which seems to have worked adequately in preliminary calculations,

is to use the bi-characteristic corresponding to $\alpha = \pi$ in place of the one above which would ordinarily be in the interval where the operational mode changes. If the operational mode changes in both intervals immediately adjacent to a mesh point, then only the $\alpha = \pi$ bi-characteristic is taken and V = 0 is set at that point.

As in the quasi-one-dimensional problem, values at the exit plane are, at a given time, determined by extrapolation from interior points.

The results so far achieved in the two-dimensional case are preliminary and incomplete. However, they are complete enough so that the soundness of the procedure is verified. This is not to say, of course, that there is not a significant amount of work left to be done in working out the details of the computational technique to arrive at a good computational tool for the entrance discontinuity surface.

The geometry of the nozzle considered, which is symmetric about the x axis (Figure 46), consisted of

a straight segment of constant area followed by ($dy/dx = -.261$)

a straight segment of constant slope, where the area contracts, followed by

a circular arc, and ending in

a straight segment making a 45^{o} angle to the centerline.

The constant area region has a cross-sectional area equal to 1.59 times the minimum area. The specified entrance flow was uniform with a Mach number of 0.4. Pressures are all divided by the stagnation pressure of the entrance flow. Entropies shown are the difference between the local entropy and the

entrance flow entropy all divided by the specific heat at constant volume. There were five mesh intervals between the centerline and the wall and fourteen mesh intervals between the entrance plane and the exit plane.

The time variation of pressure and velocity exiting the box at the centerline and at the wall are shown in Figure 47. It appears that the steady limit of the solution being computed has a jump of about 5% and a velocity jump of about 10% at the wall. These numbers are probably so high because of numerical problems arising from one or more of the following:

- too rough a mesh, (particularly important with the sharp corner on the upper wall),
- the computational procedure at the discontinuity is not entirely satisfactory,
- special numerical problems at the wall-discontinuity juncture.

It was not possible to carry this study further under current funding, so these problems must be left unresolved for the moment. However, it is probable that all three items contributed to the steady state jumps.

The entropy jump histories at the wall and centerline (Figure 48) also show that the strength of the discontinuity does not tend to zero as a steady state is approached (since the entropy jump is a difference in logs, numbers on the order of 0.01 or less would numerically indicate zero strength at the jump).

The steady state distribution of pressure (Figure 49) and Mach number (Figure 50) along the wall and the centerline, indicate that probably too rough a mesh was used. This is not unexpected, however, since the mesh used was only 10 x 5. Considering the fact that the computational procedure at the discontinuity is in an early stage of development and that no effort was made to average coefficients, there or in the wall characteristic computation, these results can be considered quite good. However, additional studies should be made to improve the computational technique and to resolve the above mentioned problems.

E. Conclusion

A unique procedure is presented for obtaining the solution of a steady flow in a deLaval nozzle. Application of the procedure to a quasi-one-dimensional case has yielded results which lend credence to the technique. In two dimensions these preliminary results substantiate the basic procedure but indicate that additional work is necessary to improve the numerics, particularly at the discontinuity.

The previous discussions focused on the fluid mechanical structure of plume flow fields. These problems are further complicated, however, by chemical and multiphase phenomenon which must be considered if realistic predictions are to be made of the thermal and electromagnetic effects relevant to the problems of environmental heating, contamination and communication.

The purpose of the following discussion is to describe some of chemical and phase transition processes which are characteristic of present and future plume flow fields.

IX. CHEMICAL KINETICS IN PLUME FLOWS

A wide variety of propellent and propellent combinations exist and are used according to the mission application. Of particular interest here are engines burning hydrogen or RP1 (Kerosene)/LOX. However, the chemical systems and kinetic mechanisms associated with these propellents are relevant to virtually all propellents whether they are solid, hybrid, slurry or pure liquid since these generally contain substantial amounts of hydrocarbons. Thus, in addition to the usefulness of providing the details of specific hydrogen and RP1 systems the results are applicable to the formulation of general propellent combustion behavior.

Previous studies of these systems and, in particular, of the RP1/LOX system have led to a conputerized formulation of the reaction mechanism with hydrogen as a subsystem, References 33 and 34. For the present purpose; which is the inclusion of the hydrocarbon kinetics into the MOCV programs, a summary of the results of the work of References 33 and 34 will be sufficient.

The kinetic mechanism for the combustion of hydrocarbons is very complex involving in general, over 30 active species entering into over 200 elementary reversible reactions. A study of a typical hydrocarbon system, Reference 35, has shown, however, that a much smaller reaction mechanism could be postulated while retaining the necessary detail for an accurate description of the combustion process. This mechanism involves 31 species entering into 69 elementary reversible reactions. Using the high speed solution technique developed at GASL, References 6 and 33, make it feasible to make pure kinetics calculations in time periods measured in minutes. This represents up to two orders of magnitude reduction in computational time compared with standard integration techniques such as Runge-Kutta. However, even with this improvement the inclusion of the "full" 69 reaction mechanism into the MOCV flow field program would result in calculation times measured in hours. Although in the analysis of certain problems it is desirable to examine the detail offered by the "full" system many applications of interest do not require such detailed species fields. To this end a study was made on the feasibility of developing a "quasi-global" representation for the "full"

sixty-nine reaction mechanism, Reference 33. The "quasi-global" mechanism provides a bridge between the high molecular weight fuel and the more stable equilibrium products of combustion. Of course, many intermediate species are not included in this representation, but the macroscopic properties including ignition delay, reaction time, equilibrium products of combustion, density, temperature, etc., are given with a remarkable degree of accuracy.

The chemical system considered includes the following species:

(1)	H_2	(7)	CO	
(2)	O_2	(8)	CO_2	
(3)	H_2O	(9)	C_nH_m	(43)
(4)	H	(10)	$C_{(s)}$	
(5)	O	(11)	N_2	
(6)	H			

Where C_nH_m is the high molecular weight hydrocarbon fuel and $C_{(s)}$ represents carbon present as a dispersion of solid particles. Also, N_2 is considered to be an inert diluent. The elementary reactions involving the first eight active species are those given in Table I and the species entering into these reactions are the essential stable products of combustion. To bridge the gap between these species and the high molecular weight reactant, an intermediate global type oxidation equation is required.

In the present "quasi-global" treatment the required overall equation must represent an intermediate, or bridging reaction. Several reactions have been considered, Reference 33, and the results of a comparative study indicates that a good representation is provided by the partial oxidation equation:

$$C_nH_{2n+2} + \frac{n}{2} O_2 \rightarrow nCO + (n+1) H_2 \qquad (44)$$

To complete the describing equations for the chemical system a global rate equation for the consumption of fuel is required. In Reference 37, it is shown that for paraffin hydrocarbons from ethane (C_2H_6) up to kerosene, the combustion times are of the same order of magnitude. Thus, available data for butane, propane and ethane were considered relevant for the kerosene oxidation process.

The rate expression is assumed to be of the following, Arrehnius type, form:

$$-\frac{dC_F}{dt} = A\ C_F^{\alpha}\ C_{O_2}^{\beta}\ e^{-\frac{13,740}{RT}} \qquad (45)$$

where the effective activation energy was fixed at the value appropriate to the propane oxidation process. The results of the study gave the following rate equation (Ref. 33):

$$-\frac{dC_F}{dt} = AC_F^{\frac{1}{2}}\ C_{O_2}^{1}\ e^{-\frac{13,740}{RT}}$$

where

$$A = 1.0 \times 10^{13}\ \left(\frac{1}{P}\right)^{.825}\ \left[.9\ \frac{T_i}{1000} - .5\right] \qquad (46)$$

The oxidation equation, Equation (44), and the associated unidirectional rate equation, Equation (46) together with the elementary reversible reactions given in Table I constitute the "quasi-global" mechanism for the homogeneous gas phase combustion process.

Because of a combination of non-uniform O/F ratio and of film cooling of the skirt using fuel rich auxilliary turbine exhaust there will be regions of the plume flow containing soot particles. The effect of these particles upon the plume flow field structure and, in particular, thermal radiation heating motivate an attempt to quantify the soot oxidation process.

The finite-rate oxidation process for soot particles already present in hydrocarbon flames also is not well understood. However, Lee, Thring, and Beer (Ref. 38) have performed a set of experiments which make it possible to form a global reaction for the combustion of the carbon particles. This global rate equation should not be though of as a firmly established analysis, but rather as a useful first estimate which will probably be modified and extended by future experimental and analytical work.

The basic experimental apparatus was a laminar diffusion flame inside a quartz tube. The fuel was predominantly propane, with some propylene and ethylene, and was burned with oxygen-enriched, preheated air. Solid and gas samples were taken starting at the axial position at which soot particles were formed in the flow field. The gas samples were analyzed by a chromotographic

method, and by an Orsat apparatus. An electron microscope was used in determining the size of the soot particles. A series of runs was made for different overall stoichiometric ratios. Temperatures of from 1200°K to almost 1700°K occurred in the sampling region. The authors were able to correlate the experimental results for the soot combustion by the relation

$$\frac{dm_c}{dt} = \frac{6(1.085) \times 10^4}{\rho_c d_c} \dot{m}_{c_{initial}}^{1/3} \dot{m}_c^{2/3} \frac{p0_2}{\sqrt{T}} e^{-\frac{39,300}{RT}}$$

which is readily transformed to

$$\frac{d\alpha_c}{dt} = .8138 \times 10^{12} \alpha_c \alpha_{0_2} \left(\frac{\alpha_{c_{initial}}}{\alpha_c} \right) \frac{p}{\sqrt{T}} e^{-\frac{39,300}{RT}} \qquad (47)$$

by assuming that the soot density ρ_c is 2 gm/cm^3 and that the mean particle diameter, d_c is 400°A.

Based on this work of Reference 38 the oxidation equation is assumed to be:

$$C_{(s)} + 0_2 \rightarrow CO_2 \qquad (48)$$

This formulation has been incorporated into the "quasi-global" chemistry package but it must be regarded as tentative.

Various versions of the MOCV program were extended to include this "quasi-global" package. In particular, all supersonic versions of the program contain this chemistry capability. It should be emphasized, however, that the extended version with the internal shock structure has been set-up for entry and exit from this kinetics package but only a "dummy" routine is currently included. However, all the thermodynamic properties (enthalpy and specific heat "fits") have been integrated into the program. It should be noted that a mixed subsonic/supersonic ducted flow version based upon the MOCV framework is under development on a separate NASA Contract and is discussed in Reference 39. However, this kinetics capability remains to be added to this version.

In addition to the kinetics of combustion, the problem of phase transition is also relevant in the underexpanded plume flow. In plumes involving large expansion ratios many of the species may become saturated and condense out of the vapor phase. In hydrocarbon systems two potential condensibles are H_2O and CO_2 and because of the short residence times the process will be a finite rate one. The next section will describe a method of including classical nucleation and growth theory into multi-dimensional flow field calculations.

X. PHASE TRANSITION

The present analysis describes some of these coupled processes as applied to specific flow configurations. In particular, the equations describing turbulent flow characterized by parabolic equations with equilibrium chemistry and finite rate phase change, are considered. This includes ducted flows appropriate for the analysis of rocket combustion chambers, thrust augmentation chambers, and ejectors. In addition, unbounded flows are analyzed including discrete jets, and plume-free shear layers.

The analysis includes a description of the conservation equations of mass, energy, and momentum, including a detailed discussion of the constitutive relations describing interphase mass transport. The important gas phase and particulate phase parameters governing the behavior of the turbulent transport of particles are described. The solution of the describing equations for all flows, bounded and unbounded, is by an explicit finite difference scheme. Either an arbitrary wall contour or streamwise pressure variation may be specified. The unique feature of this work is the coupling of a number of two-phase processes in configurations including mixing and combustion.

A. Analysis

A comprehensive description of the conservation equations governing a (utilizing the boundary layer assumptions) multi-dimensional, multi-phase system, is much more complex than the familiar gas-phase conservation equations. In addition to describing the conservation of mass, momentum and energy for the condensed phase, it is necessary to also describe the dynamic and thermodynamic interactions between the phases (dynamic nonequilibrium), temperature differences (thermal nonequilibrium), and mass transfer between the phases (nonequilibrium phase change). This highly general system of equations was formulated in Reference 40.

In this investigation we are concerned with phase transition in configurations involving mixing and combustion. The emphasis is on the finite rate interphase mass transfer process under the following assumptions: dynamic and thermal

equilibrium for the mean and turbulent components of velocity and temperature, and quasi-complete combustion. These assumptions provide a reasonable estimate for flows involving ($\sim 1\mu$). Certain combustion chamber processes associated with direct liquid fueled rockets and air breathers are additional examples of practical applications of this analysis.

For a plane two-dimensional, or axisymmetric system, the governing equations may be written as Reference 40 and 41

Mass:

$$\frac{\partial}{\partial x}(\rho u y^N) + \frac{\partial}{\partial y}(\rho v y^N) = 0 \tag{49}$$

Momentum:

$$\rho u \frac{\partial u}{\partial x} + \rho v \frac{\partial u}{\partial y} = - \frac{dp}{dx} + \frac{1}{y^N} \frac{\partial}{\partial y}(\mu y^N \frac{\partial u}{\partial y}) \tag{50}$$

Energy:

$$\rho u \frac{\partial H}{\partial x} + \rho v \frac{\partial H}{\partial y} = \frac{1}{y^N} \frac{\partial}{\partial y} [y^N \mu_t \{ \frac{1}{Pr} \frac{\partial H}{\partial y} + (1 - \frac{1}{Pr}) \frac{2(\frac{u^2}{2})}{\partial y} +$$

$$+ \Sigma [(\frac{1}{Sc} - \frac{1}{Pr}) h^i \frac{\partial \beta^i}{\partial y}] \}] \tag{51}$$

Diffusion:

$$\rho u \frac{\partial \beta^i}{\partial x} + \rho v \frac{\partial \beta^i}{\partial y} = \frac{1}{y^N} \frac{\partial}{\partial y} [\frac{y^N}{Sc} \mu_t \frac{\partial \beta^i}{\partial x}] +$$

$$+ \dot{w}^i_{\text{chemistry}} + \dot{w}^i_{\text{phase change}} \tag{52}$$

where

$$N = \begin{cases} 0 - \text{two-dimensional flow coordinates} \\ 1 - \text{axisymmetric flow coordinates} \end{cases}$$

Initial and Boundary Conditions:

$$x = 0;\ 0 \le y \le y_p \quad \begin{cases} u = u_p(y) \\ T = T_p(y) \\ \beta_i = \beta_{i_p}(y) \end{cases}$$

$$y_p < y < y_w \quad \begin{cases} u = u_s(y) \\ T = T_s(y) \\ \beta_i = \beta_{i_s}(y) \end{cases}$$

$$x \ge 0;\ y = y_w \quad \begin{cases} \dfrac{\partial \beta_i}{\partial y} = 0 \ \text{(impermeable wall)} \\ \dfrac{\partial H}{\partial y} = 0 \ \text{(adiabatic wall)} \\ \text{or} \\ T = T_w(x) \ \text{(cooled or heated wall)} \\ \dfrac{\partial u}{\partial y} = \left(\dfrac{\rho u^2}{\mu} \right)_m \dfrac{c_f}{2} \end{cases}$$

$$y = 0 \quad \begin{cases} \dfrac{\partial \beta_i}{\partial y} = \dfrac{\partial T}{\partial y} = \dfrac{\partial u}{\partial y} = 0 \\ v = 0 \end{cases}$$

This set of equations has been solved for hydrocarbon chemical systems and includes condensation for the species H_2O and CO_2 using the classical finite rate nucleation and droplet growth law treatment described in Section B. Since in this work, emphasis is placed on the kinetics of phase transition, it is appropriate to employ a simple equilibrium-like complete combustion chemistry model (Section C) to describe the burning process. Thus, we have the combination of a finite-rate phase change process and an equilibrium type chemistry model.

To properly use these models requires that the species participating in the chemistry model be cast in the form of element mass fractions, while the condensed species entering into the phase kinetics process remain as specie mass fractions which act only as diluents in the local burning process.

Thus, the diffusion conservation equation must be written in two parts:

Diffusion: (element mass fractions)

$$\rho u \frac{\partial \tilde{\alpha}^j}{\partial x} + \rho v \frac{\partial \tilde{\alpha}^j}{\partial y} = \frac{1}{y^N} \frac{\partial}{\partial y} \left[\frac{y^N \mu_t}{Sc} \cdot \frac{\partial \tilde{\alpha}^j}{\partial y} \right] + \dot{\tilde{w}}^F_j \qquad (53)$$

$$j = C,\ O_2,\ H_2,\ N_2$$

Diffusion: (phase transition species)

$$\rho u \frac{\partial \alpha^i}{\partial x} + \rho v \frac{\partial \alpha^i}{\partial y} = \frac{1}{y^N} \frac{\partial}{\partial y} \left[\frac{y^N \mu_t}{Sc} \cdot \frac{\partial \alpha^i}{\partial y} \right] + \dot{w}^F_i \qquad (54)$$

$$i = CO_2 \text{ or } H_2O$$

It must be emphasized that the $\tilde{\alpha}_j$ are not total mixture element mass fractions, but involve only the species participating in the combustion process. Thus

$$\tilde{\alpha}^j = \sum_{i}^{\substack{\text{Comb.} \\ \text{species} \\ \text{only}}} \mu_{ij} \frac{w_j}{w_i} \alpha^i$$

and

$$\sum_{j}^{\text{comb.}} \tilde{\alpha}^j + \sum_{i}^{\text{Phase trans.}} \alpha^i = 1$$

$\dot{w}^F_i$, the production rate of condensed species, is determined by the condensation-evaporation models described in Section B, and hence determines $\dot{\tilde{w}}^F_j$:

$$\dot{\tilde{w}}^F_j = \sum_i \mu_{ij} \frac{w^j}{w^i} \dot{w}^F_i$$

The chemical species considered in the present application are H_2O, H_2, O_2, CO, CO_2, N_2, $C_{(c)}$ a generalized hydrocarbon fuel, C_nH_m, whose thermodynamic properties must be specified, and either $H_2O_{(c)}$ or $CO_{2(c)}$ as a specie undergoing finite rate phast transition. Because the phase transition kinetics is a function of particle size it is necessary to track the particles through the flow and account for the size distribution. The droplet particle size array is discussed in Section X.B.

The solution of the above system of equations provides the details of the flow field including the velocity, temperature, and species fields.

The global continuity equation can be eliminated from the system of differential equations by introducing the von Mises coordinates as the independent variables. The transformation (x,y) to (x,Ψ) is defined according to the relations:

$$\rho u y^N = \Psi^N \Psi_y \tag{54a}$$

$$-\rho v y^N = \Psi^N \Psi_x \tag{54b}$$

Introduction of (54a) and (54b) into the differential equations results in:

Element Conservation

$$\frac{\partial \tilde{\alpha}_j}{\partial x} = \frac{1}{\Psi^N} \frac{\partial}{\partial \Psi} \left[\frac{Le_t}{Pr_t} \frac{\mu_t \rho u}{\Psi^N} y^{2N} \frac{\partial \alpha_j}{\partial \Psi}\right] + \dot{\tilde{w}}^F_j/\rho u \quad , \; j=C,O_2,H_2,N_2$$

$$\frac{\partial \alpha_i}{\partial x} = \frac{1}{\Psi^N} \frac{\partial}{\partial \Psi} \left[\frac{Le_t}{Pr_t} \frac{\mu_t \rho u}{\Psi^N} y^{2N} \frac{\partial \alpha_i}{\partial \Psi}\right] + \dot{w}_L, \; L = CO_2 \text{ or } H_2O \tag{55}$$

Momentum

$$\frac{\partial u}{\partial x} = \frac{1}{\Psi^N} \frac{\partial}{\partial \Psi} \left[\frac{\mu_t \rho u}{\Psi^N} \, y^{2N} \frac{\partial u}{\partial \Psi} \right] - \frac{1}{\rho u} \frac{dp}{dx} \tag{56}$$

Energy

$$\frac{\partial H}{\partial x} = \frac{1}{\Psi^N} \frac{\partial}{\partial \Psi} \left[\frac{\mu_t \rho u}{\Psi^N} \, y^{2N} \frac{1}{Pr} \left\{ \frac{\partial H}{\partial \Psi} + (Pr_t - 1) \frac{\partial u^2/2}{\partial \Psi} + \right. \right. \tag{57}$$

$$\left. \left. + \sum_i h_i (Le_t - 1) \frac{\partial \alpha_i}{\partial \Psi} \right\} \right]$$

The physical y coordinate is obtained by the inverse transformation:

$$y^{N+1} = (N + 1) \int_o^{\Psi} \frac{\Psi^N}{\rho u} \, d\Psi \tag{58}$$

and the transverse component of velocity, v, is given by

$$v = - \frac{\Psi^N \Psi_x}{\rho y^N} \tag{59}$$

Boundary Conditions:

The governing equations are parabolic and require initial conditions at $x = 0$ and boundary conditions at $\Psi = \infty$ and $\Psi = 0$. The initial and boundary conditions are:

at $\Psi = 0$;

$$\frac{\partial u}{\partial \Psi} = \frac{\partial \alpha_i}{\partial \Psi} = \frac{\partial T}{\partial \Psi} = 0 \tag{60}$$

at $\Psi = \Psi_w$;

$$\frac{\partial u}{\partial \Psi} = \left(\frac{\Psi}{\rho u y} \right)_w \left(\frac{\rho u^2}{\mu} \right)_m \frac{Cf}{2}$$

$$\frac{\partial H}{\partial \Psi} = 0, \text{ or } T = T_w \tag{61}$$

$$\frac{\partial \alpha_i}{\partial \Psi} = 0$$

Initial Conditions:

$$x = 0 \qquad 0 \le \Psi \le \Psi_p \qquad \begin{cases} u = u_p(\Psi) \\ T = T_p(\Psi) \\ \tilde{\alpha}_j = \tilde{\alpha}_{jp}(\Psi) \\ \alpha_L = \alpha_{Lp}(r,\Psi) \end{cases}$$

$$\Psi_p < \Psi < \Psi_w \qquad \begin{cases} u = u_s(\Psi) \\ T = T_s(\Psi) \\ \tilde{\alpha}_j = \tilde{\alpha}_{js}(\Psi) \\ \alpha_L = \alpha_L(r,\Psi) \end{cases} \qquad (62)$$

The conditions expressed by (60), (61), and (62) with symmetry at $\Psi = 0$ completes the specification of initial and boundary conditions.

The solution of the above system has been carried out by an explicit finite difference scheme and the details are given in various references including References 33, 41 and 42.

B. The Condensation Process

The condensation process is initiated by the formulation of critically sized clusters of droplets in the new phase. This phenomena, defined as nucleation, is generally divided into two types: homogeneous, wherein the new phase deposits on nuclei spontaneously formed when vapor molecules collide and stick; and heterogeneous nucleation in which the condensate initially deposits on foreign particles serving as centers for condensation. For simplicity, the present analysis is concerned only with the first of these phenomena.

The Nucleation Rate Equation:

The model for homogeneous nucleation according to classical theory consists of specifying expressions for the radius of a critical drop r*, work required for cluster formation w*,

droplet surface tension σ and a growth law. The nucleation rate J can be written in general form as

$$J = B_1 B_2 \frac{P_V}{\rho_L T^2} \exp X_7$$

where J is defined as the number of droplets created per unit time per unit volume. The pre-exponential factors are closely related to the collision frequency of molecules in the gaseous state and the exponential is an expression of the work of cluster formation. Since a particular model may be best for only certain flow conditions or types of condensate, six models are included in this analysis. These expressions are summarized in Table II . Once the droplet is formed its subsequent history is determined by some growth law. A particularly simple and useful one is given by kinetic theory:

$$F = \frac{\alpha(p_v - p_{v\infty})}{\rho_L u} \left(\frac{M_L}{2\pi kT} \right)^{\frac{1}{2}}$$

where

F = dr/dx the rate of change of droplet radius and
α is the accommodation coefficient.

To apply these expressions to condensation of a supersaturated vapor, the values of A*, n*, w* and σ, must be determined. These variables depend upon the state and shape of the droplets of condensate, and involve the surface tension of the droplets. The area of the droplet is given by

$$A^* = s^* r^{*2}$$

where s* is a shape factor. For spherical droplets, $s^* = 4\pi$. The number of molecules in a critical droplet is:

$$n^* = \frac{s^* r^{*3} \rho_c}{3m}$$

The work of formation is

$$w^* = \frac{4\pi}{3} \sigma r^{*2}$$

The Particle Array:

The total amount of condensate present at every point in the flow field is divided into categories (current computer program has ten) based on particle size. Within each size range all the particles are combined to form an average with a volume to surface area ratio equal to that of the summation overall contributions. This equivalent particle size is identical to the Sauter mean diameter or radius and be expressed as

$$r_s = \frac{\Sigma n_i r_i^3}{\Sigma n_i r_i^2} \quad \text{where } n_i \text{ particles have radius } r_i$$

This representation is exact for dynamic and thermal equilibrium between phases assuming a mass transfer rate based on condensation from kinetic theory. The mass fraction of each category is equal to the sum of the mass fraction of each contribution. With the average size of category particles and the total category mass fraction known, the appropriate number of equivalent particles is established for every class.

The particle distribution array in terms of size, mass fraction, and number in each category at every grid point can only be altered by three phenomena: the creation of new droplets by nucleation, the growth of old droplets, and the diffusion of droplets from adjoining grid points. Each of these effects is treated separately in the following sections wherein expressions for the particle array variables resulting from these prccesses are developed.

Nucleation:

Whenever new particles are created by the condensation of droplets from the vapor phase, the resulting particle size is defined in terms of the local pressure and temperature as r*

where

$$r^* = \frac{2\sigma m_v}{\rho_c R \ell n \varphi}$$

φ=saturation ratio= $\frac{\text{partial pressure of the vapor}}{\text{equilibrium partial pressure}}$

$\rho_c \equiv$condensate density

The number density of critical size particles created over a given length is defined as N_S where:

$$N_S = \int_{x_o}^{x} \frac{J(\xi)d\xi}{u}$$

The mass fraction created is then

$$g_s = \int_{x_o}^{x} \frac{n^* M_L}{\rho u} J(\xi)d\xi$$

$n^* \equiv$number of molecules in critical droplet

$M_L \equiv$mass of molecule

These particles are then categorized into the proper size group and averaged with those already in the category using the Sauter criteria to form a new class radius, mass fraction and number density, defined as $R(J,I)_{AVE}$, $G(J,I)$, and $N(J,I)$ where the J indexes the categories and I the points in the grid.

Growth:

All droplets are formed with an initial radius r* that changes in accordance with the growth law as the flow field develops. Thus, after every step, the updated radius array must be reclassified in order to account for the transition of particles from one category to another. Since it is possible for more than one contribution to be made to a particular category, the total mass in each category must then be re-averaged to establish the category radius using the Sauter criteria. The resulting expressions for the particle array in terms of radius, mass fraction and number density become:

$$R(J,I)_{AVE} = \frac{\Sigma n_i r_i^3}{\Sigma n_i r_i^2}$$

where r_i represents the radius and n_i the number density for each contribution that has been sorted into the same category. Since the total mass is equal to the sum of the mass contributions, the number density of particles is given by

$$N)J,I) = \frac{\Sigma n_i r_i^3}{R(J,I)^3_{AVE}}$$

With the new size and number established the mass fraction can be expressed as

$$F(J,I) = \frac{N(J,I)}{N(J,I)_{old}} \left(\frac{R(J,I)_{AVE}}{R(J,I)_{old}} \right)^3 G(J,I)_{old}$$

Where the subscript "old" denotes values of the variables prior to the last integration step.

The effects of the condensation process of creation and growth on the particle array parameters are summarized below. The particle array in terms of mass fractions, sizes and number density is traced from an initial station to a downstream position one step away.

The Condensation Process Summarized

For every grid point I the initial values of the particle array are initially:

G(J,I)
R(J,I) where J indexes the categories
N(J,I)

The rate of growth of old droplets is computed based on the growth law.

$$\frac{dR}{dx} = \frac{\alpha(p_v - p_{v\infty})}{\rho_c u} \left(\frac{M_L}{2\pi kT} \right)$$

Knowing the numerical step size based on the stability criteria for the finite rate scheme, these two rate equations are integrated numerically over this step Δx.

The number density of new droplets created is computed

$$N_s = \frac{J\Delta x}{u}$$

The change in radius of old droplets is evaluated

$$\Delta R = \frac{dR}{dx} \Delta x$$

The initial radius array R(J,I) is now updated

$$R(J,I) = R(J,I) + \Delta R$$

The new particle sizes are sorted into the proper categories and the number of contributions to each category is defined as n(J).

The average particle size in each category is established using the Sauter criteria

$$R(J,I)_{new} = \frac{\sum_{i=1}^{n} R_i^3 N_i}{\sum_{i=1}^{n} R_i^2 N_i}$$

The new number density of particles in each category having the updated size is established

$$N(J,I)_{new} = \sum_{i=1}^{n} R_i^3 N_i / R(J,I)_{new}^3$$

The new mass fraction of each category is established

$$G(J,I)_{new} = \frac{N(J,I)_{new}}{N(J,I)} \qquad \frac{R(J,I)^3_{new}}{R(J,I)} \cdot G(J,I)$$

Now, knowing the size r* of the droplets created over this step, the mass fraction created is added to the appropriate category

$$G'(J,I)_{new} = G(J,I) + g_s$$

Then having established the number of droplets created N_s with radius r*, the category radius is reaveraged to include this last contribution

$$R'(J,I)_{new} = \frac{R(J,I)^3_{new} N(J,I)_{new} + N_s r^{*3}}{R(J,I)^3_{new} N(J,I)_{new} + N_s r^{*2}}$$

The category number density is adjusted by

$$N'(J,I)_{new} = R(J,I)^3_{new} N(J,I)_{new} / R'(J,I)^3$$

The particle array parameters thus established

$$G'(J,I)_{new}$$
$$R'(J,I)_{new}$$
$$N'(J,I)_{new}$$

represent the condensate at the downstream station

$$X = X_o + \Delta x$$

as it has been altered by the kinetic process. For simplicity it will be referred to using a subscript K. Thus, we have established

$$G'(J,I)_{new} = G(J,I)_K$$

$$R'(J,I)_{new} = R(J,I)_K$$

$$N'(J,I)_{new} = R(J,I)_K$$

Diffusion

Each category in the particle array is altered by the diffusion of condensate of the mass categories from neighboring upstream locations. Considering each particle category as a quasi-element, the conservation equation for the "category elements" can be written in finite difference form (forn non-axis points) as:

$$\alpha^j_{\substack{n+1\\m}} = \Delta x \left(\frac{w_j}{u}\right) + \alpha^j_{\substack{n\\m}} + \frac{\Delta x}{M^N \Delta \Psi^{2+n}} \left\{ \left(\frac{Le\ b}{Pr}\right)_{\substack{n\\m+\frac{1}{2}}} \alpha^j_{\substack{n\\m+1}} \right.$$

$$\left. \left[\left(\frac{Le\ b}{Pr}\right)_{\substack{n\\m+\frac{1}{2}}} + \left(\frac{Le\ b}{Pr}\right)_{\substack{n\\m+\frac{1}{2}}} \right] \alpha^j_{\substack{n\\m}} + \left(\frac{Le\ b}{Pr}\right)_{\substack{n\\m-\frac{1}{2}}} \alpha^j_{\substack{n\\m-1}} \right\}$$

where n,m subscripts refer to the grid point locations shown in the sketch below. The first term in the equation above represents the change in α^j due to the condensation process as the flow moves downstream from n to n+1. The sum of the first two terms is the total mass fraction of category j condensate present downstream due to kinetic processes, and the remaining term represents the contribution to the mass fraction from diffusion. Based on sketch below, this diffusional term can be split into the contributions from each of the three upstream points:

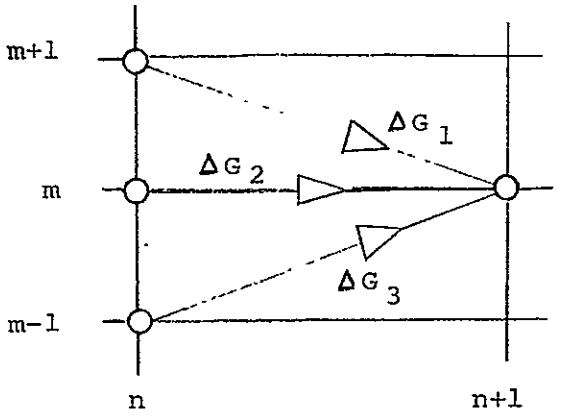

$$\Delta G_1 \equiv \frac{\Delta x}{M^N \Delta\Psi^{2+N}} \left(\frac{Le\ b}{Pr} \right)_{\substack{n \\ m+\frac{1}{2}}} \alpha^j_{\substack{n \\ m+1}}$$

$$\Delta G_2 \equiv - \frac{\Delta x}{M^N \Delta\Psi^{2+N}} \left[\left(\frac{Le\ b}{Pr} \right)_{\substack{n \\ m+\frac{1}{2}}} - \left(\frac{Le\ b}{Pr} \right)_{\substack{n \\ m-\frac{1}{2}}} \right] \alpha^j_{\substack{n \\ m}}$$

$$\Delta G_3 \equiv \frac{\Delta x}{M^N \Delta\Psi^{2+N}} \left(\frac{Le\ b}{Pr} \right)_{\substack{n \\ m-\frac{1}{2}}} \alpha^j_{\substack{n \\ m-1}}$$

For each of the 10 categories present at a given grid point we may express the category mass fraction as

$$G(J,I)_{\substack{n+1 \\ m}} = \left[\Delta x \left(\frac{\dot{w}^j}{u} \right)_{\substack{n \\ m}} + \alpha^j_{\substack{n \\ m}} \right] + \Delta G_1 + \Delta G_2 + \Delta G_3$$

where the kinetics contribution is evaluated as outlined in the previous two sections on growth and creation of condensate and is represented by $G(J,I)_K$ with its associated $R(J,I)_K$ and $Q(J,I)_K$. Knowing the category sizes associated with each upstream contribution the Sauter criteria can be used to define the new category radius:

$$R(J,I)_{n+1} = \frac{G(J,I)_K + \Delta G_1 + \Delta G_2 + \Delta G_3}{\frac{G(J,I)_K}{R(J,I)_K} + \frac{\Delta G_1}{R(J,I)_{\substack{n \\ m+1}}} + \frac{\Delta G_2}{R(J,I)_{\substack{n \\ m}}} + \frac{\Delta G_3}{R(J,I)_{\substack{n \\ m-1}}}}$$

Knowing the new mass fraction and size, the number density of particles is determined from

$$N(J,I)_{\substack{n+1 \\ m}} = \frac{\rho_{n+1} \; G(J,I)_{\substack{n+1 \\ m}}}{\frac{4}{3}\pi\rho_c \; R(J,I)^3_{\substack{n+1 \\ m}}}$$

For points on the axis, the finite rate category element conservation equation becomes

$$\alpha^j_{\substack{n+1 \\ o}} = \Delta x \left(\frac{\dot{w}^j}{u}\right)_{\substack{n \\ o}} + \alpha^j_{\substack{n \\ o}} + \frac{(1+N)2\Delta x}{\Delta\Psi^2}\left[\rho u^{(1-N)}\left(\frac{Le}{Pr}\,\mu\right)\right]_{\substack{n \\ o}}\left[\alpha^j_{\substack{n \\ 1}} - \alpha^j_{\substack{n \\ o}}\right]$$

Here once again the first two terms represent the mass fraction of category j due to the condensation process and the last term, the effect of diffusion. In the sketch below the diffusional contribution of each upstream point is defined.

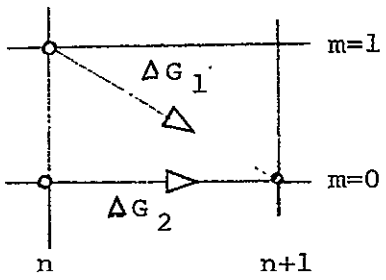

$$\Delta G_1 \cong (1+N)\frac{2\Delta x}{\Delta \Psi^2}\left(\rho u^{(1-N)}\left(\frac{Le\mu}{Pr}\right)\right)_{\substack{n \\ o}} \alpha^{j}_{\substack{n \\ 1}}$$

$$\Delta G_2 \cong -(1+N)\frac{2\Delta x}{\Delta \Psi^2}\left(\rho u^{(1-N)}\left(\frac{Le\mu}{Pr}\right)\right)_{\substack{n \\ o}} \alpha^{j}_{\substack{n \\ o}}$$

The total mass fraction of category j for grid point i at (N+1) can then be written as

$$G(J,I)_{\substack{n+1 \\ o}} = \left[\Delta x\left(\frac{\dot{w}^j}{u}\right)_{\substack{n \\ o}} + \alpha^{j}_{\substack{n \\ o}}\right] + \Delta G_1 + \Delta G_2$$

where the first term is obtained from the kinetics condensations outlined in the previous section and is defined as $G(J,I)_K$ with the associated $R(J,I)_K$ and $Q(J,I)_K$. Applying the Sauter criteria to determine the average size of the resultant collection of condensate we obtain

$$R(J,I)_{\substack{n+1 \\ o}} = \frac{G(J,I)_K + \Delta G_1 + \Delta G_2}{\frac{G(J,I)_K}{R(J,I)_K} + \frac{\Delta G_1}{R(J,I)_{\substack{n \\ 1}}} + \frac{\Delta G_2}{R(J,I)_{\substack{n \\ o}}}}$$

Knowing the total mass fraction and size, the number density of particles is then

$$N(J,I)_{n+1}^{o} = \frac{\rho_{n+1}^{o} \; G(J,I)_{n+1}^{o}}{\frac{4}{3}\pi\rho_c \; R(J,I)_{n+1}^{3\,o}}$$

C. Chemistry Model

In making preliminary design studies for a proposed propulsion system, it is alwasy desirable to investigate the extremes of no burning ("frozen chemistry") and maximum burning ("complete combustion chemistry"). The standard complete combustion model for a hydrocarbon-oxygen system is

$$C_nH_m + pO_2 \rightarrow nCO_2 + m/2\ H_2O + q \qquad \begin{matrix} O_2 - \text{fuel lean} \\ C_nH_m = \text{fuel rich} \end{matrix}$$

Obviously, this model ignores the effects of dissociation. For fuel-lean mixtures with flame temperatures less than 2500°K this simple model is an acceptable approximation to the equilibrium composition. For fuel-rich mixtures the above model is not as satisfactory, since CO and $C_{(s)}$ are present in significant amounts at equilibrium. A study[s] of tabulated hydrocarbon-air equilibrium compositions indicated that it would be possible to formulate a simple, algebraic fuel-rich "quasi-complete combustion" model by using three distinct regions of fuel/air ratios. The first attempt to formulate the model is shown in Figure 51.

This model yields flame temperatures that are only slightly above that at true equilibrium. However, the representation of the relative amounts of the major chemical species in zones A and B was not very realistic for most combinations of pressure and initial mixture temperature. This led to a revision of zones A and B, resulting in the model shown in Figure 52. This model, as shown in Figures 53 and 54, yields a flame temperature very near that of equilibrium except for mixtures very close to stoichiometric. In this region, the flame temperatures are high enough so that chemical dissociation is a significant phenomena, and hence the flame temperature of the complete combustion model, which ignores dissociation is, noticably higher than the flame

temperature of the equilibrium chemistry model which takes dissociation into account with respect to the species H, O, and OH.

It should be noted that methane (CH_4) is a significant equilibrium specie in very fuel rich regions ($O/F < 1$ or $\phi > 3$) for fuels such as kerosene (C_9H_{20}), and that at low temperatures in highly fuel rich regions the original fuel specie is present at equilibrium in significant amounts rather than being completely broken down into $C_{(s)}$ and H_2.

As an example of the application of this analysis, a nozzle type expansion process was investigated. To demonstrate the coupling between the mixing process and the finite rate evaporation process a non-uniform entrance condition was imposed consisting of the products of the complete combustion of a lean hydrogen/O_2 mixture surrounded by cold air. As the flow field develops, the gaseous H_2O spreads into the secondary air stream and cools. When saturation conditions are achieved, the finite rate condensation of water vapor begins. Profiles of the important flow variables are given in Figures 55 to 58. Velocity and static temperature profiles for the system are given in Figure 55. Figure 56 shows the gaseous specie mass fraction distributions at a streamwise location where two phase phenomena have occurred. An indication of the spread of condensate in both the radial and streamwise direction is given by the results of Figure 57. As the flow moves downstream both the amount of condensate and its radial extent increases. The radius distribution of a condensate in the first size category (0 to 10^{-3} microns) is given in Figure 58. The secondary peak in the vicinity of the wall is due to the creation of "new" droplets as the gaseous H_2O diffuses.

The primary distribution (y/y_w = .77 to .95) represents the size variation of "old" droplets created upstream as effected by their growth history. These droplets comprise the majority of condensate present. Near the wall ($y/y_w > .95$) the saturation ratio is relatively high and the small condensate mass fraction (below 10^{-13}) in this region is essentially comprised of critical sized droplets.

XI. SUMMARY

The work presented in this report consists of both analysis and numerical implementation of a number of processes relevant to chemically reacting plume flows.

The basic GASL MOCV (Method of Characteristics with Viscosity) program has been extended to include the intercepting shock-Mach disc structure of an underexpanded exhaust plume. Although various aspects of the computer program have been checked the total capability has not been exercised as of this time. Limited tests for inviscid flows with frozen chemistry have been made demonstrating that the modifications are working. Also, in the existing version the detection of the intercepting (barrel) shock is done by noting a local pressure peak in the vicinity of the nozzle lip. Furthermore, the Mach disc location must be specified.

The Mach disc problem was studied in some detail and its location, or more specifically the location of the triple point, in relationship to the subsequent downstream subsonic flow has been analyzed. This investigation suggests a theoretical rather than an empirical method for treating this problem.

The transonic flow problem was investigated and various methods of analysis were reviewed. The result of this study indicates that an unsteady approach should be used for the transonic flow downstream of the Mach disc. Additional work is, however, required to establish a feasible unsteady computational technique which includes viscosity and kinetics processes simultaneously.

In addition to studying the various fluid mechanical problems, some relevant aspects of chemical and multiphase processes were investigated. A chemical kinetics mechanism for the oxidation of hydrocarbons (hydrogen included) has been introduced into the plume version of the MOCV program (ducted flow versions are described in Reference 39). Phase transition kinetics has been analyzed and implemented for computations within the parabolic mixing and combustion programs and currently treats the finite rate phase transition of CO_2 and H_2O. Inclusion of this capability into the MOCV programs will be made in the near future.

APPENDIX A

The computations reported herein were obtained using a modification of a method of characteristics computer program originally developed to compute internal flows with multiple shock intersections[44]. Envelope shocks of either family are detected by the crossing of characteristics of that family. In outline, the plume computations proceed as follows (Figure 57).

The flow (p,T,M,θ) across the exit plane (in this case uniform and parallel) was specified along with the ambient pressure. The computation procedes along right running characteristics. A concentrated expansion is put at the nozzle lip to match the exit and ambient pressures. After each interior point is computed, a test is made to determine whether or not two characteristics of the same family have crossed. If not, the computation proceeds to the next regular interior or boundary point. If two such characteristics cross, a shock is initiated. Subsequently, the shock slope and the flow immediately behind it are obtained by matching the Rankine-Hugonoit jump conditions with the solution of the characteristic compatability equations behind the shock. Since characteristic computations are familiar to most fluid dynamicists, the details of the interior, boundary, and shock point computations which can be found in Reference 44 are not given here. However, two comments are in order. First, in all finite difference equations the coefficients were averaged between initial and final points except that, strictly as a matter of computational convenience, the shock slope was not averaged in determining shock point locations. Second, the entropy and total enthalpy (in this computation the latter was constant) along a streamline are determined from a mass flow entropy, total enthalpy table which is constructed from initial data and modified when a shock is traversed. This procedure is much more accurate[45] than the more usual one of directly interpolating on the computational mesh.

In the present computations, the triple point abscissa was specified. So, after each internal mesh point was computed, a test was made to determine whether its abscissa was greater than or less than that specified for the triple point. If greater,

the ordinate of, and flow before the shock at the triple point, were obtained by linear interpolation. Then the intercepting shock alope and the flow behind it were obtained from a regular shock computation.

The triple point solution is obtained by first assuming a value for the strong shock slope and computing the corresponding pressure and flow direction in region 4, Figure 58. Then the reflected shock angle, σ_r corresponding to the pressure $p_3 = p_4$ is determined. A test is then made to determine if $\theta_3 = \theta_4$. If not, a new value of the strong shock slope is guessed and the process is repeated. The strong shock slope is iterated on until $p_3 = p_4$ and $\theta_3 = \theta_4$ simultaneously.

The triple point solution includes the slope of the separating slip-stream (SS), θ_{SS}, which is necessary to continue the flow field solution further downstream. Recall that this streamline separates the flow into two regions, a quasi-one-dimensional streamtube centered along the axis and an outer region where the complete steady Euler equations are used. The separating slip-stream shape (i.e., the streamtube cross-sectional area distribution) and the axial pressure distribution are obtained by matching the solutions of these two regions along the slipstream.

REFERENCES

1. Farmer, R.C., Prozan, R.J., McGimsey, L.R., and Ratliff, A.W., "Verification of a Mathematical Model which Represents Large, Liquid Rocke-Engine Exhaust Plumes," AIAA Second Propulsion Joint Specialist Conference, Colorado Springs, Colorado, June 13-17, 1966, Paper No. 66-650.

2. Edelman, R., and Fortune, O., "Some Recent Developments on the Analysis of Exhaust Plume Afterburning," Presented at the Rocket Plume Specialists' Meeting, San Bernardino, California, July 11-12, 1968.

3. Smoot, L.D., and Farmer, R.C., "Rocket Plume Technology," Second Joint AICHe- 11 QPR Meeting, Tampa, Florida, May 19-22, 1968.

4. Moretti, G., "A New Technique for the Numerical Analysis of Non-Equilibrium Flows," AIAA Journal, Vol. 3, No. 2, February 1965, pp. 223-229.

5. DeGroat, J., and Abbett, M., "A Computation of One-Dimensional Combustion of Methane," AIAA Journal, Vol. 3, No. 2, February 1965, pp. 381-383.

6. Magnus, D., and Schechter, H., "Analysis and Application of the Pade Approximation for the Integration of Chemical Kinetic Equations," GASL TR-642, May 1967.

7. Moretti, G.,"Analysis of Two-Dimensional Problems of Supersonic Combustion Controlled by Mixing," AIAA Preprint 64-69, January 1964.

8. Ferri, A., Moretti, G., and Slutsky, S., "Mixing Processes in Supersonic Combustion," J. Soc. Indust. Appl. Math., 13, 1, March 1965, pp. 229-258.

9. Edelman, R., and Weilerstein, G.,"Mixing and Combustion in Supersonic Flow with Lateral Pressure Gradient Effects," GASL TR 636, August 1968.

10. Adamson, T.C., and Nicholls, J.A., "On the Structure of Jets From Highly Underexpanded Nozzles into Still Air," JAS 26, 1, 1959, 16-24.

11. Eastman, D.W., and Radtke, L.P., "Location of the Normal Shock Wave in the Exhaust Plume on a Jet," AIAA J, Vol. 1, No. 4, April 1963.

12. Bowyer, J., D'Attore, L., and Yoshihara, H., "The Flow Field Resulting from Mach Reflection of a Convergent Conical Shock at the Axis of a Supersonic Axially Symmetric Jet," General Dynamics/Astronautics, San Diego, Calif., GDA63-0586, 1963.

13. Abdelhamid, A.N., and Dosanje, D.S., "Mach Disc and Reimann Wave in Underexpanded Jet Flows," AIAA Paper 69-665, June 1969.

14. Crocco, L., "One Dimensional Steady Flow," in Fundamental of Gas Dynamics, ed. by H. W. Emmons, Vol. IV of High Speed Aerodynamics and Jet Propulsion, Princeton U. Press, Princeton, N.J.

15. Crocco, L., "Considerations on the Shock-Boundary Layer Interaction," in High Speed Aeronautics, ed. by A. Ferri, N. J. Hoff, and P. Libby, Polytechnic Inst. of Bklyn, 1955.

16. Love, E.S., et al., "Experimental and Theoretical Studies of Axisymmetric Free Jets," NACA R6, 1959.

17. Hayes, W.P., and Probstein, R.F., "Hypersonic Flow Theory, Vol. 1, Inviscid Flows, end ed., Academic Press, 1966, N.Y. Section 6.3, 6.4.

18. Belotserkovskiy, O.M., ed., "Supersonic Gas Flow Around Blund Bodies," Theoretical and Experimental Investigations, NASA TTF-453, June 1967 (translation of "Obtekaniye Zatuplennykh Tel Sverkhzvukovym Potokom Gaza. Teoreticheskoye i Eksperimental'noye Issledovaniya," Computer Center of Academy of Sciences, USSR, Moscow, 1966)

19. Holt, Maurice, "The Design of Plane and Axisymmetric Nozzles by the Method of Integral Relation," Symposium Transonieum ed by Oswatitsch, Springer-Verlag, Berlin, 1963.

20. Belotserkovskii, O.M., and Chuskin, P.I., "The Numerical Solution of Problems in Gas Dynamics," in Basic Developments in Fluid Dynamics, Vol. 1, ed. by M. Holt, Academic Press, New York, 1965.

21. Kentzer, Czeslaw, P., "Instability of Numerical Solutions of the steady, Supersonic Blunt Body Problem, AIAA J., 5, 5, May 1967, 1035-7.

22. Kentzer, C.P., "Singular Line of the Method of Integral Relations," AIAA J., 1, 4, April 1963, 928-929.

23. Moretti, G., and Abbett, M., "A Two Dependent Calculation Method for Blunt Body Flows," AIAA J., 4, 12, Dec. 1966 2136-2141.

24. Moretti, G., and Bleich, G., "Three Dimensional Flow About Blunt Bodies," AIAA J, 5, 9, Sept. 67, 1557-1562.

25. Armitage, J., "The Lax Wendroff Method Applied to Axial Symmetric Swirl Flow," Blanch Anniversary Volume, Aerospace Research Labs., Office of Aerospace Research, USAF, February 1967.

26. Private Communication from R. Prozan, Lockheed Missiles ans Space Co., Huntsville, Ala., October 1, 1968.

27. "Computation of Axial-Symmetric Transonic Swirl Flows by the Unsteady Flow Approach," Aerospace Research Labs, Office of Aerospace Research, United States Air Force, ARL 68-0070, April 1968.

28. Saunders, Lee, M., "Numerical Solution of the Flow Field in the Throat Region of a Nozzle," Brown Engineering Co., Inc., Propulsion Rept. Technical Report R-66-3, Aug. 19,1966.

29. Migdal, David, Klein, Kenneth, and Moretti, G., "Time Dependent Calculations for Transonic Nozzle Flow," AIAA J, 7, 2, February 1969, 372-374.

30. Lax, P.D., and Wendroff, B., "Difference Schemes for Hyperbolic Equations with High Order of Accuracy," Comm. Pure Appl. Math. XVII, 1964, 381-398.

31. Ames Research Staff, Equations, Tables and Charts for Compressible Flow, NACA Report 1135, 1953.

32. Moretti, G., and Abbett, M., "A Time Dependent Computational Method for Blunt Body Flow," AIAA J, 4, 12, December 1966, 2136-2141.

33. Edelman, R., and Fortune, O., "Mixing and Combustion in the Exhaust Plumes of Rocket Engines Burning RP1 and Liquid Oxygen," GASL TR 631, November 1966.

34. Fortune, O., and Edelman, R., "The Effect of Mixing, Radiation and Finite Rate Combustion Upon the Flow Field and Surroundings of the Exhaust Plumes of the Rocket Engines Burning RP1 (Kerosene) and Liquid Oxygen," GASL TR 681, December 1967.

35. Chinitz, W., and Baurer, T., "An Analysis of Non-Equilibrium Hydrocarbon-Air Combustion," PART I - Chemical Kinetics, GASL TR 546, August 1965.

36. Magnus, D., and Schecter, H., "Analysis of Error Growth and Stability for the Integration of the Equation of Chemical Kinetics, May 1966.

37. Brokow, R.S., "Selected Combustion Problems," II, Butterworths, London, 1956.

38. Lee, K.B., Thring, M.W., and Beer, J.M., "On the Rate of Combustion of Soot in a Laminar Soot Flame," Combustion & Flame, Vol. 6, pp 137-145, 1962.

39. Edelman, R.B., Weilerstein, G., Fortune, O.F., and Abbett, M., "Combustion Analyses for Propulsion Systems," GASL Annual Report No. TR-736, (in preparation).

40. Edelman, R., Rosenbaum, H., and Slutsky, S., "Generalized Viscous Multicomponent-Multiphase Flow With Application to Laminar and Turbulent Jets of Hydrogen, GASL TR-349, April 1963.

41. Edelman, R., "Turbulent Transport in Polydisperse Systems" GASL TR 735.

42. Edelman, R., "Diffusion Controlled Combustion for Scramjet Application," Part I - Analysis and Results of Calculations, GASL TR 569, December 1965.

43. Edelman, R., and Fortune, O., "A Preliminary Analysis of Mixing and Combustion in Ducted Flows with Application to Ejector Ramjet Technology," GASL TR 658, May 1967.

44. Investigation of the Low Speed Fixed Geometry Scramjet, Part I - Inlet Design Practice Manual, ed. by James Johnson, GASL TR 667, September 1967, also AFAPL-TR-68-7.

45. Powers, S.A., and O'Neill, J.B., "Determination of Hypersonic Flow Fields by the Method of Characteristics, AIAA J., 1, 7, July 1963, 1693-1694.

TABLE I REACTION MECHANISM FOR PLUME AFTERBURNING WITHOUT TURBINE EXHAUST INJECTION*

Reaction No.	Reaction		
1	$CO + OH \underset{k_{b_1}}{\overset{k_{f_1}}{\rightleftharpoons}} CO_2 + H$	$3.2 \times 10^{12} e^{(-3.1706/T)}$	$2.7 \times 10^{17} T^{-0.79} e^{(-1...5/T)}$
2	$OH + H_2 \underset{k_{b_2}}{\overset{k_{f_2}}{\rightleftharpoons}} H + H_2O$	$6.3 \times 10^{13} e^{(-2.9693/T)}$	$2.4 \times 10^{...} e^{(-2...}$
3	$OH + OH \underset{k_{b_3}}{\overset{k_{f_3}}{\rightleftharpoons}} H_2O + O$	$7.6 \times 10^{12} e^{(-.50327/T)}$	$6.9 \times 10^{...} e^{(-8.928/T}$
4	$O + H_2 \underset{k_{b_4}}{\overset{k_{f_4}}{\rightleftharpoons}} OH + H$	$3.3 \times 10^{12} e^{(-3.5934/T)}$	$1.4 \times 10^{...} e^{(-2.612/T)}$
5	$H + O_2 \underset{k_{b_5}}{\overset{k_{f_5}}{\rightleftharpoons}} OH + O$	$2.4 \times 10^{14} e^{(-8.4298/T)}$	$3.2 \times 10^{...} T^{-0.47} e^{(-.0032/T)}$
6	$O + H + M \underset{k_{b_6}}{\overset{k_{f_6}}{\rightleftharpoons}} OH + M$	3×10^{14}	$7.5 \times 10^{...} T^{-0.06} e^{(-50.976/T)}$
7	$O + O + M \underset{k_{b_7}}{\overset{k_{f_7}}{\rightleftharpoons}} O_2 + M$	2.2×10^{13}	$2.5 \times 10^{...} T^{-0.5} e^{(-59.336/T)}$
8	$H + H + M \underset{k_{b_8}}{\overset{k_{f_8}}{\rightleftharpoons}} H_2 + M$	$2 \times 10^{18} T^{-1}$	$2.4 \times 10^{...} T^{-0.65} e^{(-51.956/T)}$
9	$H + OH + M \underset{k_{b_9}}{\overset{k_{f_9}}{\rightleftharpoons}} H_2O + M$	$2.2 \times 10^{21} T^{-1.5}$	$1.2 \times 10^{...} T^{-1.34} e^{(-59.3996/T)}$

* Data from Ref.

TABLE II - NUCLEATION RATE MODELS

FORM	B_1	B_2	X_7	Used By
1	p_v	1	$X_6 - W^*$	Volmer Zeldovich Frenkel Hill
2	p_v	1	$X_6 - W^* \left[1 - 2\left(\frac{2}{n^*}\right)^{2/3} + \frac{4}{n^*}\right]$	Yang
3	p_v	$\left[\left(\frac{3M_L}{4\pi\rho_L}\right)^{1/3} \frac{1}{r^*}\right]^2$	$X_6 - W^*$	Becker & Doring
4	p_v	$\left[\left(\frac{3M_L}{4\pi\rho_L}\right)^{1/3} \frac{1}{r^*}\right]^2$	$X_6 - W^* \left[1 - 3\left(\frac{1}{n^*}\right)^{2/3} + \frac{2}{n^*}\right]$	Becker & Doring, Barnard
5	αp_v	1	$X_6 - W^*$	Thomann
6	αp_{v_∞}	1	$X_6 - W^*$	Dufour & Defay

where $X_6 = \frac{1}{2}\ell n\left(\frac{2\sigma M_L}{\pi}\right) - 2\ \ell nk + \ell n\Gamma$

α = condensation coefficient; fraction of molecules that stick on impingement

M_L = mass of one molecule of condensed phase

n^* = number of molecules in a droplet of critical size

p_{v_∞} = equilibrium vapor pressure of the condensed specie

Γ = gasification factor (generally unity)

σ = surface tension

the radius of a critical drop is given by $r^* = \frac{2\sigma M_v}{\rho_r RT} \quad \frac{1}{\ell n\alpha}$

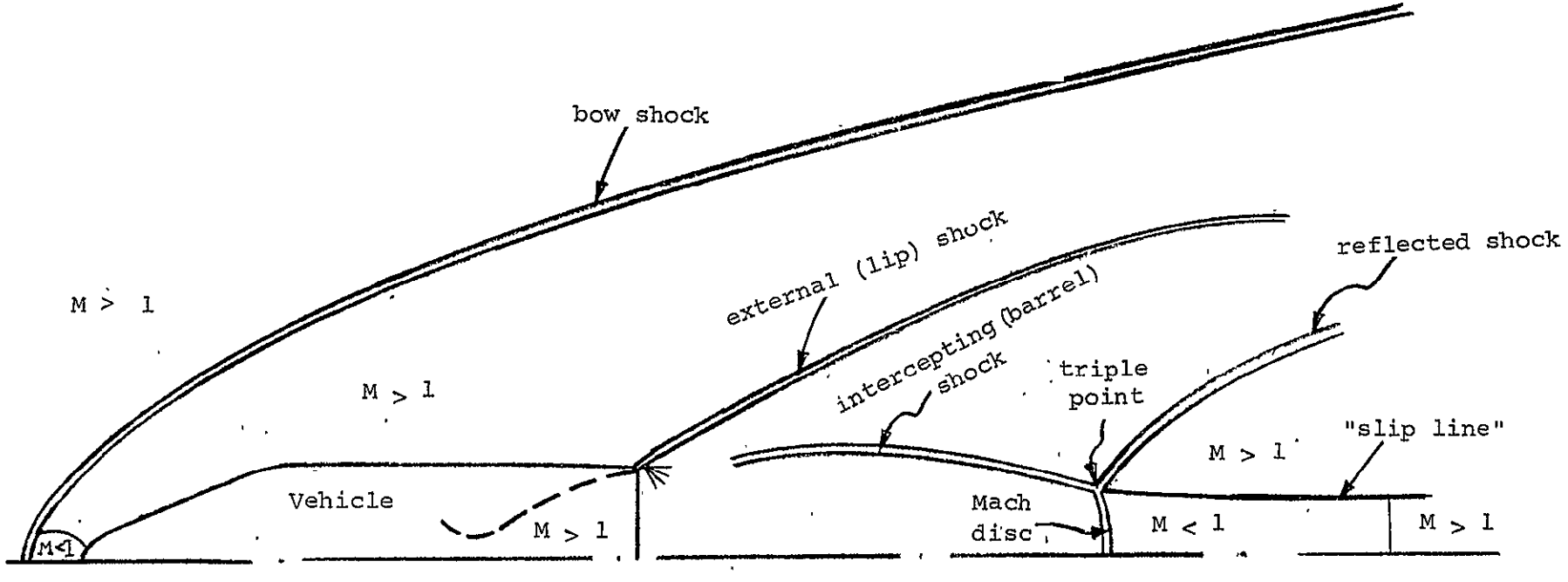

Fig. 1 - Schematic of flow field - supersonic missile with underexpanded exhaust

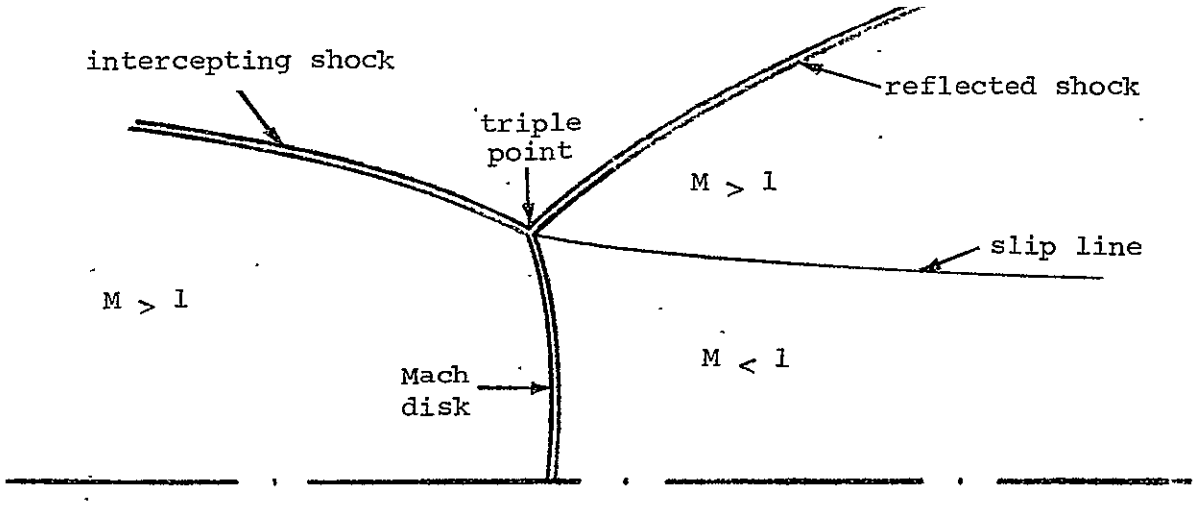

FIGURE 2 - TRIPLE POINT CONFIGURATION

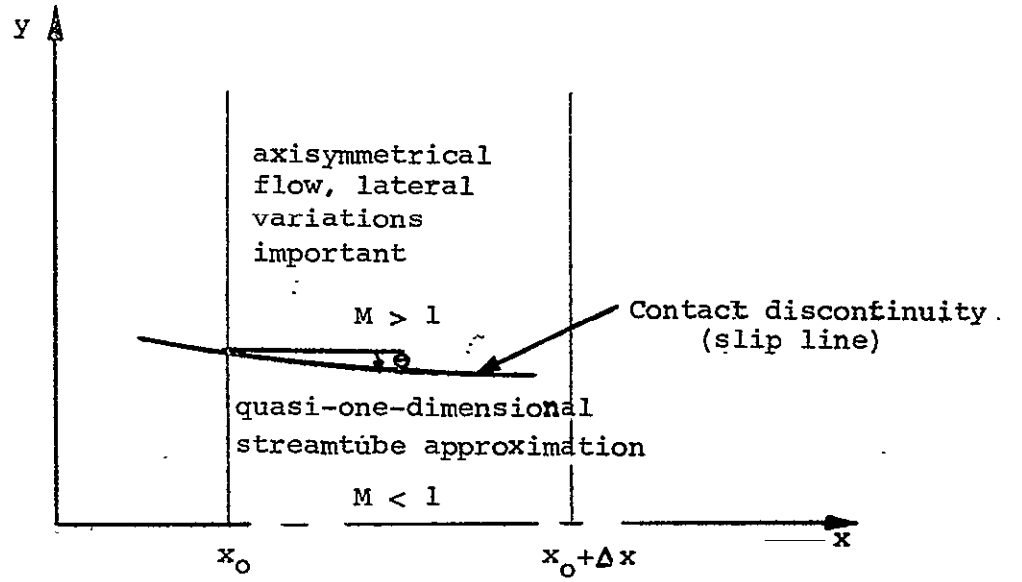

FIGURE 3 - SCHEMATIC OF FLOW DOWNSTREAM OF MACH DISC

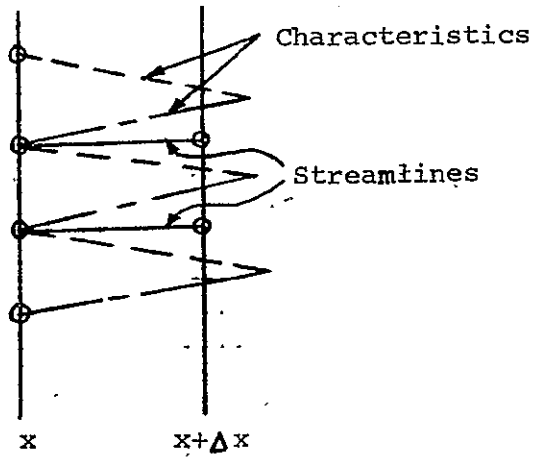

FIGURE 4 - SCHEMATIC OF MOCV COMPUTATIONAL PROCEDURE

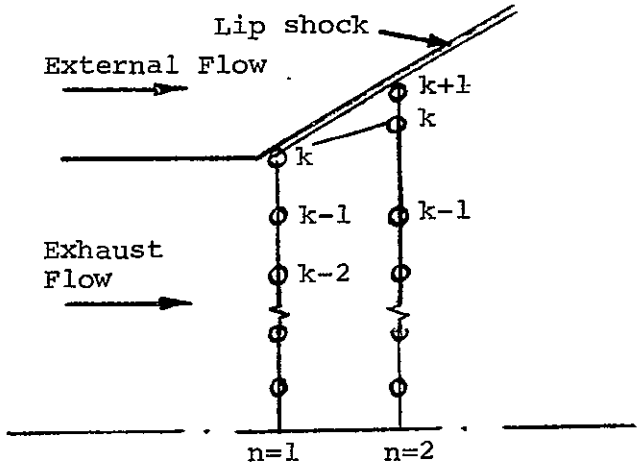

FIGURE 5 - SKETCH-STARTING MESH OF EDELMAN & WEILERSTEIN[9]

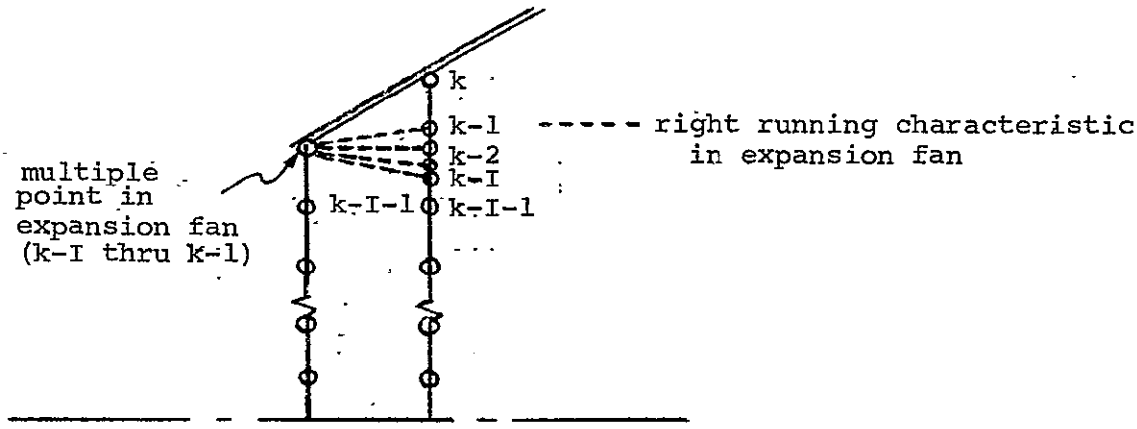

FIGURE 6 - SKETCH OF STARTING MESH FOR CURRENT EFFORT

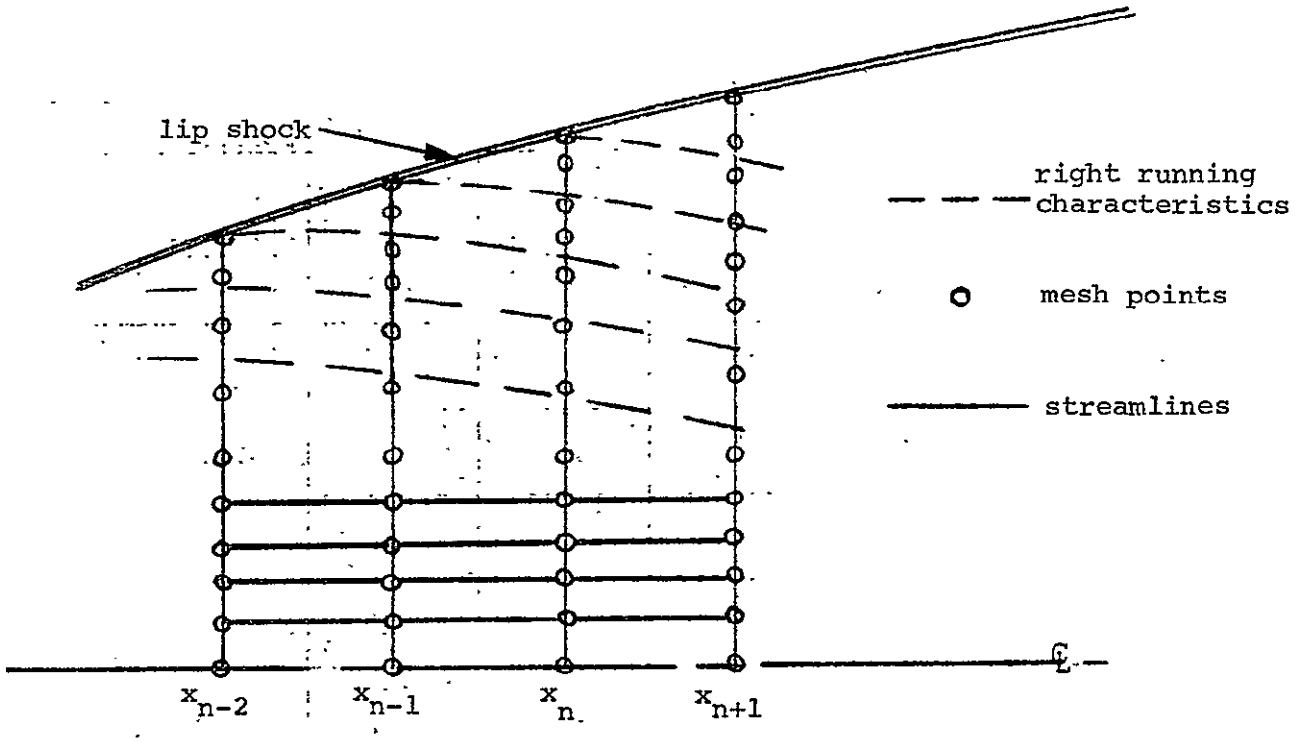

FIGURE 7 - SKETCH OF REGULAR CHARACTERISTIC MESH SUPERIMPOSED ON COMPUTATIONAL MESH

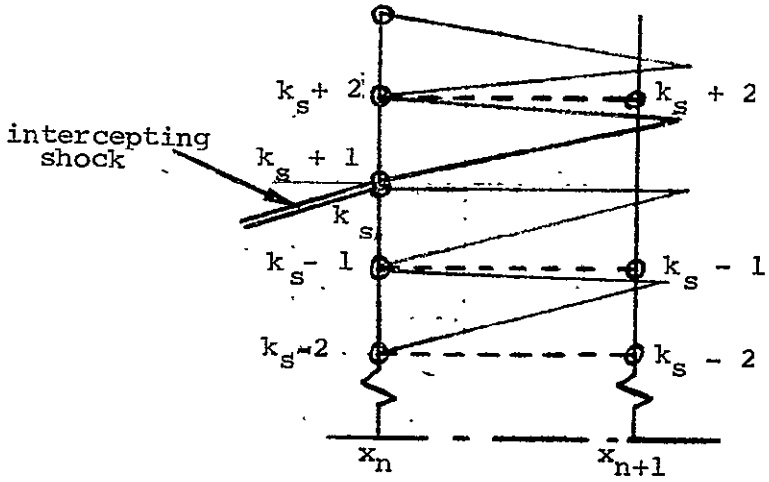

FIGURE 8a - SKETCH ILLUSTRATING COMPUTATIONAL PROCEDURE

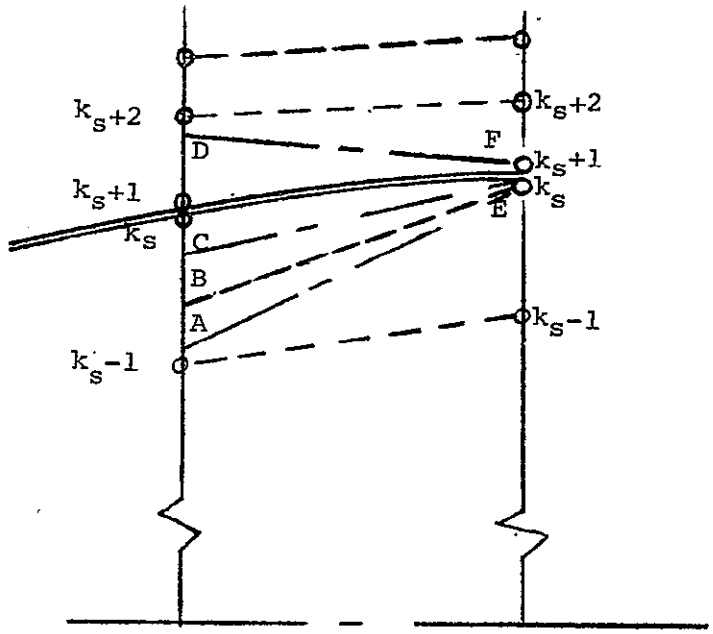

FIGURE 8b - SKETCH OF COMPUTATION AT INTERCEPTING SHOCK

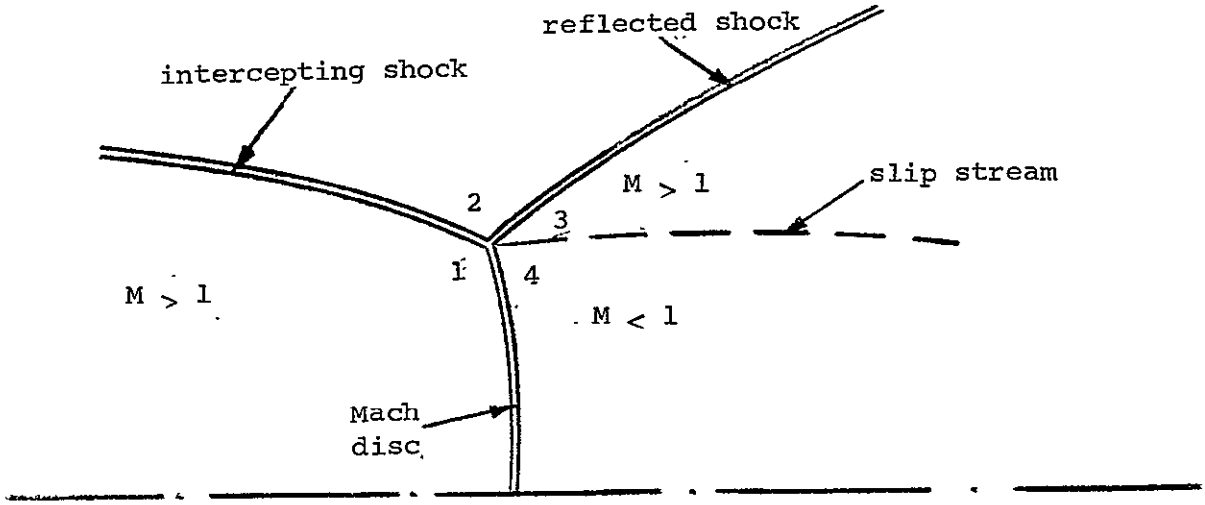

FIGURE 9 - SKETCH OF TRIPLE POINT COMPUTATION

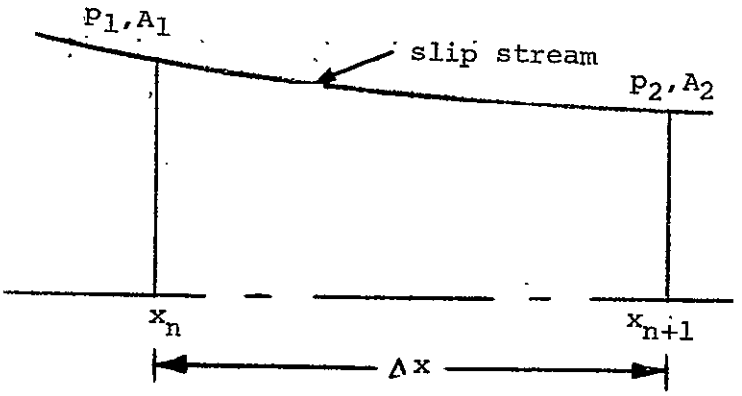

FIGURE 10 - SKETCH OF SUBSONIC CORE STREAMTUBE

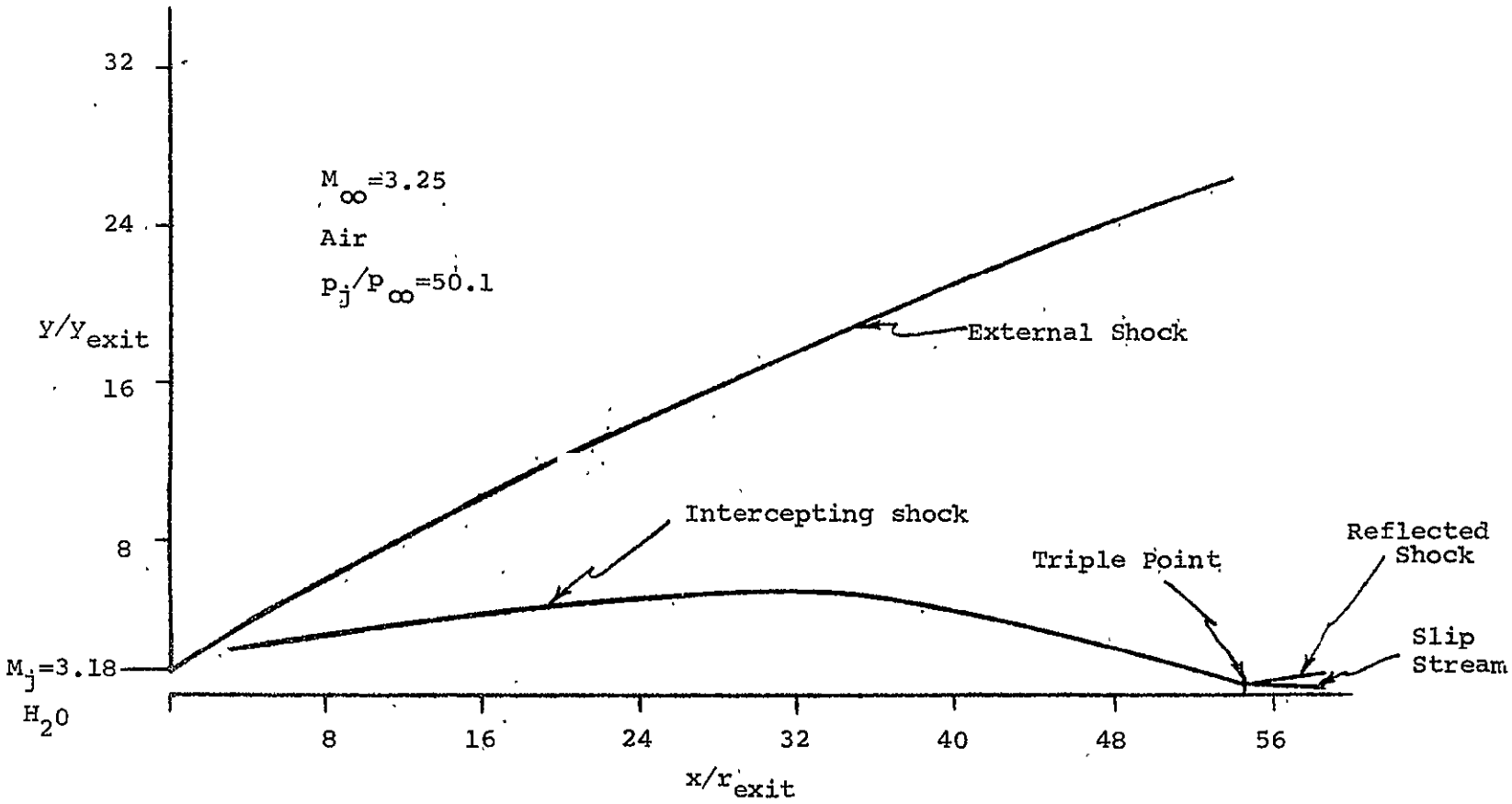

FIGURE 11 - SAMPLE CALCULATION

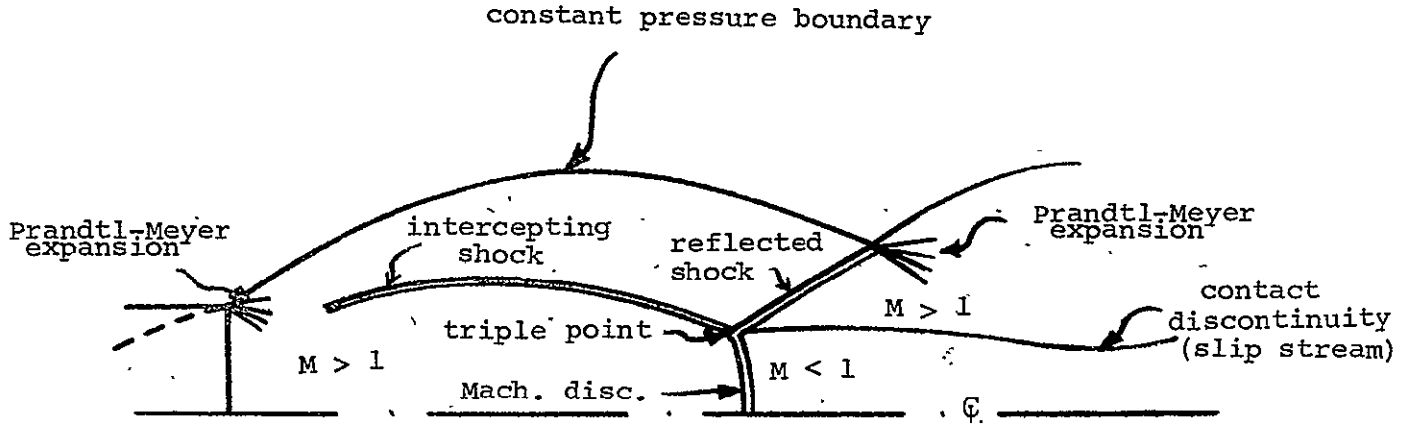

a) static ambient

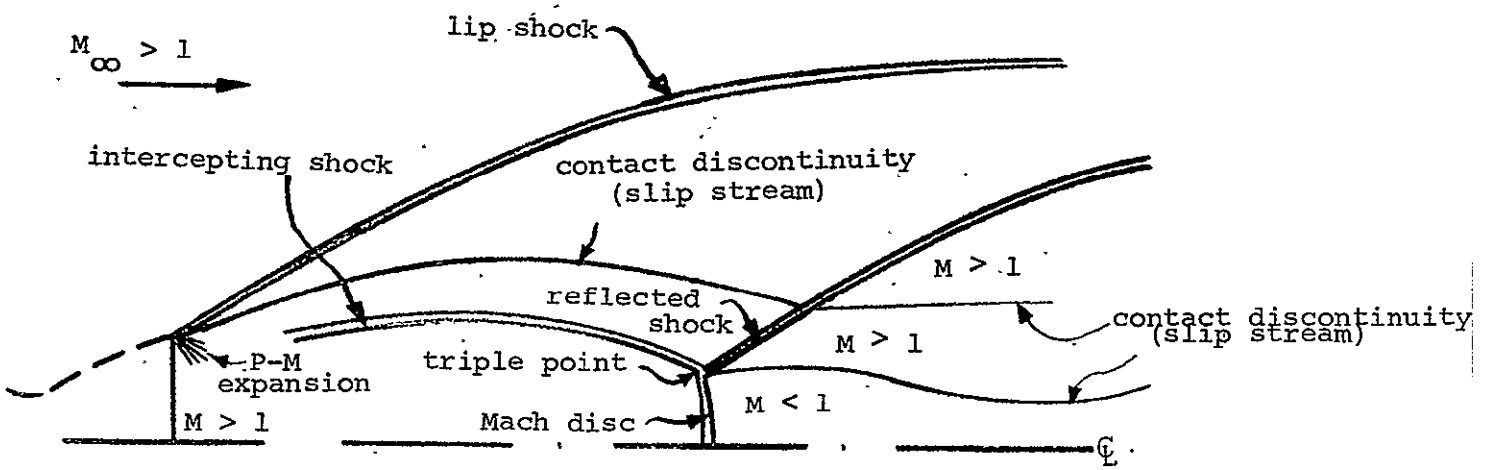

b) supersonic ambient

FIGURE 12 - INVISCID PLUME OF AN UNDEREXPANDED NOZZLE

FIGURE 13 - CORE-STREAMTUBE MACH NUMBER VS AXIAL DISTANCE FOR VARIOUS ASSUMED TRIPLE POINT LOCATIONS

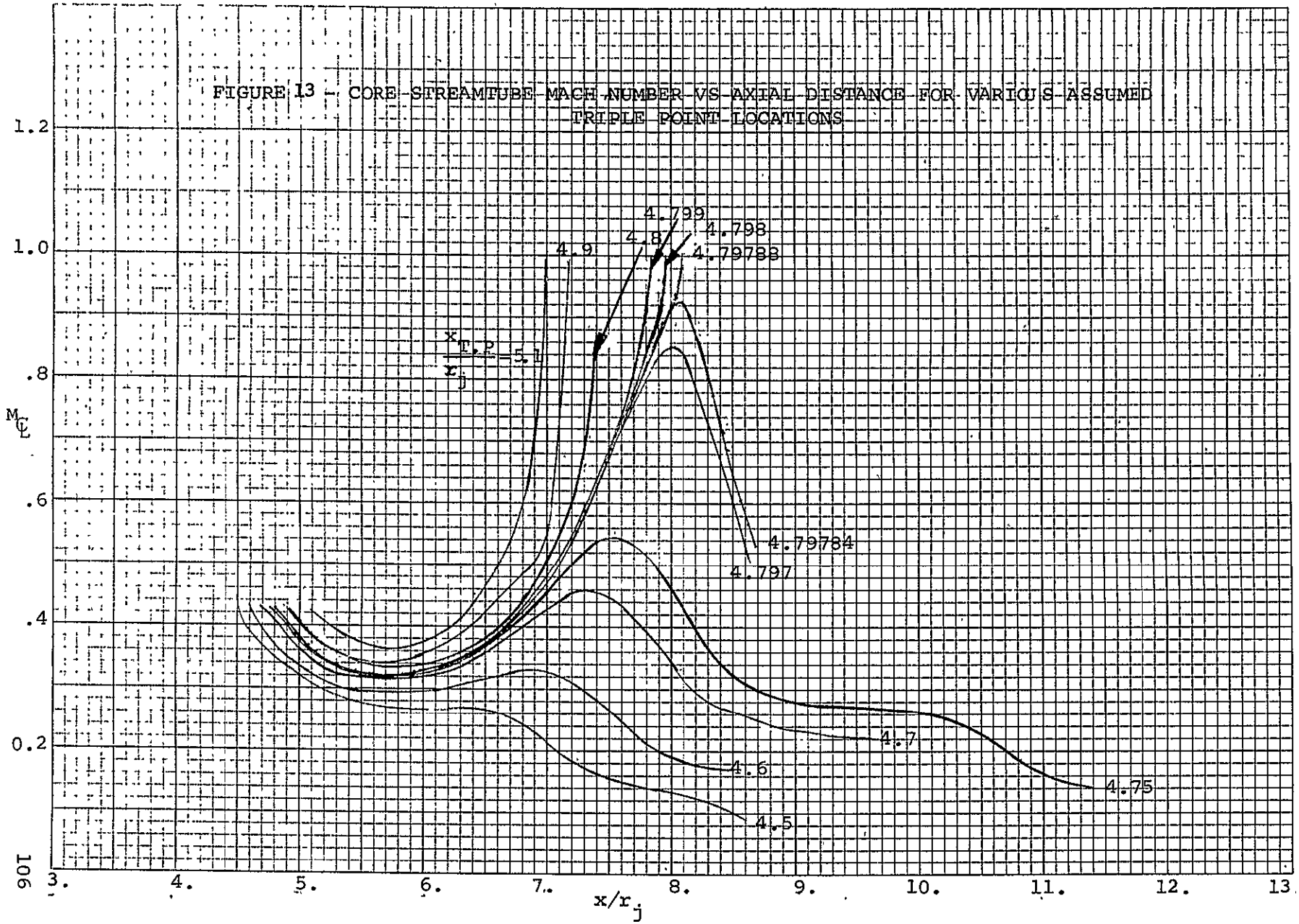

FIGURE 14 - SLIP LINE SLOPE VS CORE MACH NUMBER FOR VARIOUS ASSUMED VALUES OF TRIPLE POINT LOCATIONS

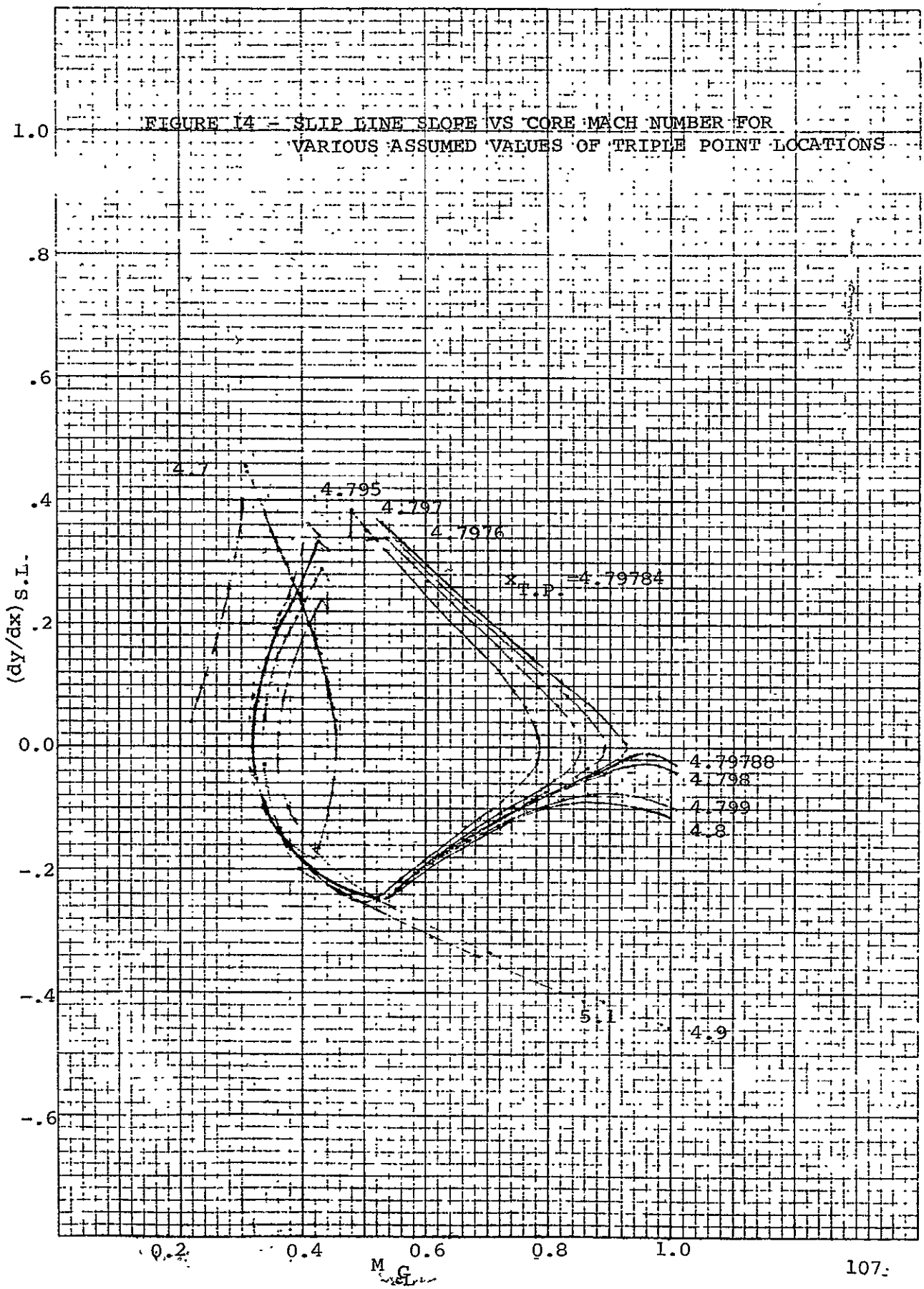

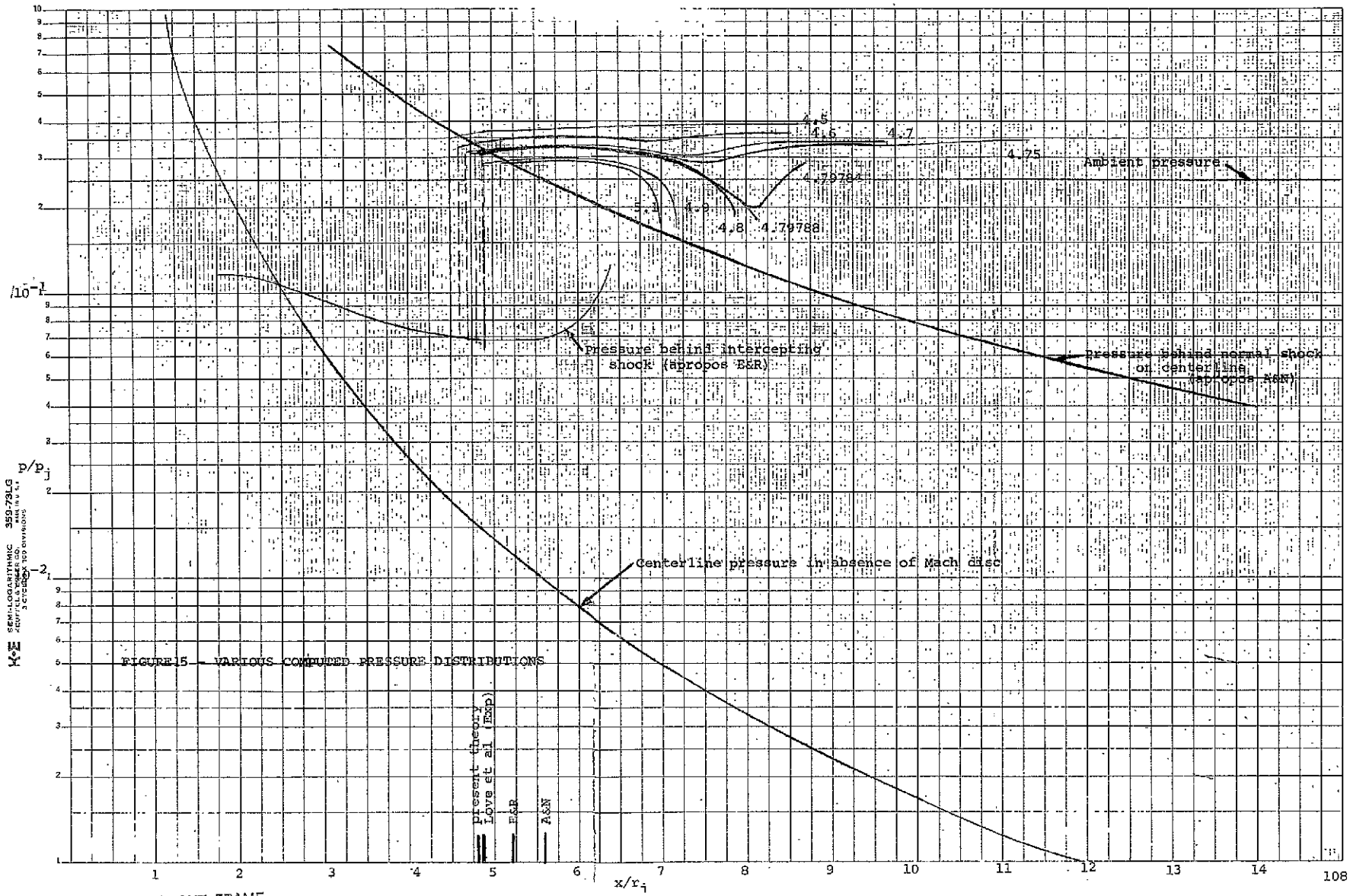

FIGURE 15 -- VARIOUS COMPUTED PRESSURE DISTRIBUTIONS

FOLDOUT FRAME

FOLDOUT FRAME 2

FIGURE 16- ANGLE BETWEEN MACH DISC AND INCIDENT FLOW VS. AXIAL POSITION OF ASSUMED TRIPLE POINT

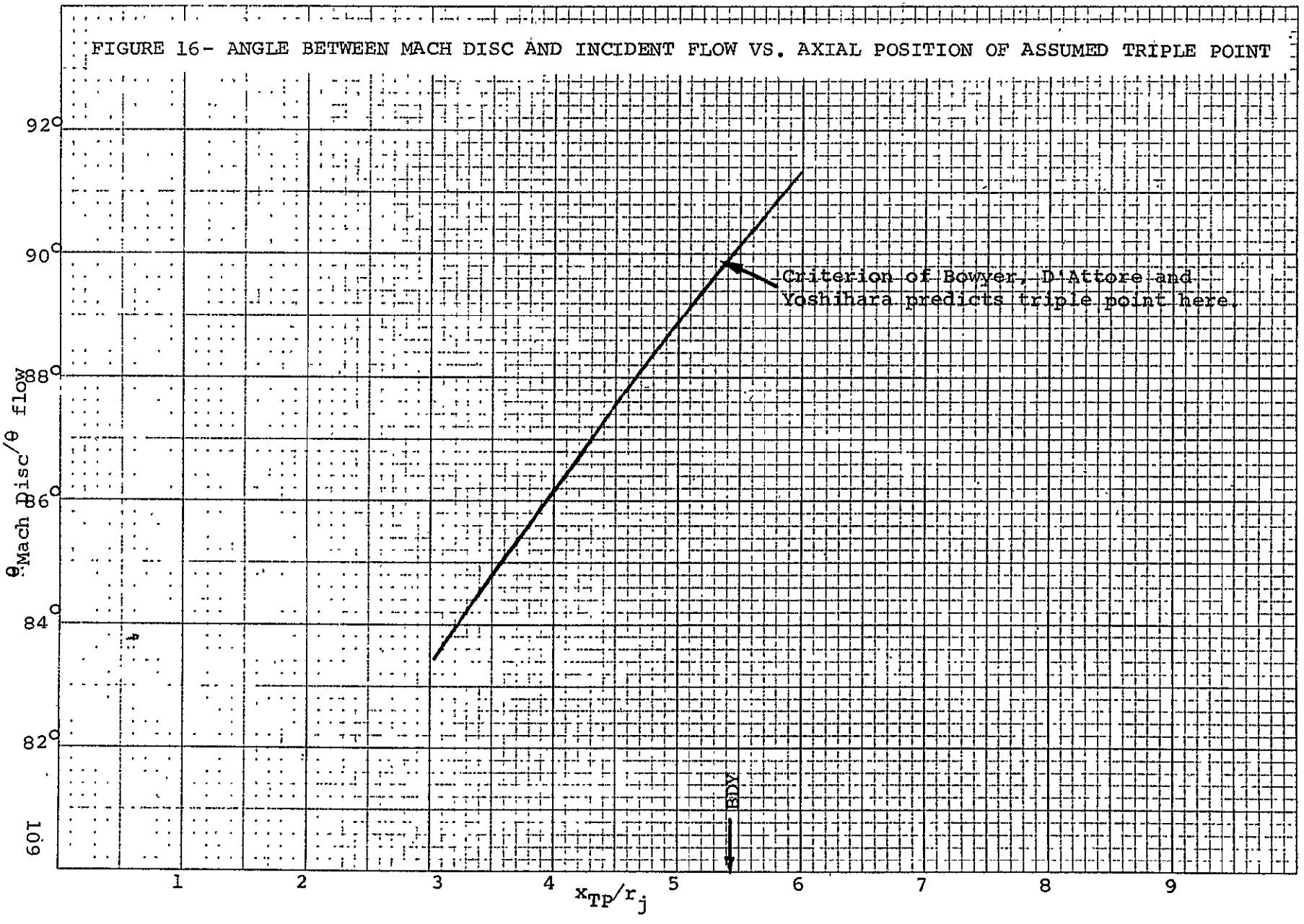

FIGURE 17- PARAMETERS PINPOINTING THE SOLUTION

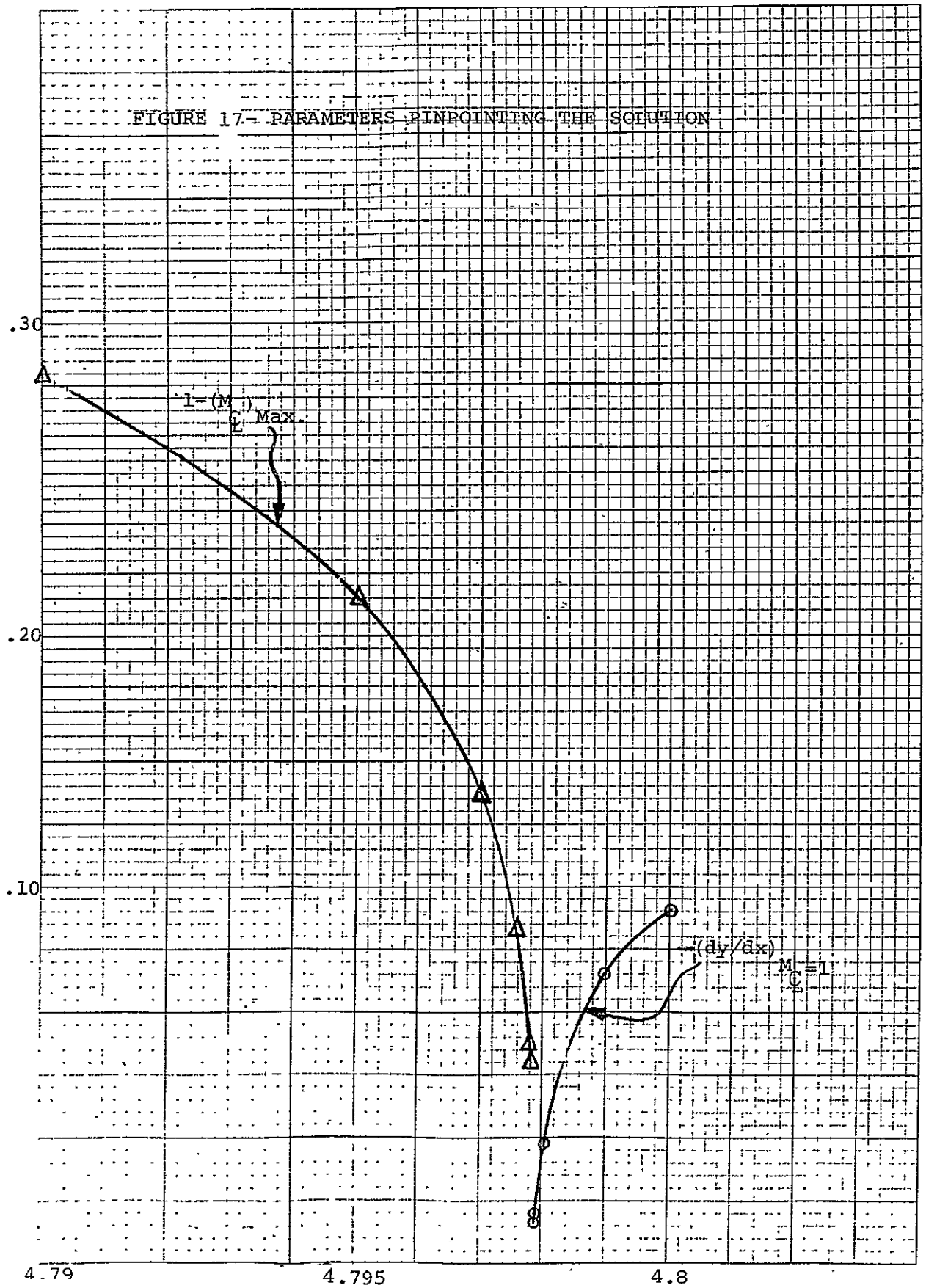

FIGURE 18 - COMPARISON OF THEORETICAL AND EXPERIMENTAL TRIPLE POINT LOCATIONS

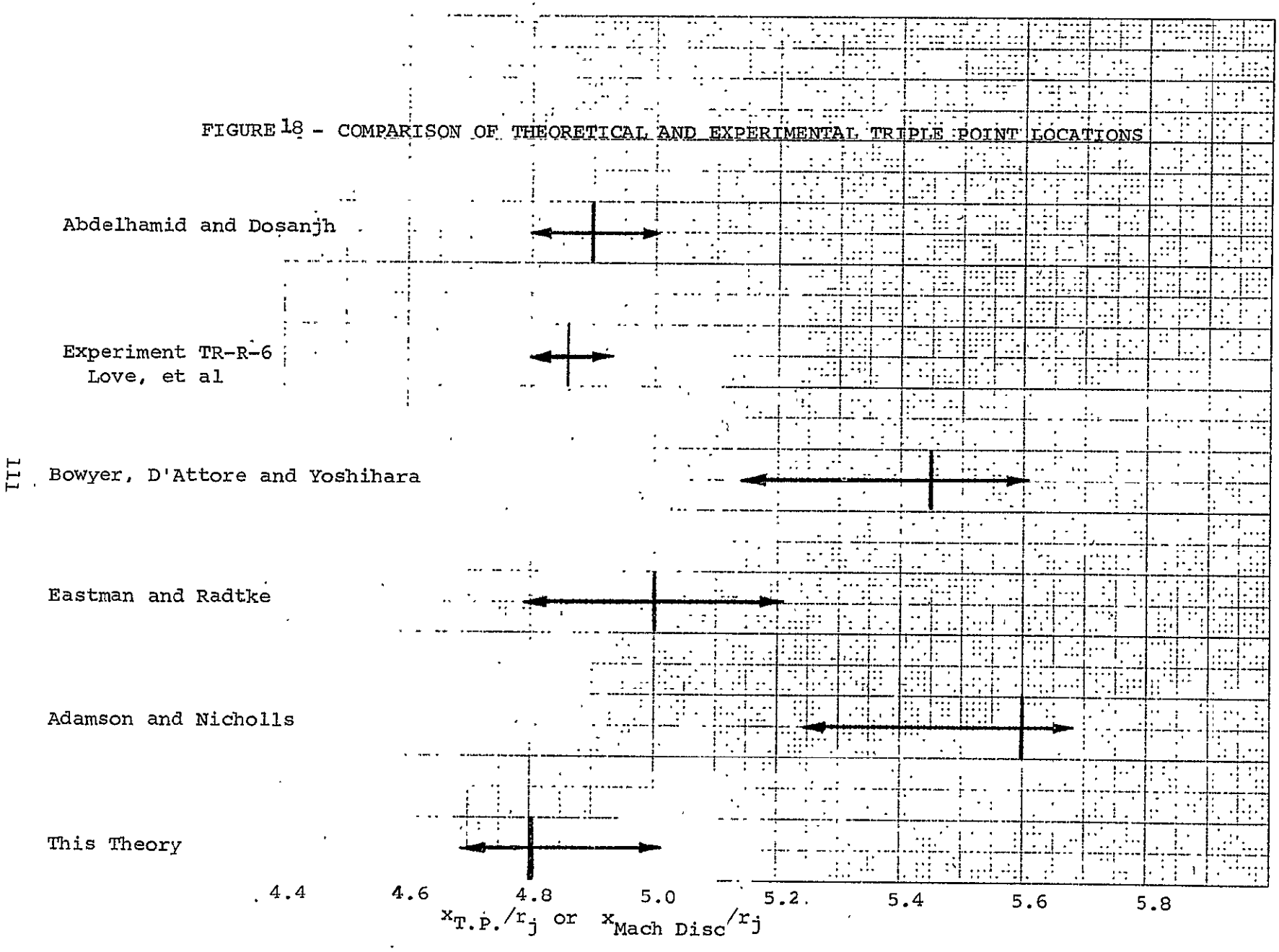

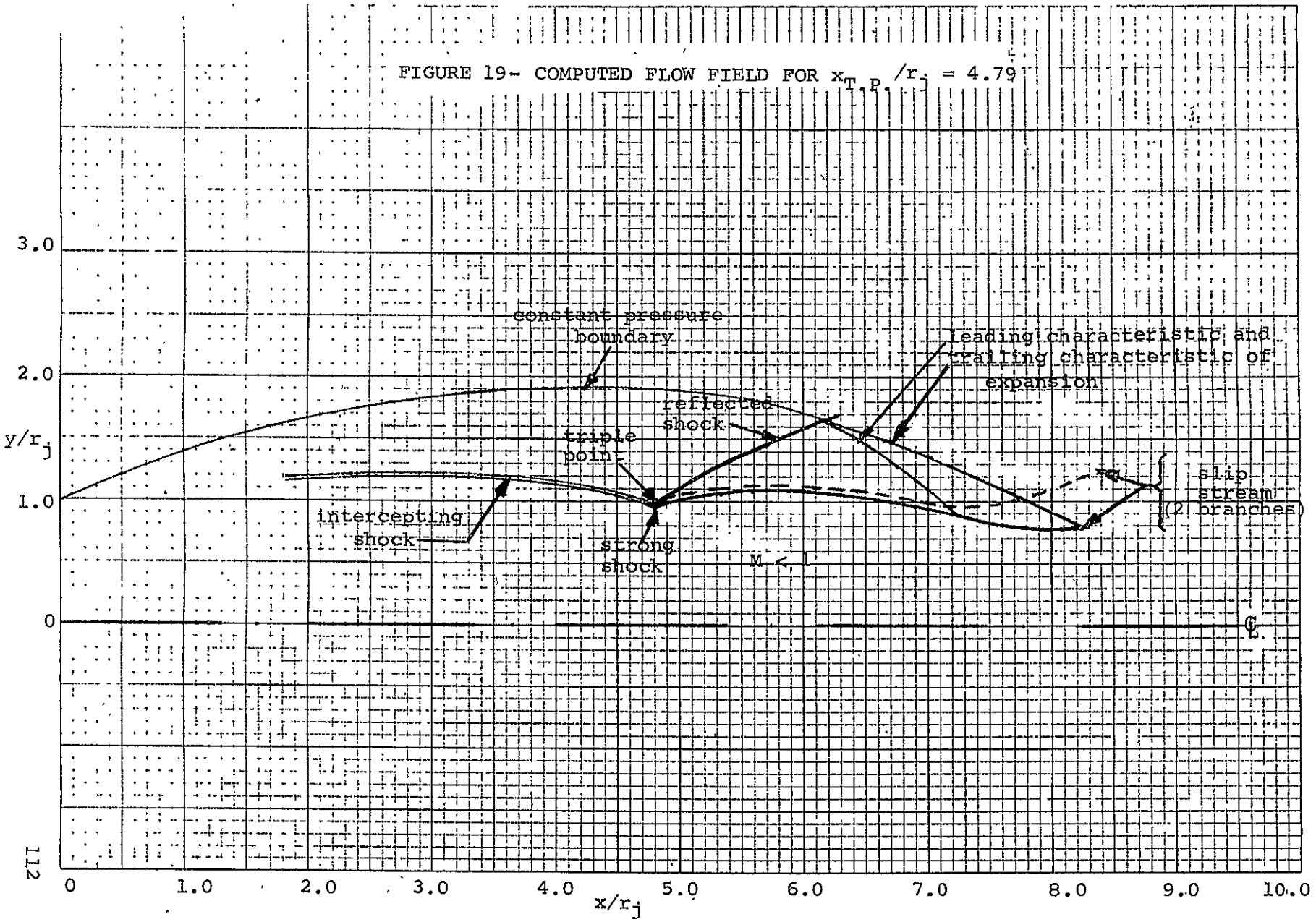
FIGURE 19- COMPUTED FLOW FIELD FOR $x_{T.P.}/r_j$ = 4.79
constant pressure boundary
leading characteristic and trailing characteristic of expansion
reflected shock
triple point
slip stream (2 branches)
intercepting shock
strong shock
M < 1
$\mathbb{C}_L$
3.0
2.0
1.0
0
y/r_j
0
1.0
2.0
3.0
4.0
5.0
6.0
7.0
8.0
9.0
10.0
x/r_j

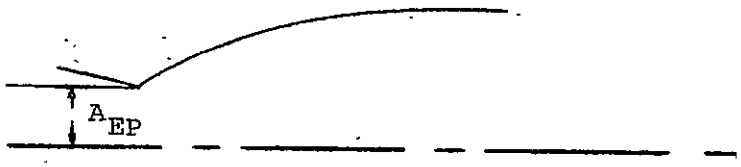

FIGURE 20 - SCHEMATIC OF UNDEREXPANDED SONIC NOZZLE IN A QUIESCENT ENVIRONMENT

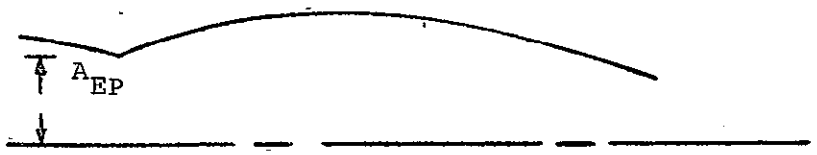

FIGURE 21 - SCHEMATIC OF UNDEREXPANDED SONIC NOZZLE IN THE ABSENCE OF INTERNAL SHOCKS

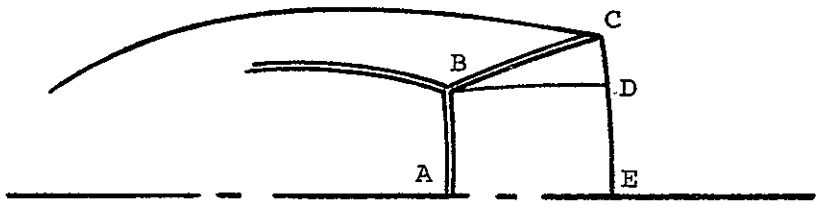

FIGURE 22 - SCHEMATIC OF INTERNAL SHOCK STRUCTURE IN THE VICINITY OF THE TRIPLE POINT

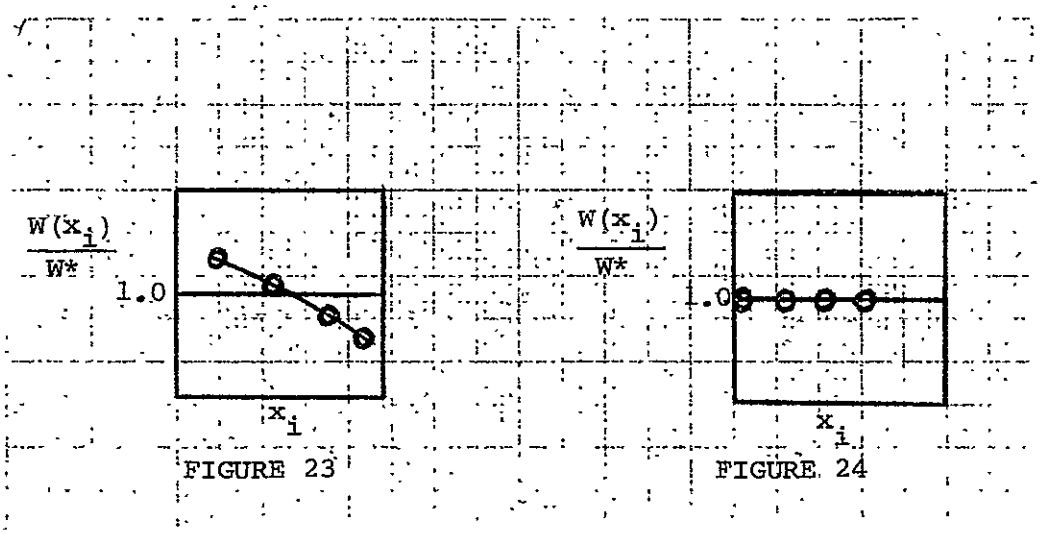

FIGURE 23 FIGURE 24

NORMALIZED MASS FLOW VS AXIAL DISTANCE

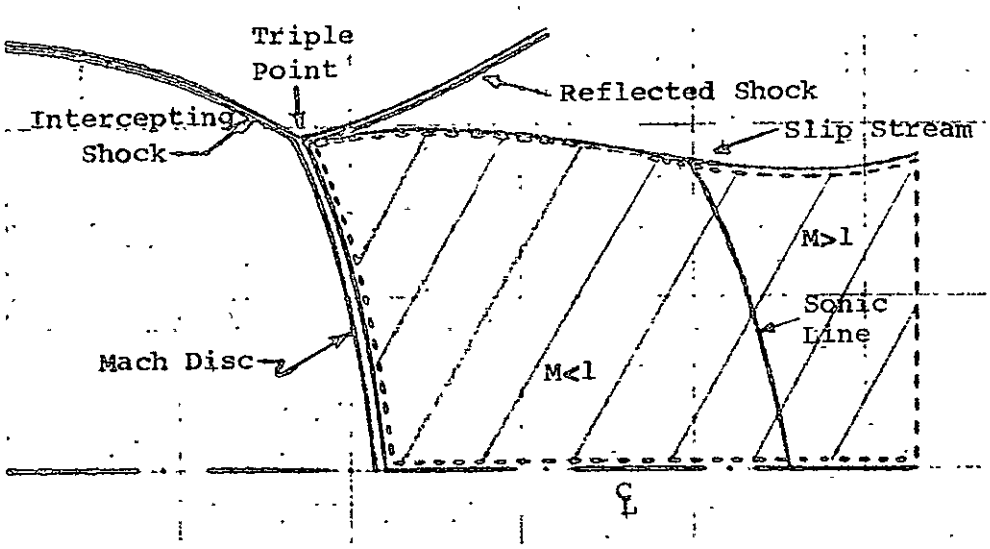

FIGURE 25 - FLOW NEAR & DOWNSTREAM OF THE TRIPLE POINT MACH DISC

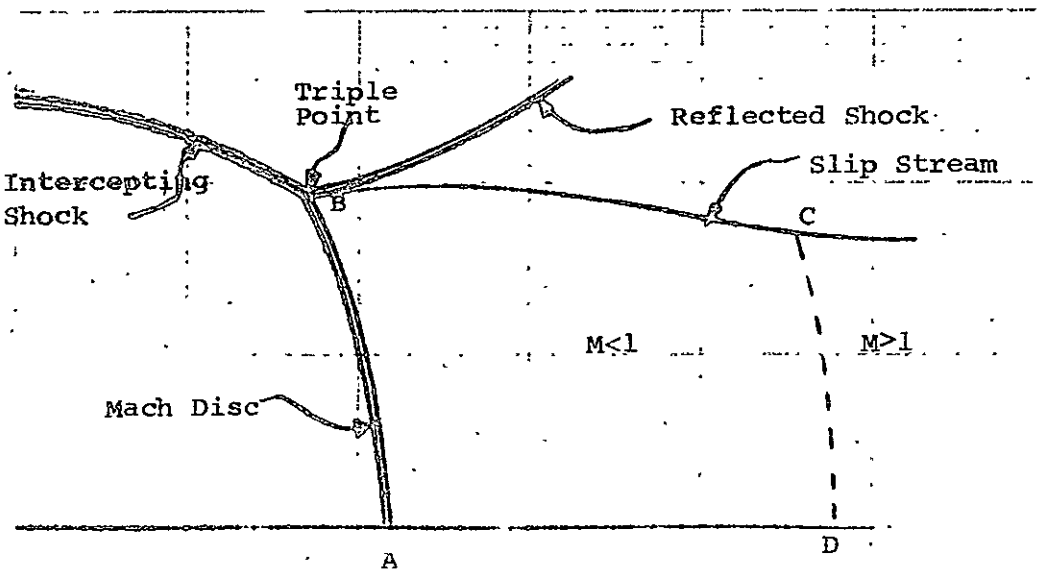

FIGURE 26 - COMPUTATIONAL REGION FOR TRANSONIC FLOW

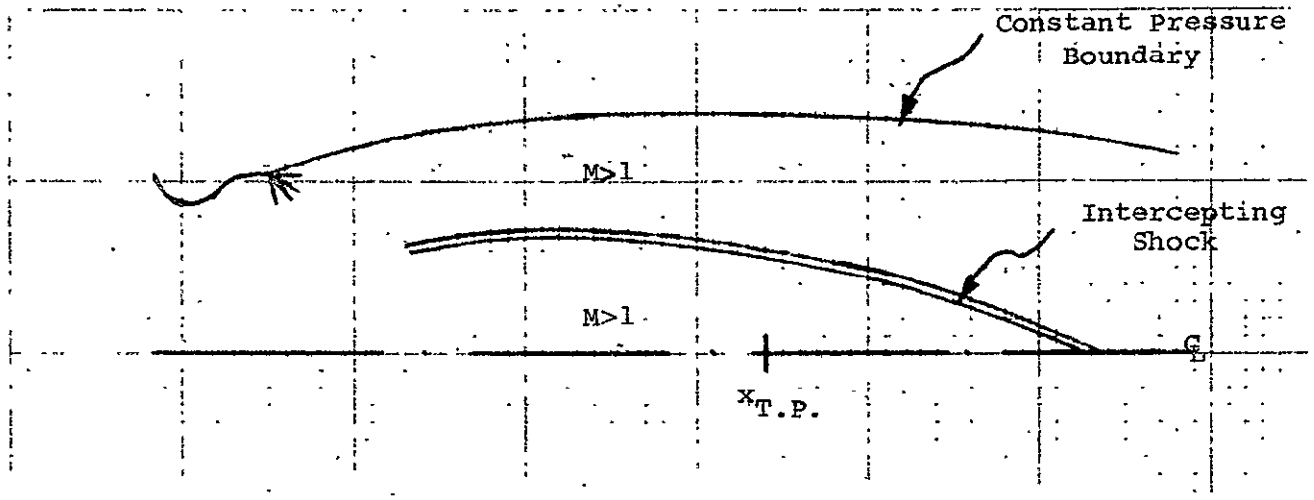

FIGURE 27a - REGION TO BE COMPUTED AS STEADY SUPERSONIC FLOW

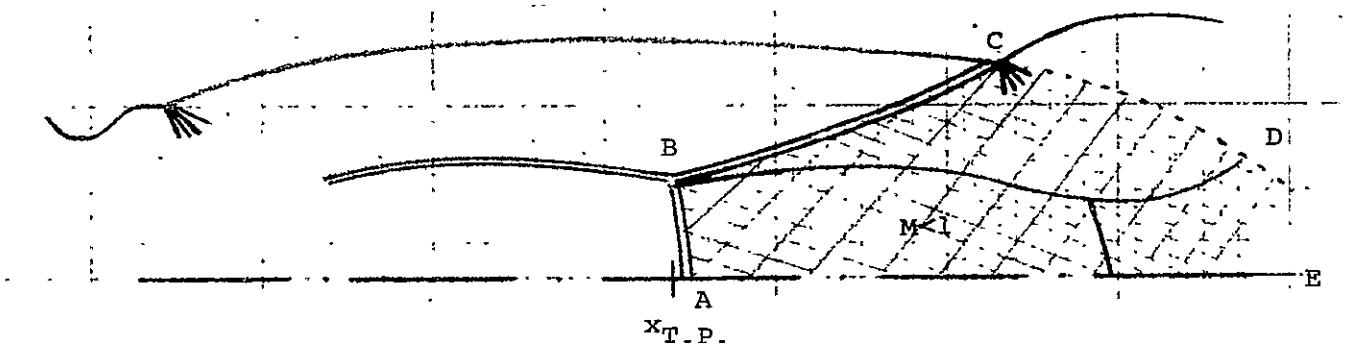

FIGURE 27b - REGION TO BE COMPUTED WITH UNSTEADY PROCEDURE

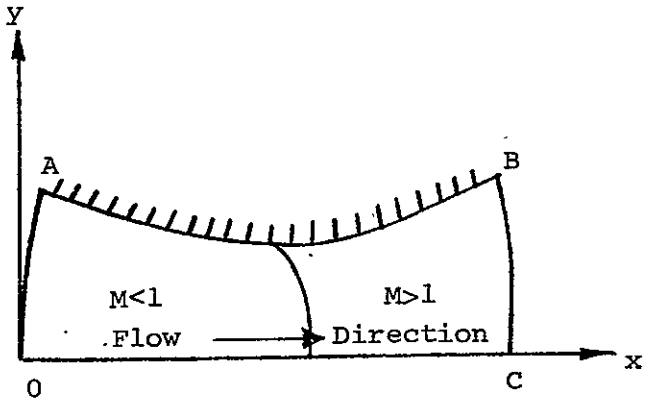

FIGURE 28 - TWO-DIMENSIONAL deLAVAL NOZZLE

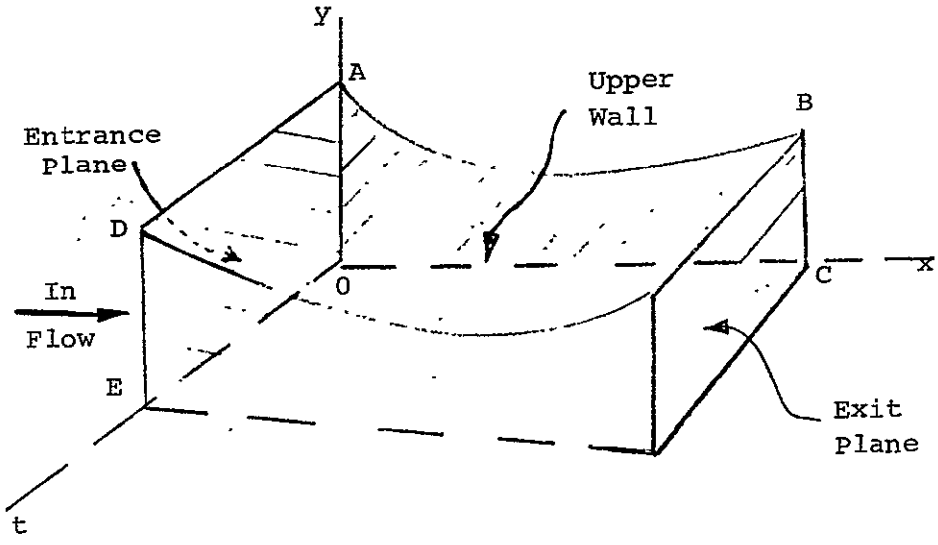

FIGURE 29 - SCHEMATIC OF THE UNSTEADY INITIAL VALUE BOUNDARY VALUE PROBLEM

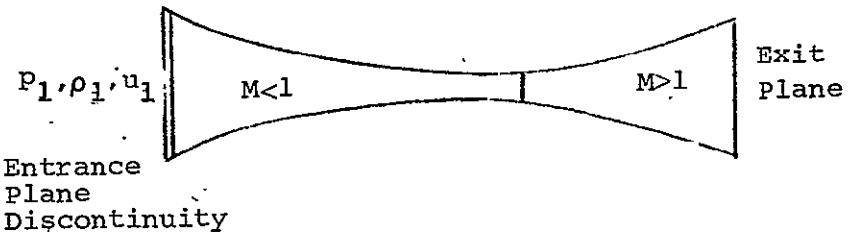

FIGURE 30 - QUASI-ONE-DIMENSIONAL deLAVAL NOZZLE UNSTEADY FLOW

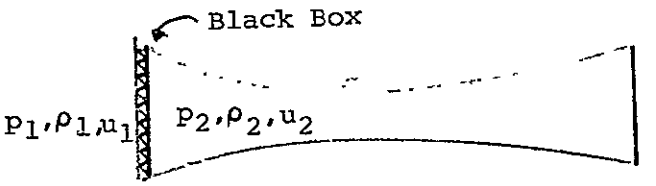

FIGURE 31 - SCHEMATIC OF THE ENTRANCE PLANE "BLACK BOX"

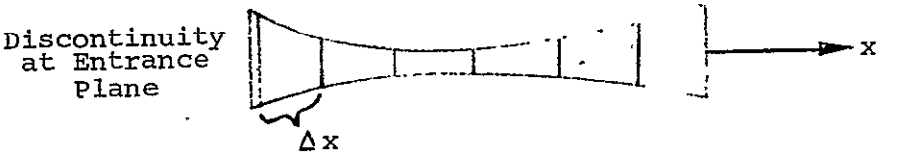

FIGURE 32 - QUASI-ONE-DIMENSIONAL deLAVAL NOZZLE COMPUTATIONAL GRID

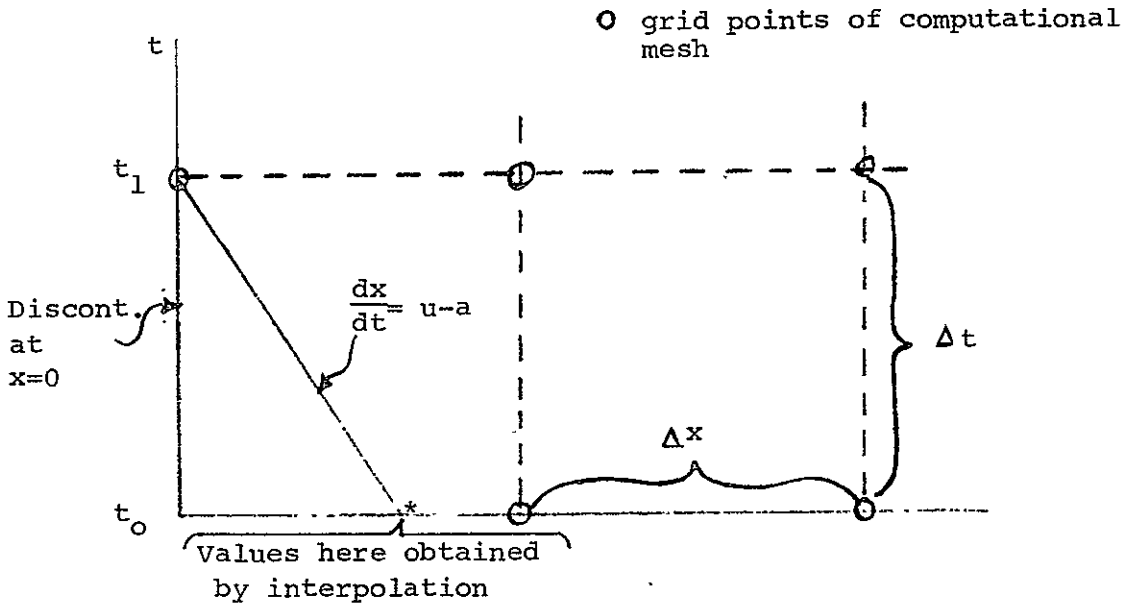

FIGURE 33 - COMPUTATIONAL SCHEME AT ENTRANCE DISCONTINUITY

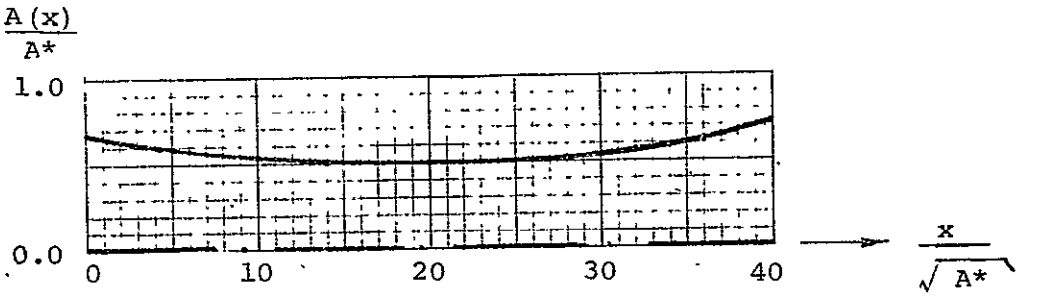

nozzle geometry
(a)

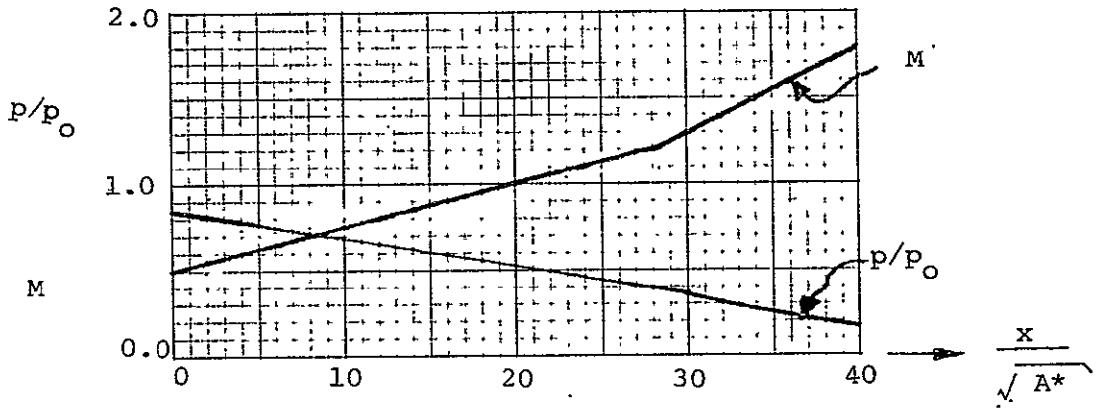

exact steady solution
(b)

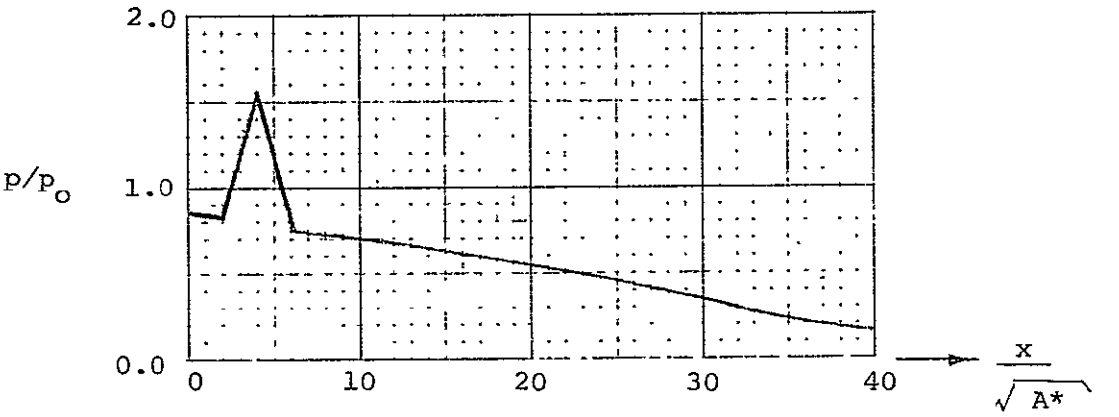

assumed initial pressure distribution
(c)

FIGURE 34- QUASI-ONE-DIMENSIONAL deLaval NOZZLE

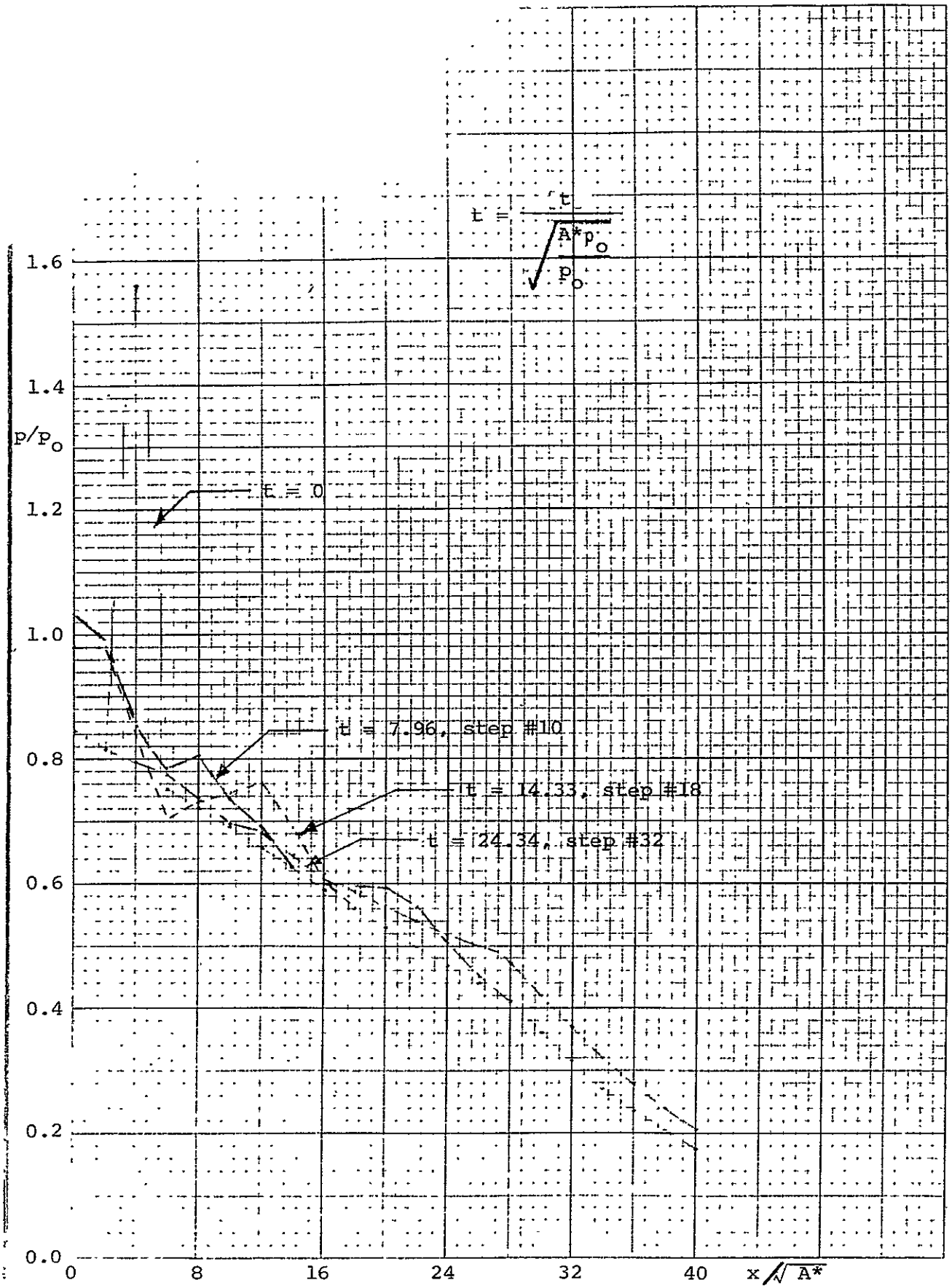

FIGURE 35 - QUASI-ONE-DIMENSIONAL deLAVAL NOZZLE - PRESSURE DISTRIBUTION AT SEVERAL TIMES

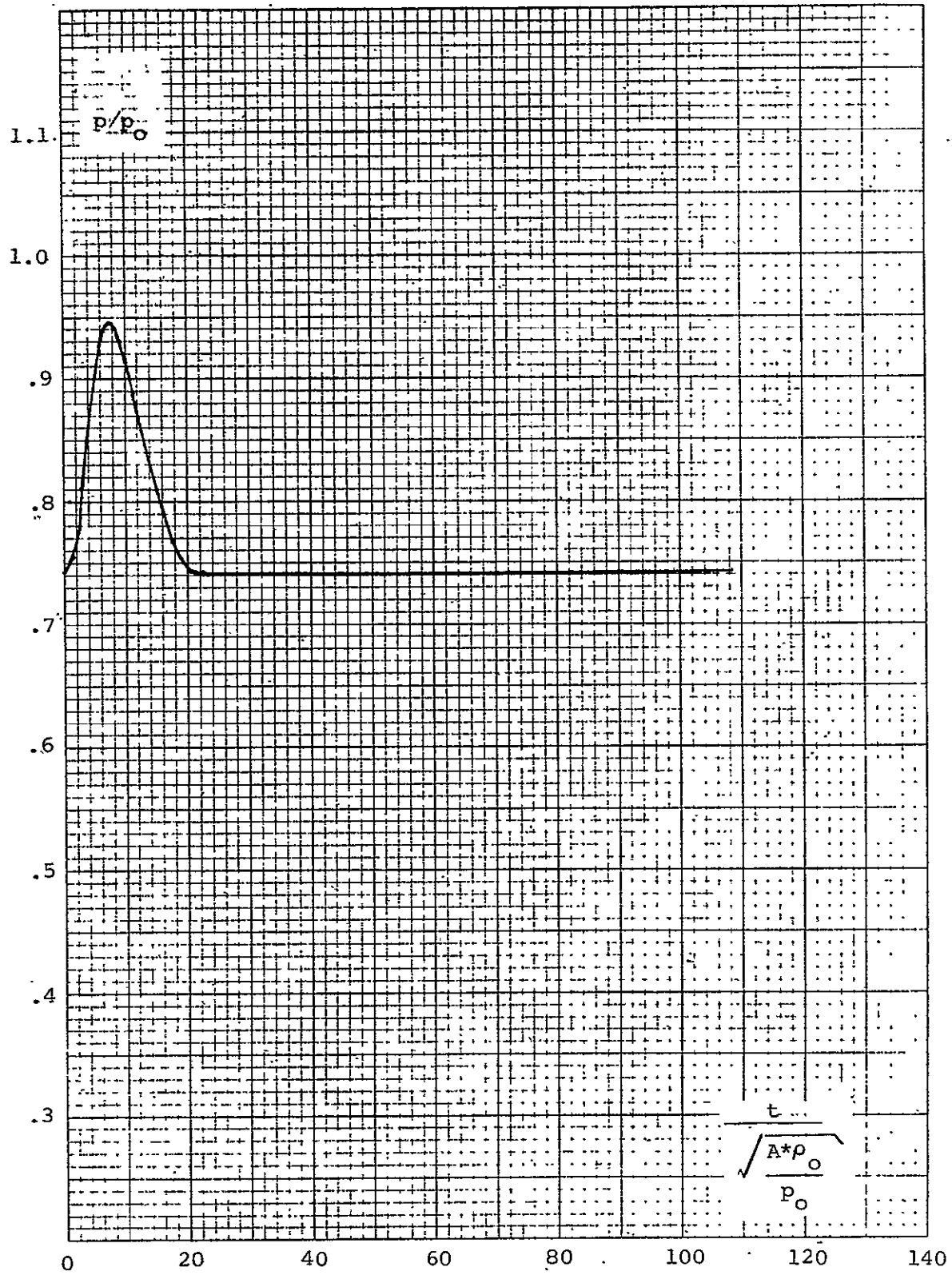

FIGURE 36- PRESSURE VS. TIME ON DOWNSTREAM SIDE OF THE DISCONTINUITY-QUASI-ONE-DIMENSIONAL deLaval NOZZLE

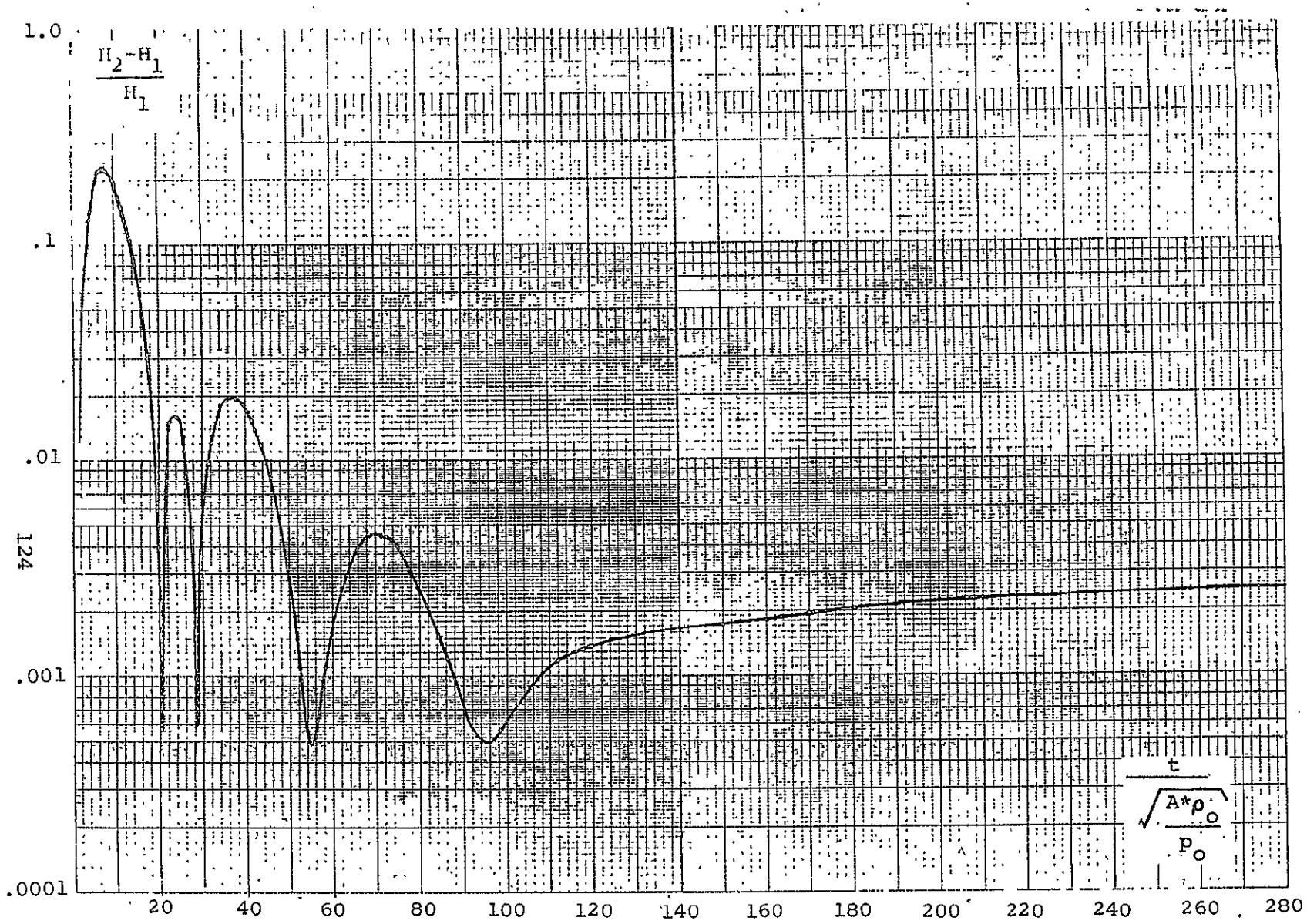

FIGURE 37- HISTORY OF WORK PERFORMED AT THE ENTRANCE PLANE- QUASI-ONE-DIMENSIONAL deLaval NOZZLE

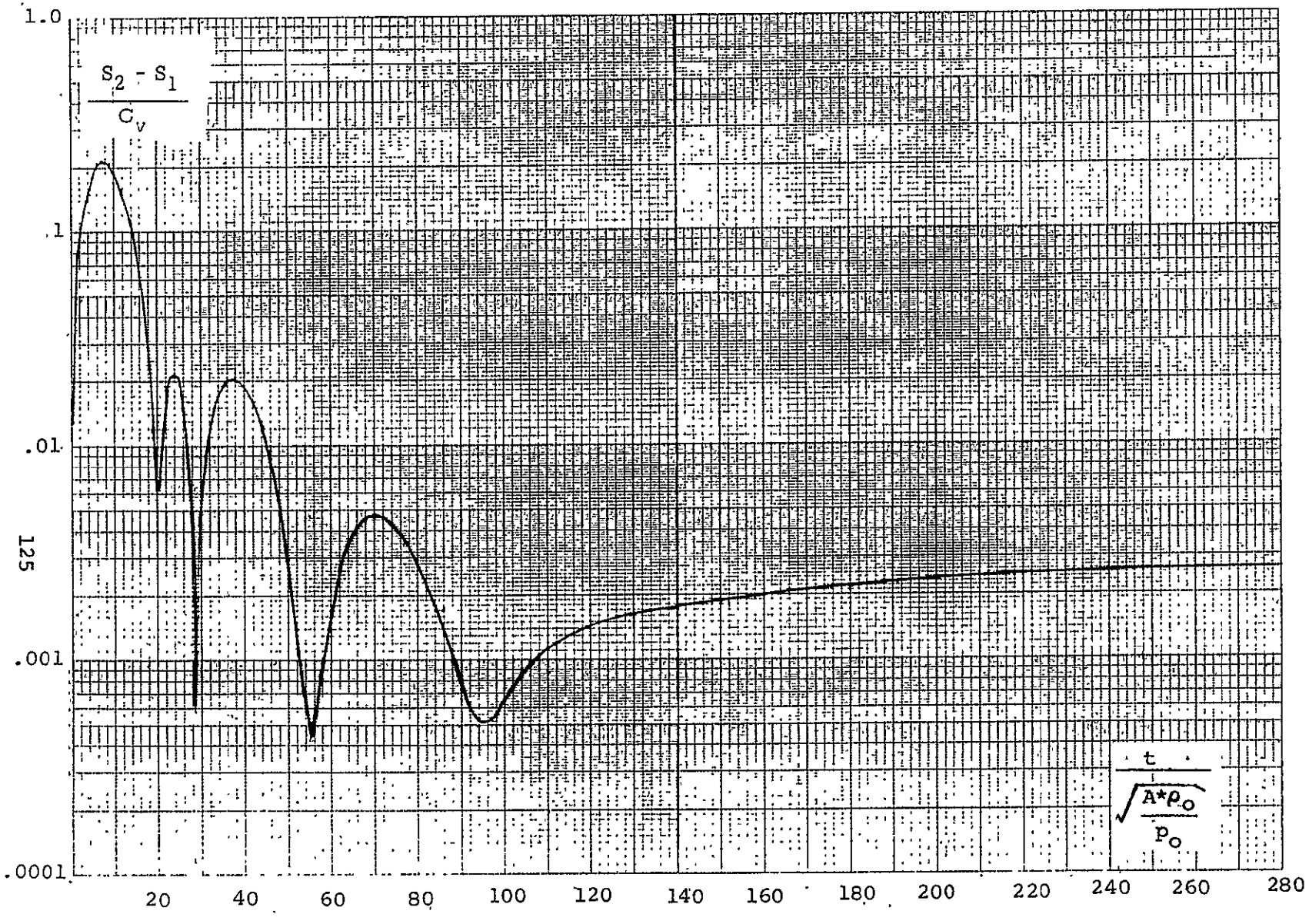

FIGURE 38 - ENTROPY JUMP AT ENTRANCE PLANE DISCONTINUITY-QUASI-ONE-DIMENSIONAL deLaval NOZZLE

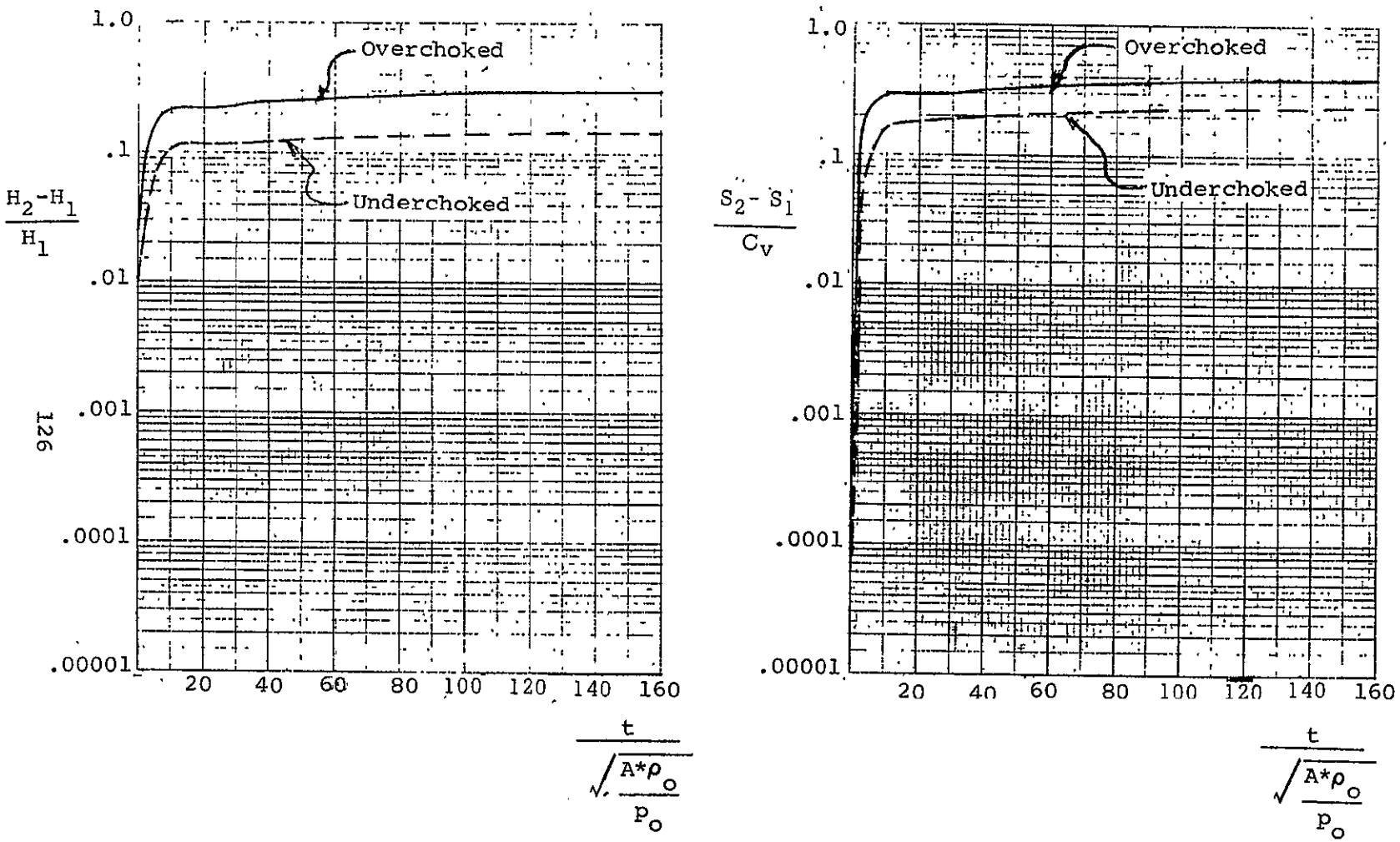

FIGURE 39- DISCONTINUITY WORK AND ENTROPY JUMP HISTORIES FOR "OVERCHOKED"AND "UNDERCHOKED" QUASI-ONE-DIMENSIONAL NOZZLES

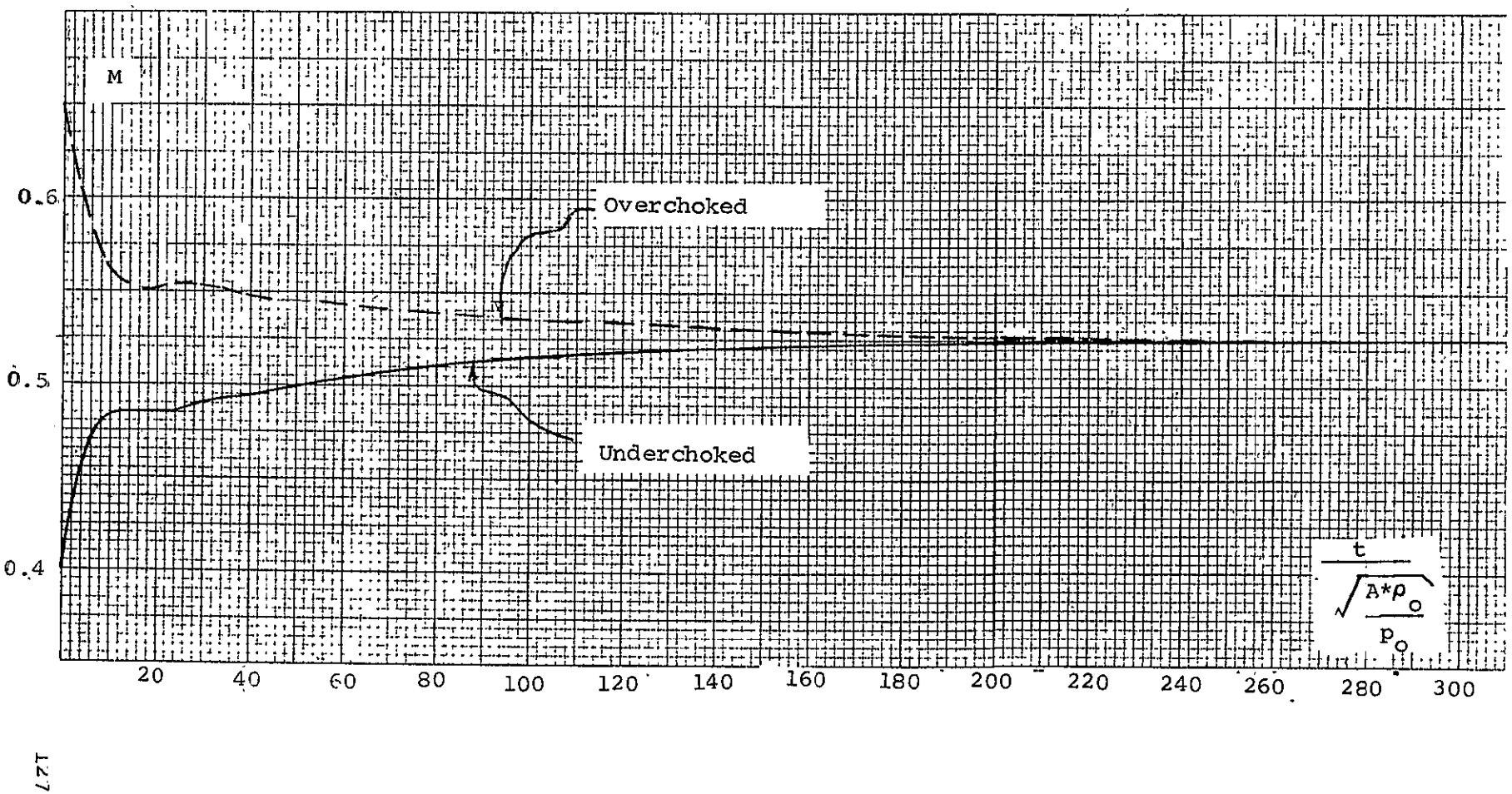

FIGURE 40- MACH NUMBER BEHIND THE DISCONTINUITY FOR "OVERCHOKED" AND "UNDERCHOKED" IN QUASI-ONE-DIMENSIONAL NOZZLES

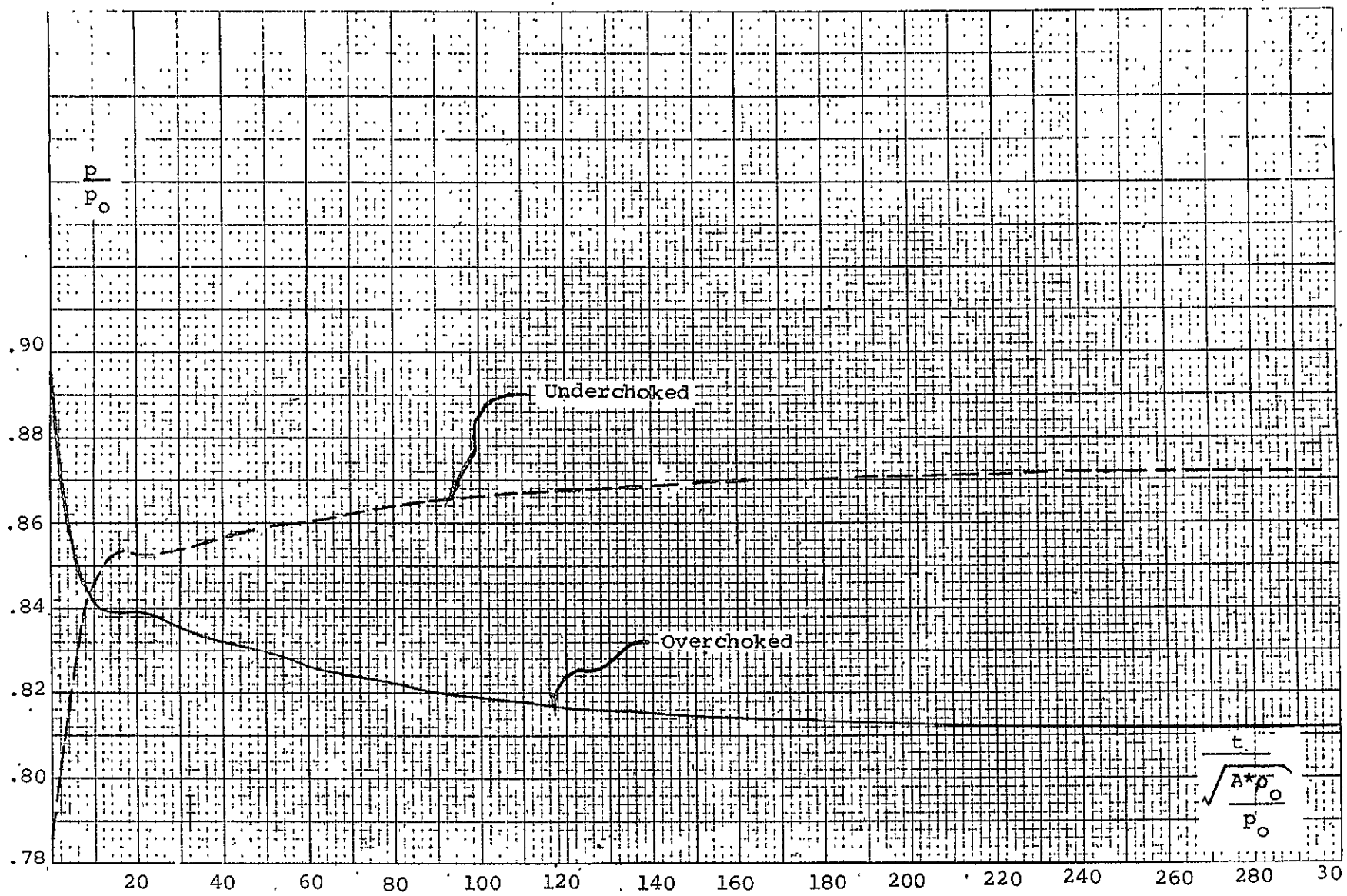

FIGURE 41- PRESSURE BEHIND THE DISCONTINUITY IN "OVERCHOKED" AND "UNDERCHOKED" QUASI-ONE-DIMENSIONAL NOZZLES

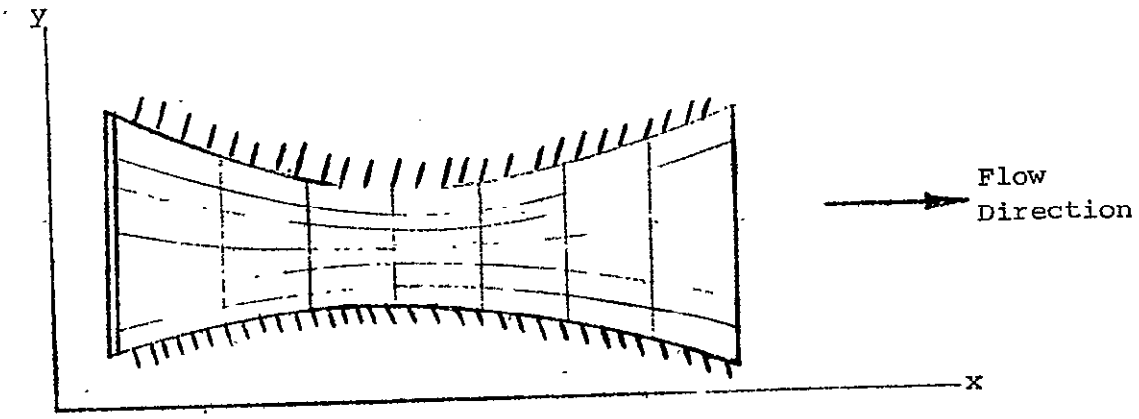

FIGURE 42 - COMPUTATIONAL GRID IN PHYSICAL SPACE
TIME = CONSTANT

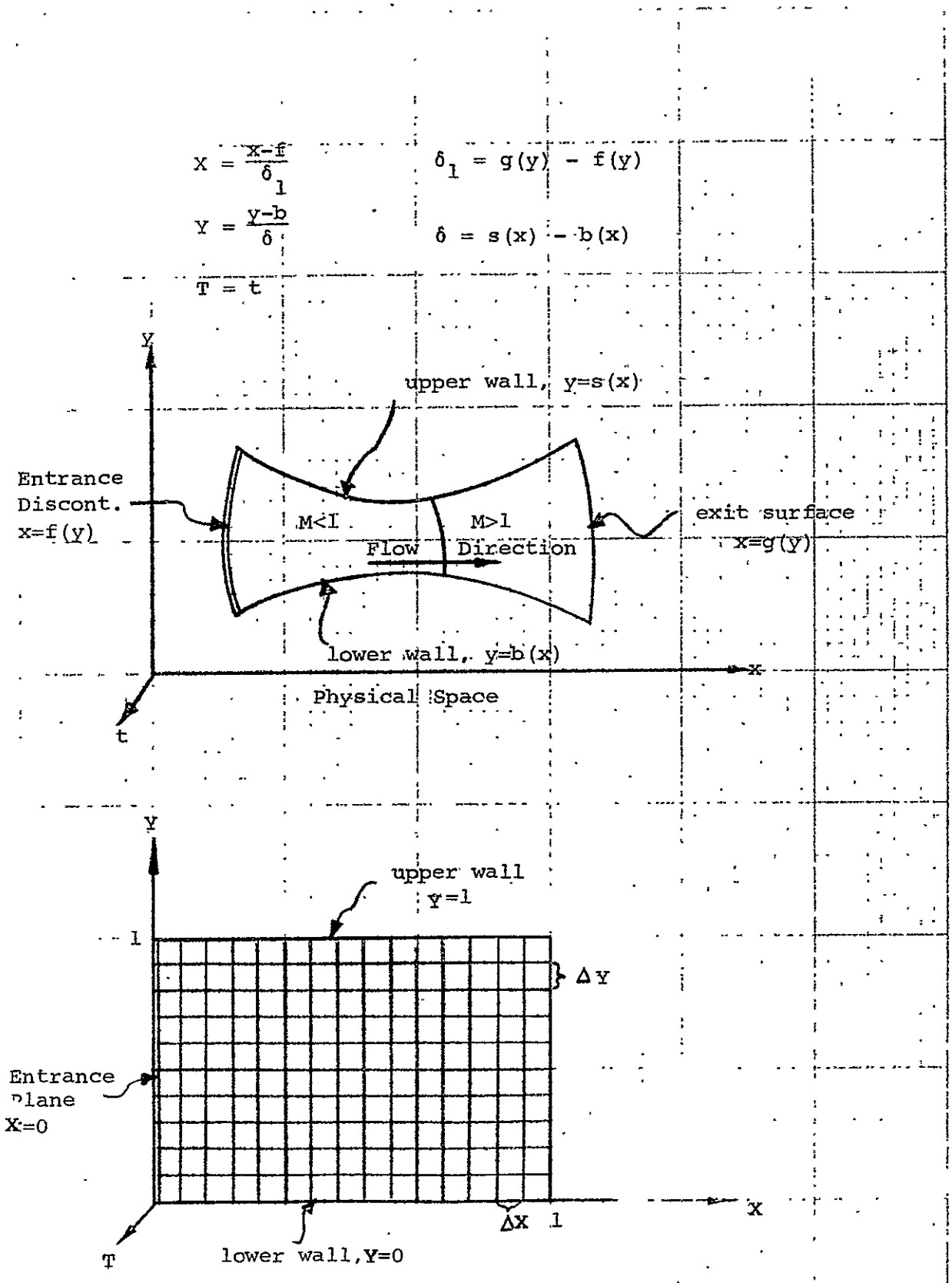

FIGURE 43 - SCHEMATIC OF MAPPING OF PHYSICAL SPACE AUTO COMPUTATION SPACE - FIXED TIME

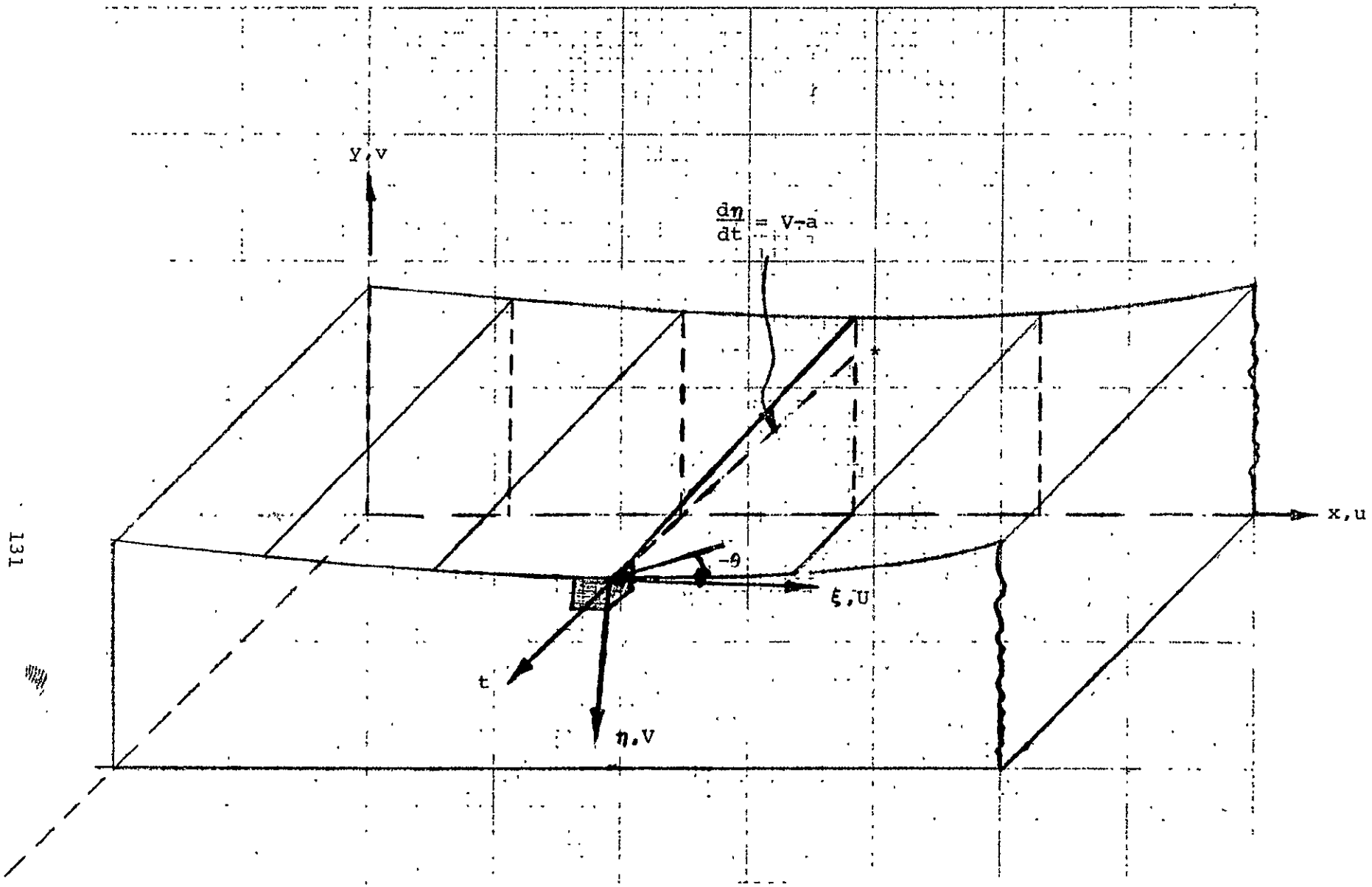

SKETCH 44- SCHEMATIC OF COMPUTATIONAL PROCEDURE AT A WALL MESH POINT (UPPER WALL SHOWN)

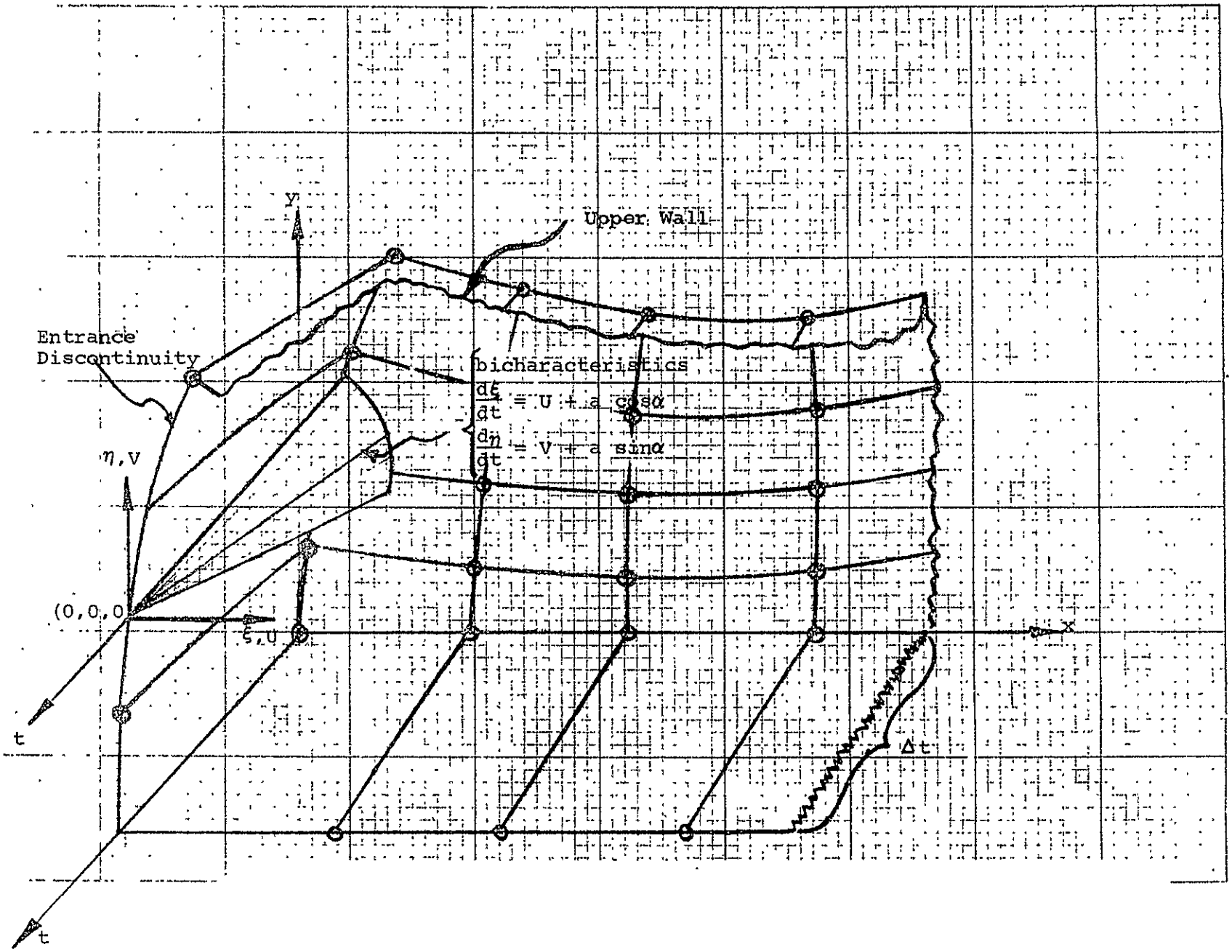

SKETCH 45. SCHEMATIC OF COMPUTATIONAL PROCEDURE ON DOWNSTREAM SIDE OF DISCONTINUITY

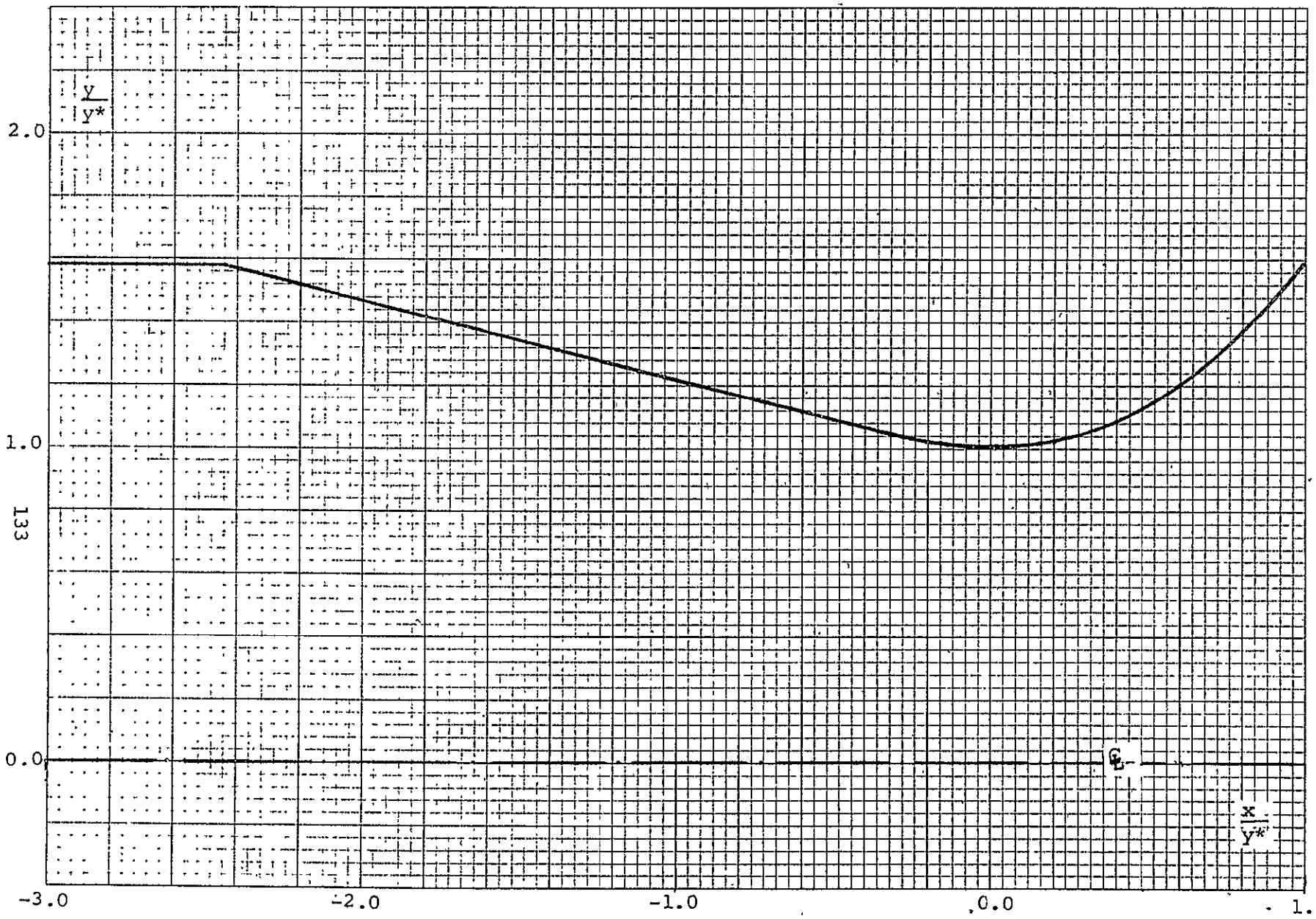

FIGURE 46 = TWO-DIMENSIONAL deLaval NOZZLE - SPECIFIED GEOMETRY

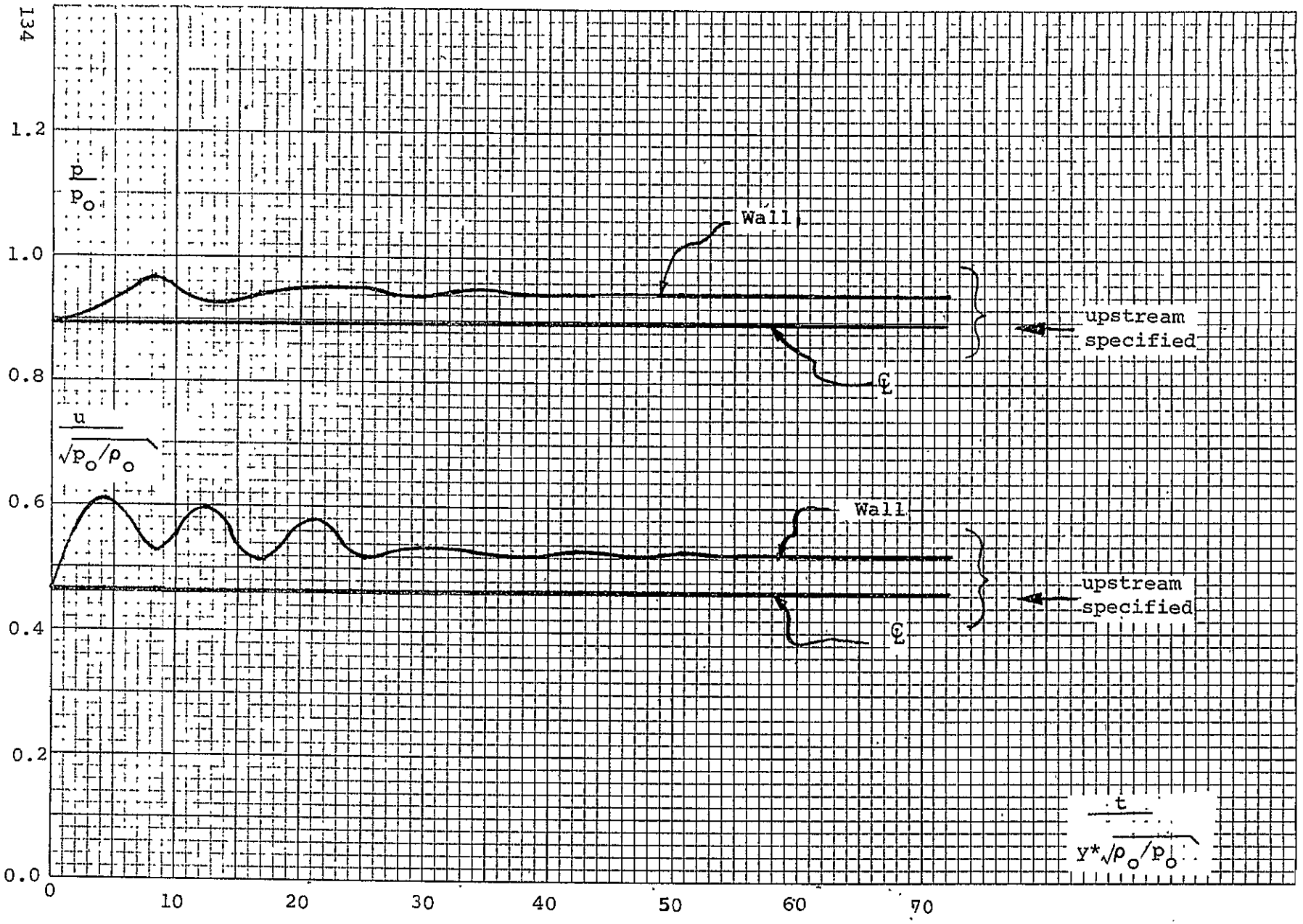

FIGURE 47 - PRESSURES AND VELOCITIES DOWNSTREAM OF DISCONTINUITY-TWO-DIMENSIONAL

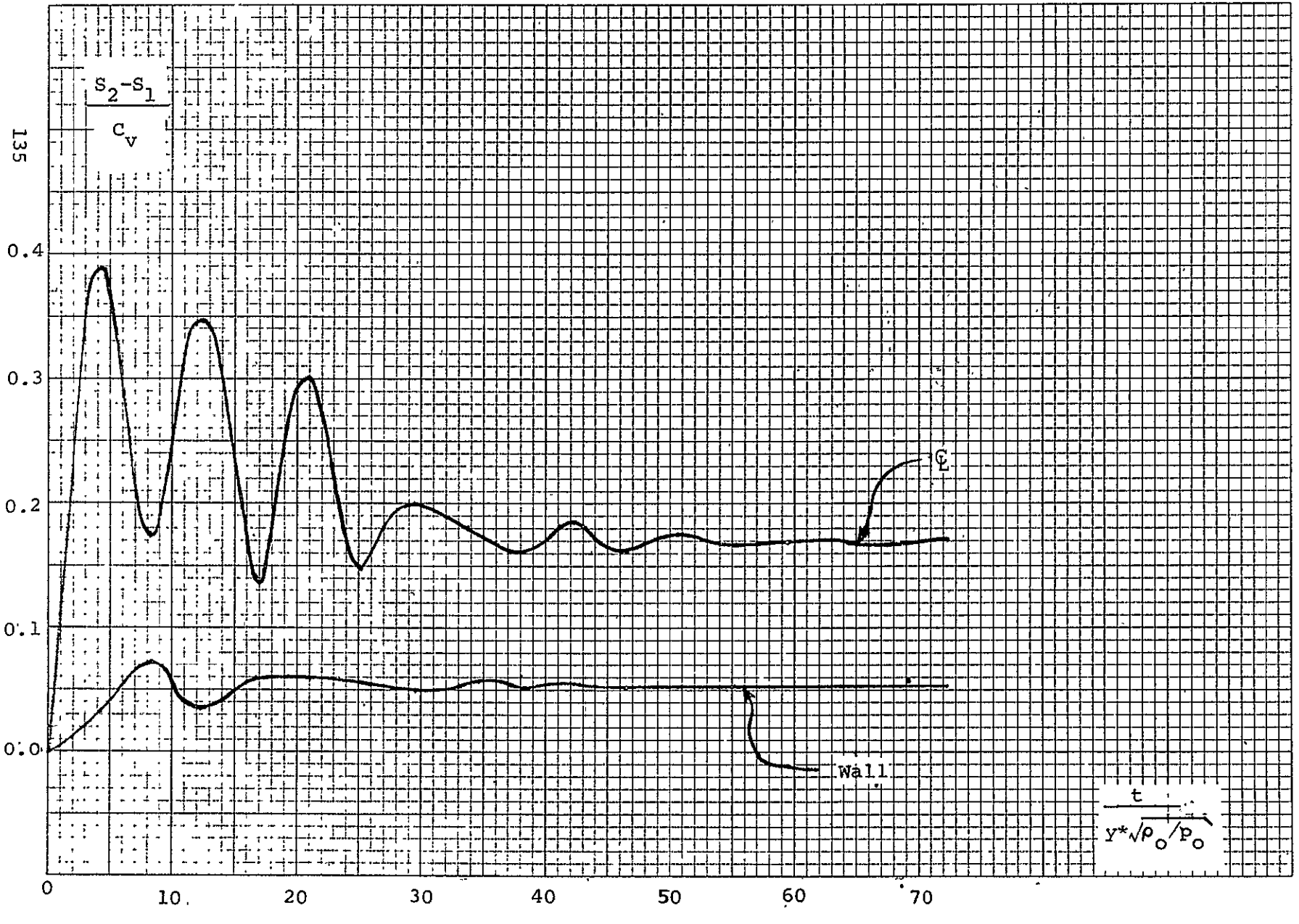

FIGURE 48 - ENTROPY JUMP AT DISCONTINUITY SURFACE-TWO-DIMENSIONAL NOZZLE

FIGURE 49 - COMPUTED STEADY CENTERLINE & WALL PRESSURE DISTRIBUTION
TWO-DIMENSIONAL NOZZLE

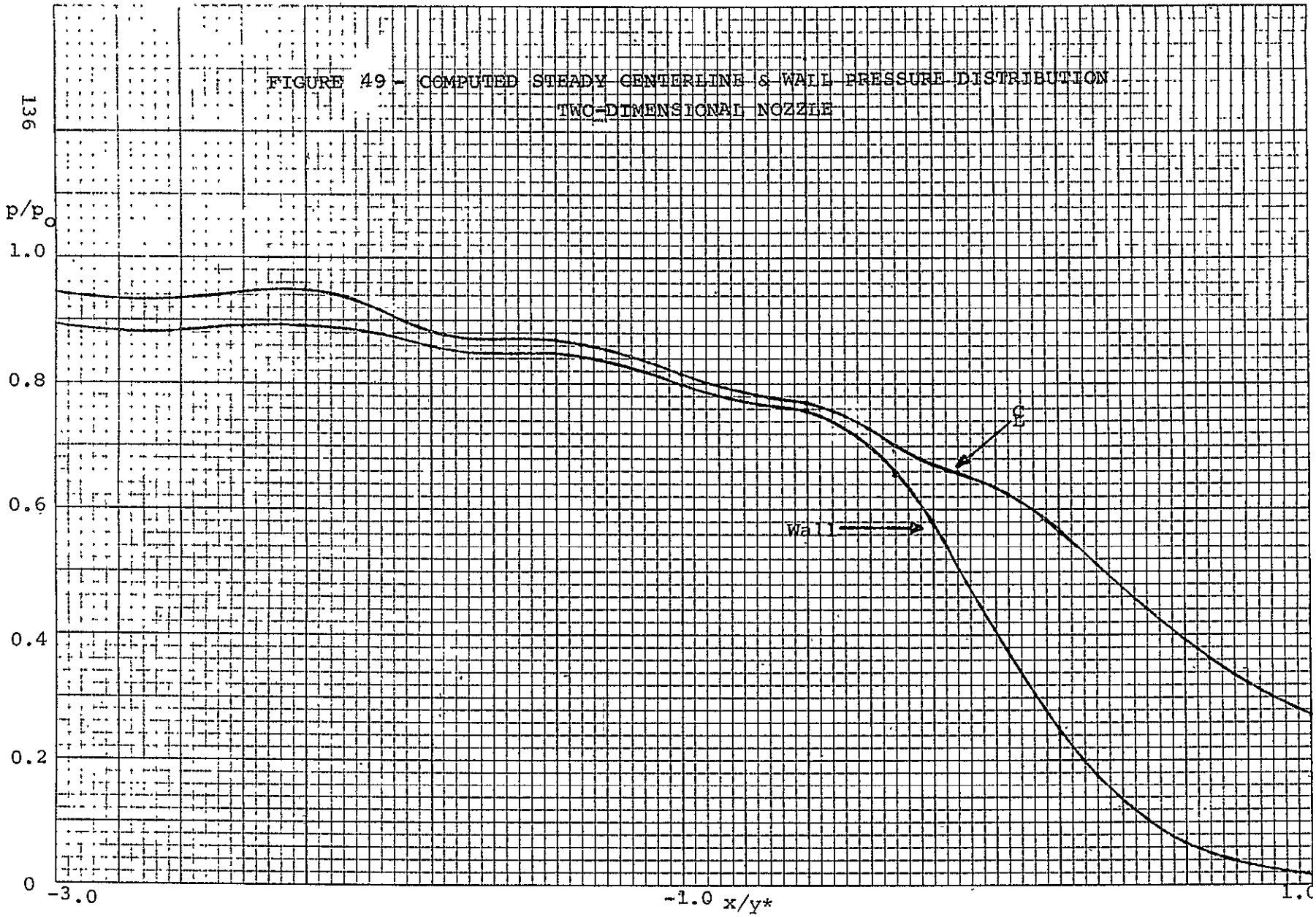

FIGURE 50 - COMPUTED STEADY STATE CENTERLINE & WALL MACH NUMBER DISTRIBUTION - TWO-DIMENSIONAL NOZZLE

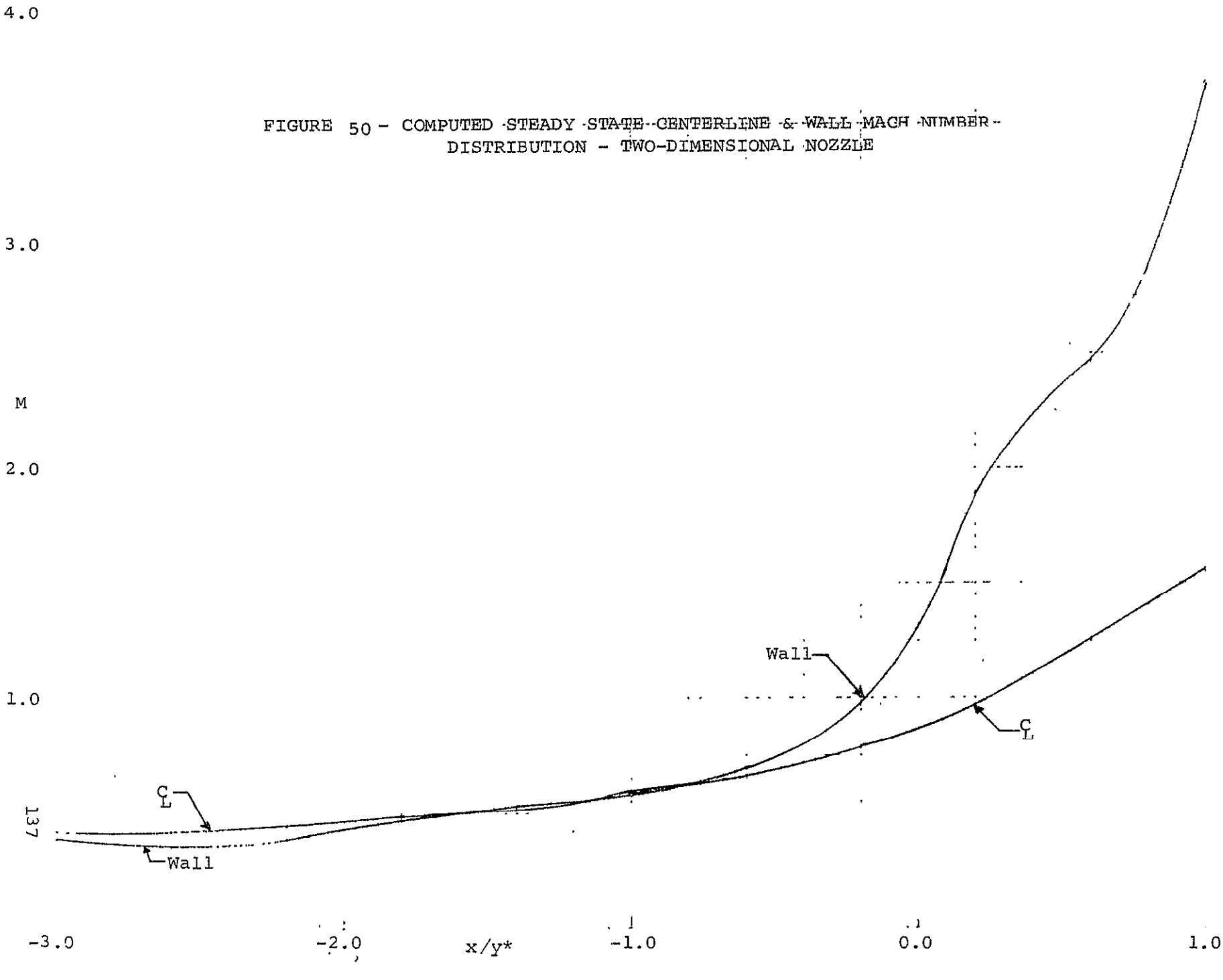

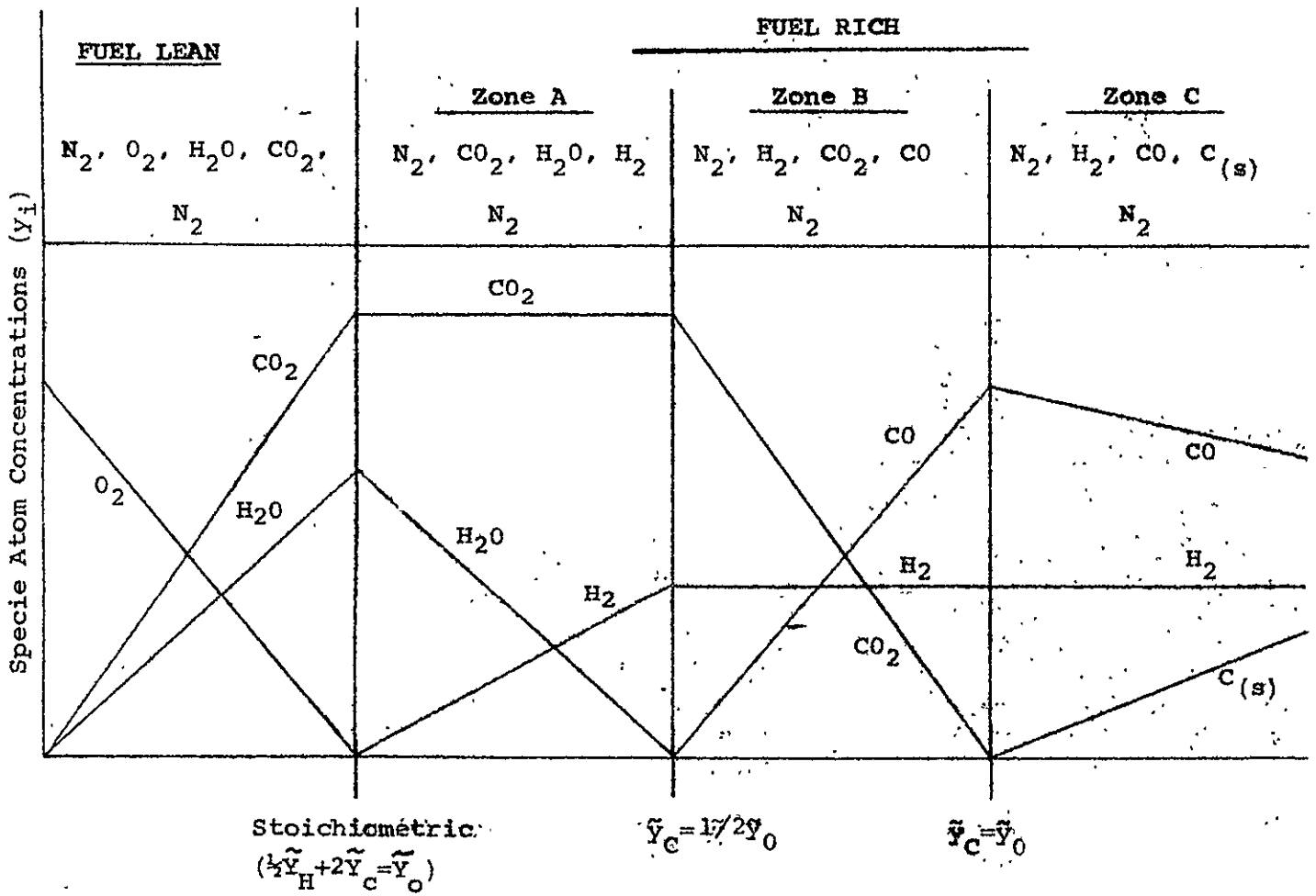

FIGURE 51 - EARLY QUASI-COMPLETE COMBUSTION OF HYDROCARBON-AIR CHEMISTRY MODEL

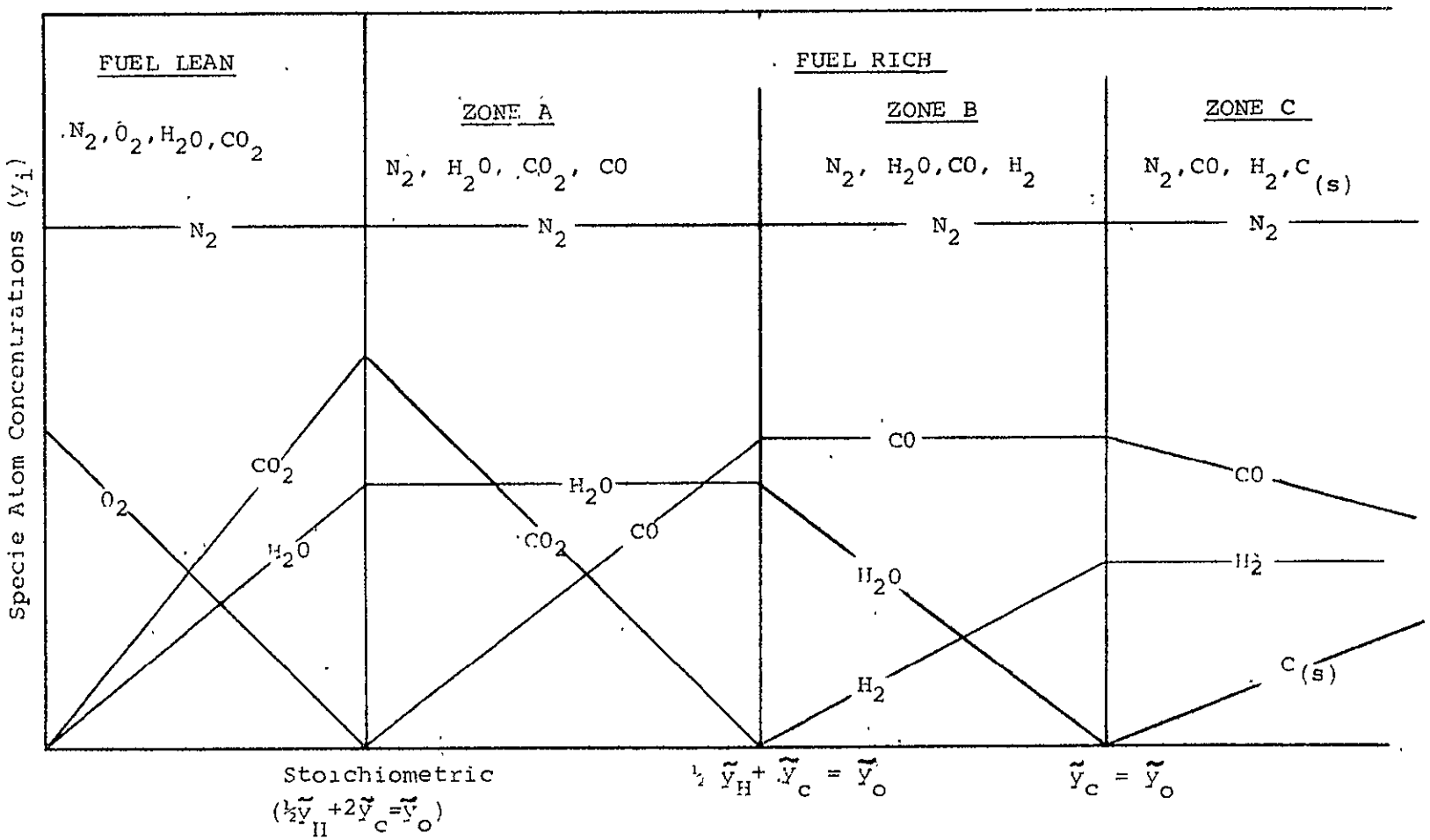

FIGURE 52 - FINAL QUASI-COMPLETE COMBUSTION HYDROCARBON-AIR CHEMISTRY MODEL

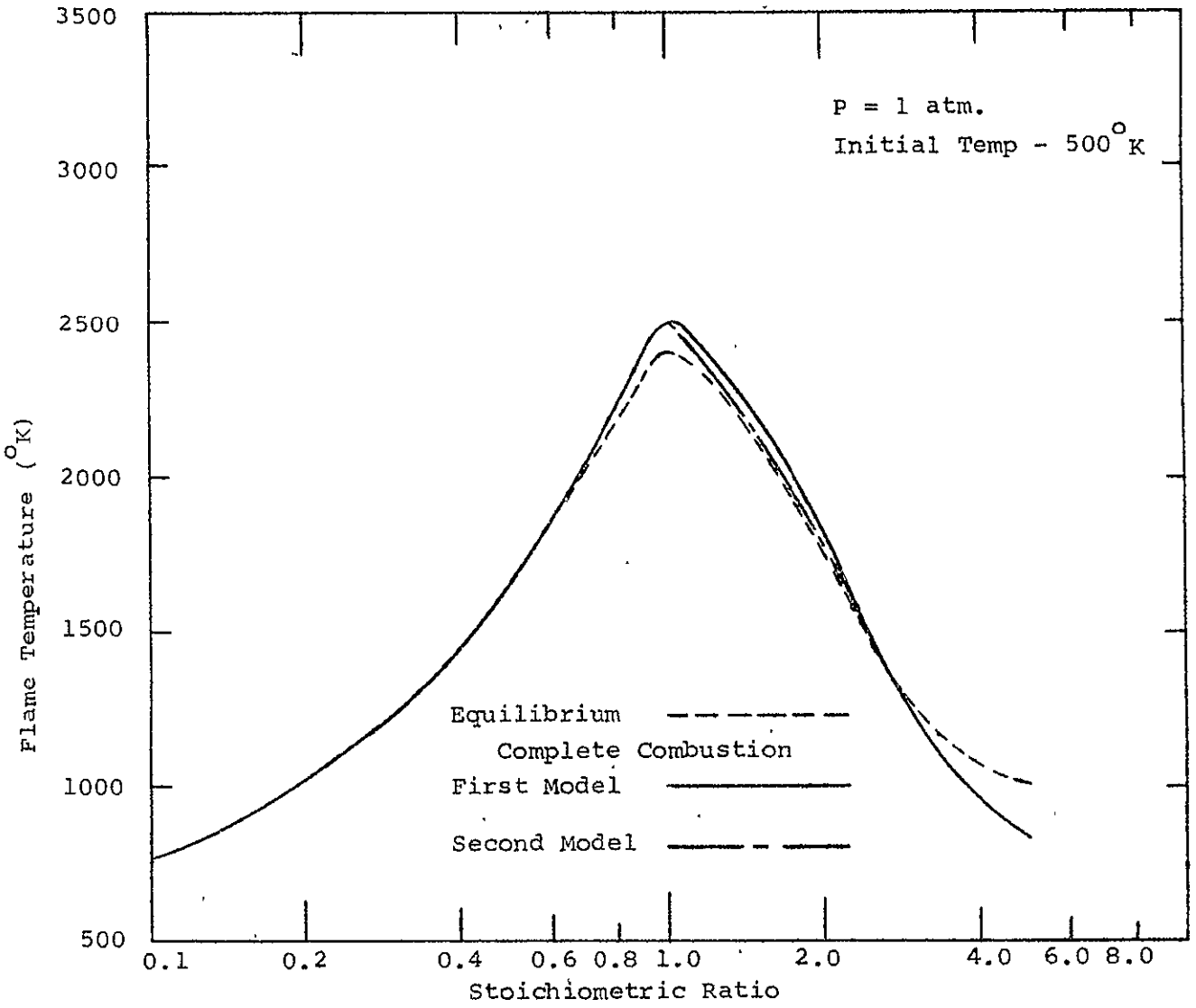

FIGURE 53 - COMPARISON OF QUASI-COMPLETE COMBUSTION MODELS WITH EQUILIBRIUM CHEMISTRY FOR A PROPANE-AIR SYSTEM

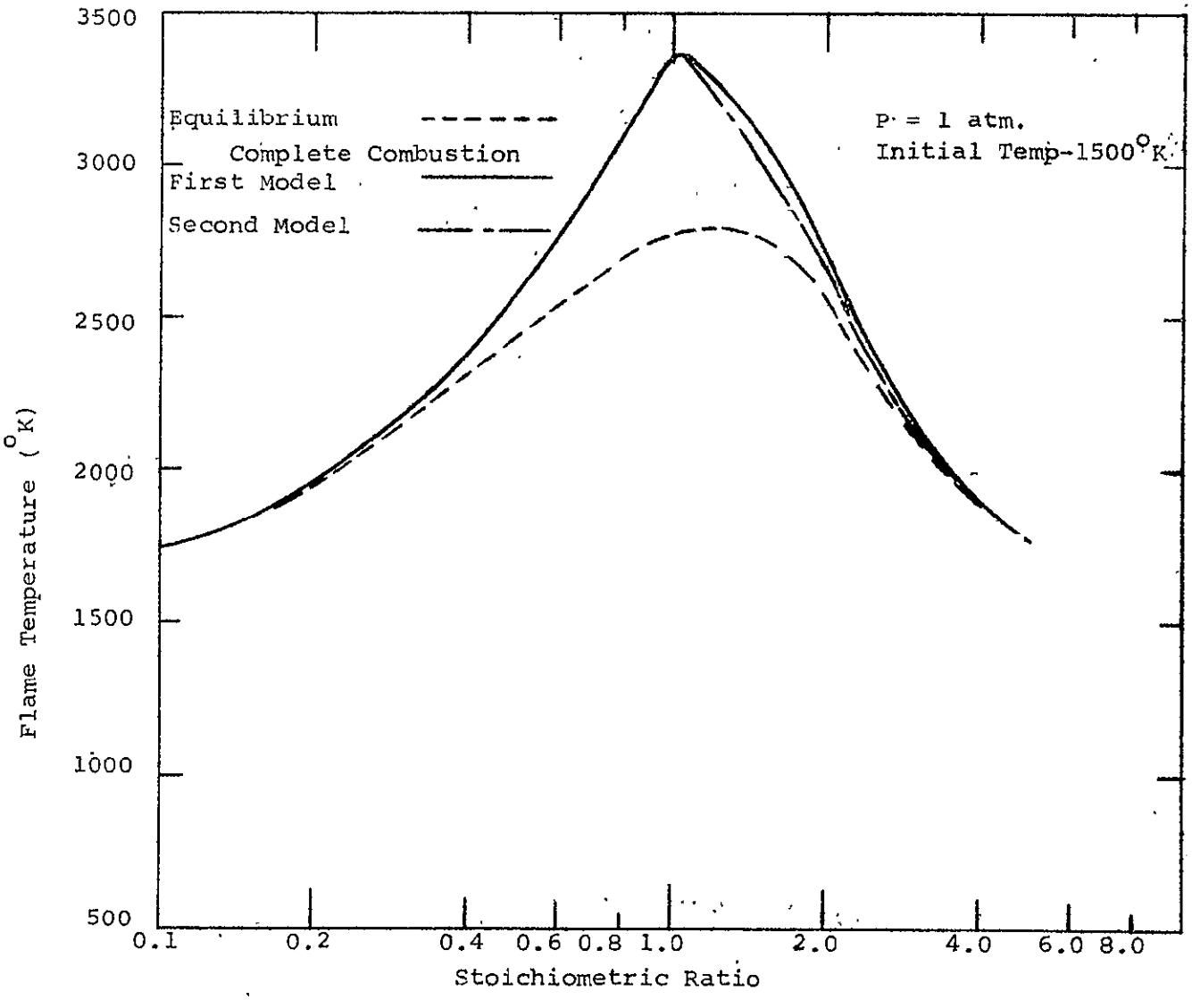

FIGURE 54 - COMPARISON OF QUASI-COMPLETE COMBUSTION MODELS WITH EQUILIBRIUM CHEMISTRY FOR A PROPANE-AIR SYSTEM

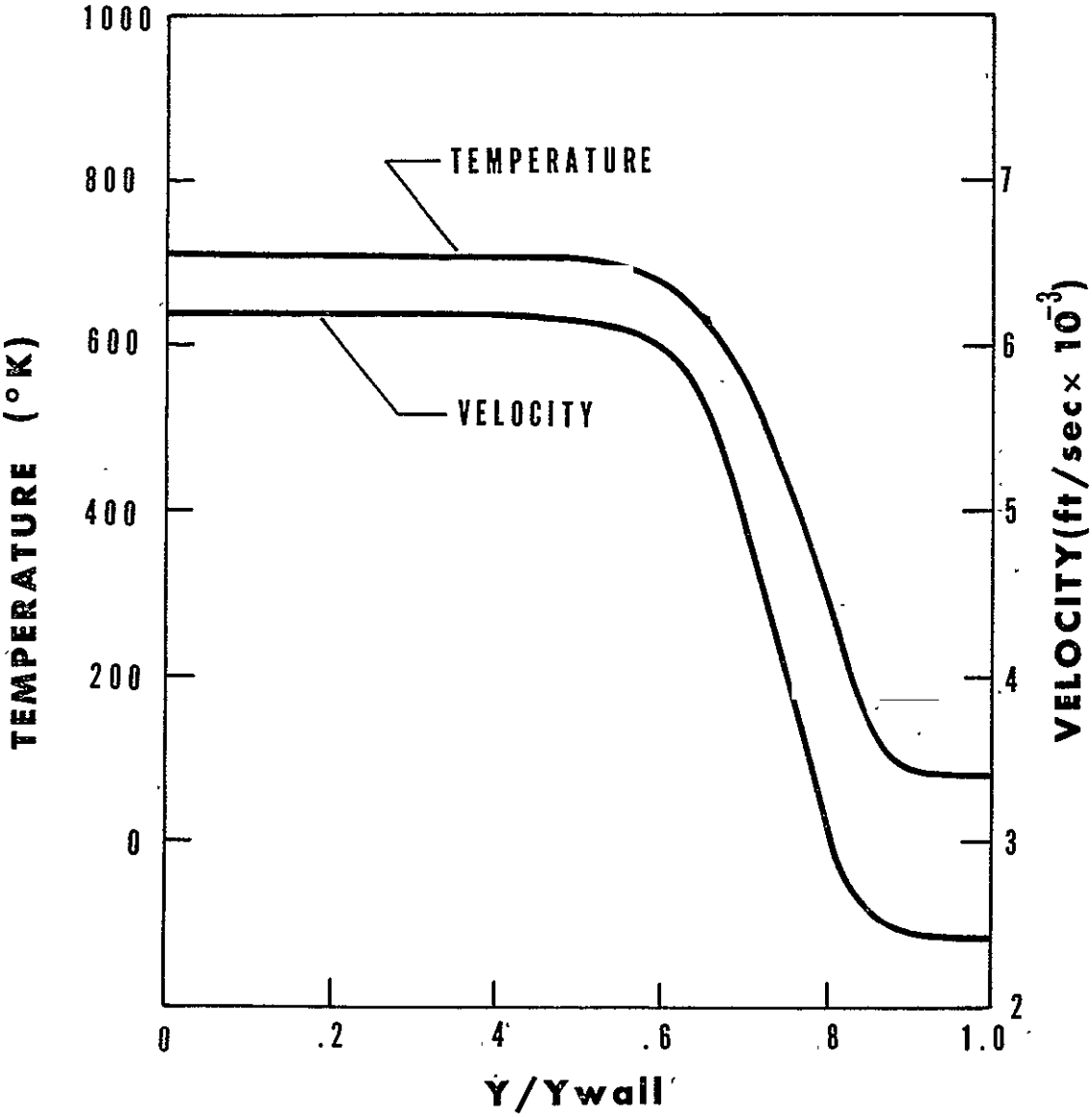

FIGURE 55 **VELOCITY AND TEMPERATURE PROFILES AT STATION $A/A_{jet} = 22$**

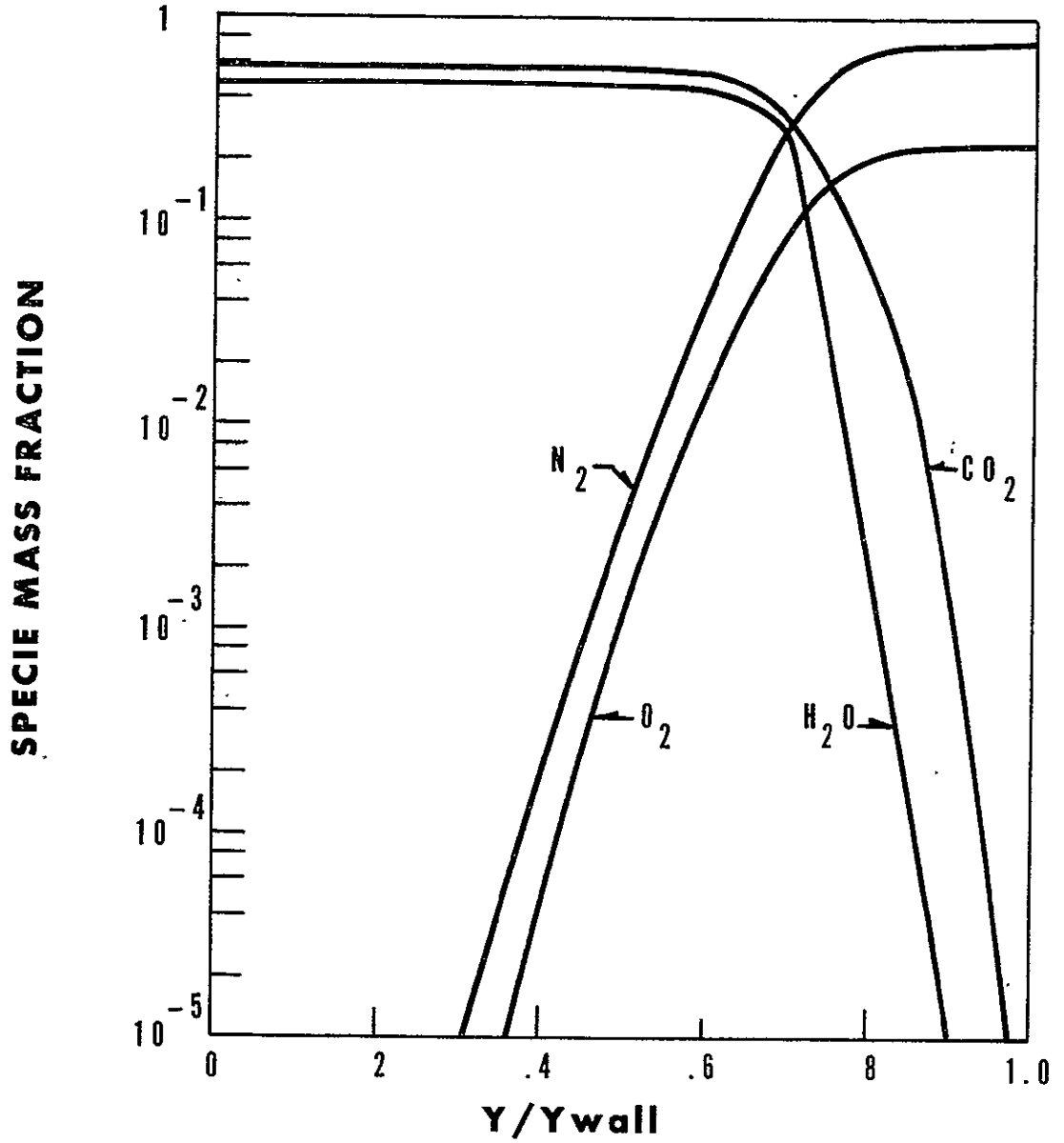

FIGURE 56 – **GASEOUS SPECIE MASS FRACTION DISTRIBUTION AT $A/A_{jet} = 22$**

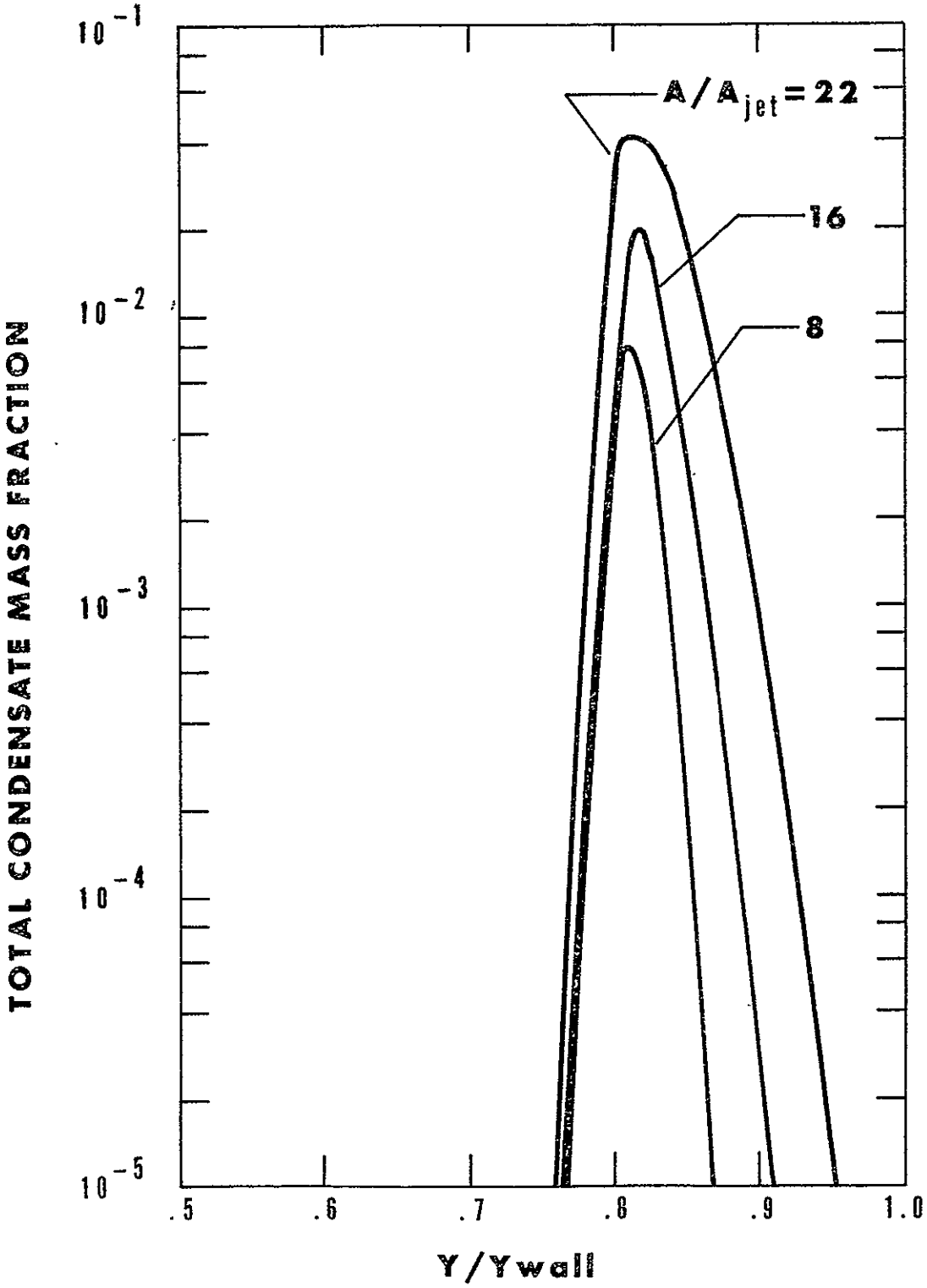

FIGURE 57 - **CONDENSED WATER PROFILES AT SEVERAL DOWNSTREAM STATIONS**

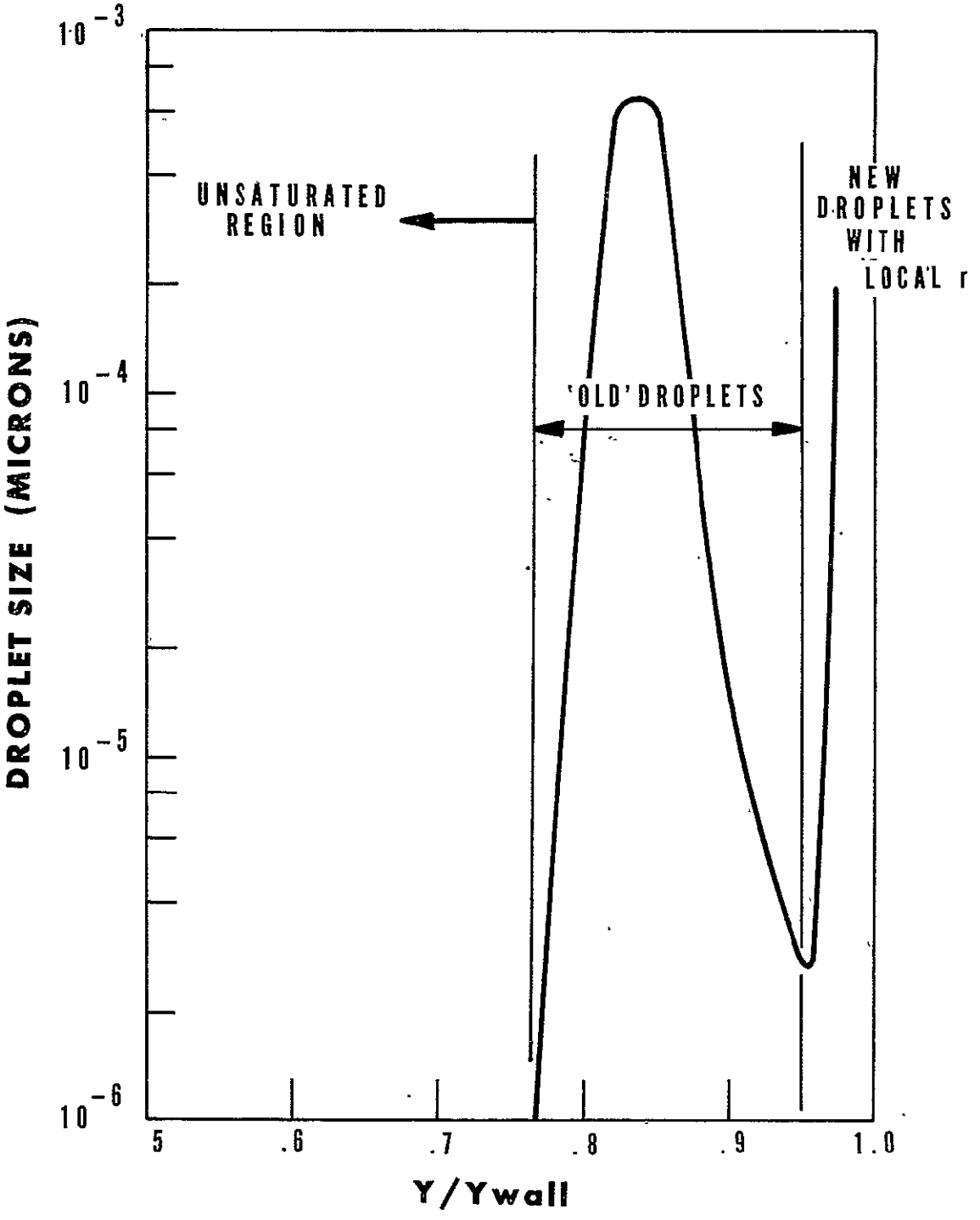

FIGURE 58 -CONDENSATE SIZE DISTRIBUTION IN THE FIRST CATAGORY AT $A/A_{jet} = 22$

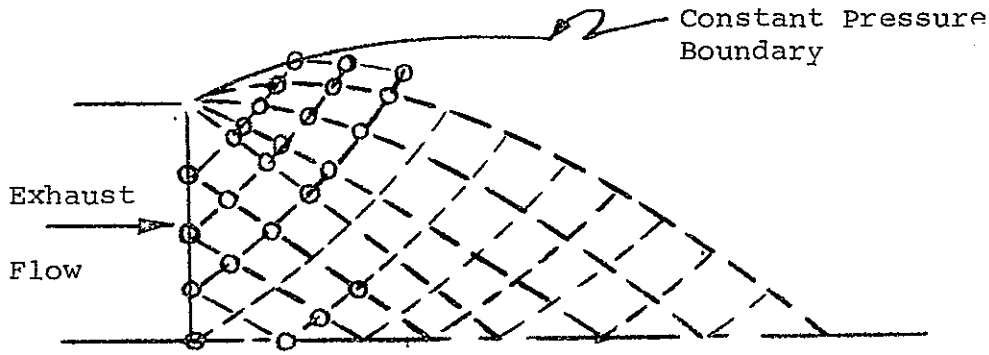

FIGURE 59 - THE CHARACTERISTIC MESH

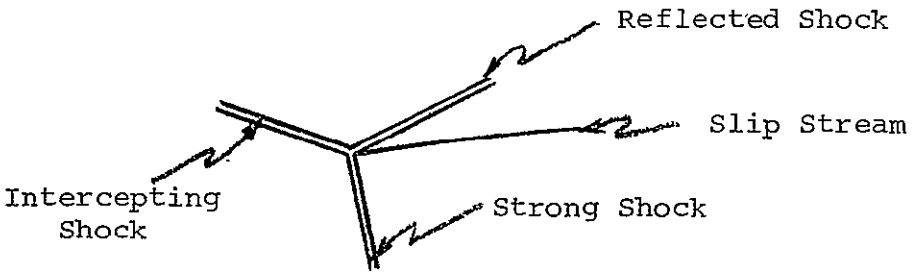

FIGURE 60 - SCHEMATIC OF TRIPLE POINT CONFIGURATION